Processing of Mullite based Ceramics Using Bauxite-Fly ash Mixture

A thesis submitted in partial fulfillment of the
Requirement for the degree of

MASTER OF TECHNOLOGY (RESEARCH)

By

DEVAVARAPU SOUMYA
(Roll no. 612CR3005)

Under the guidance of

Prof. Santanu Bhattacharyya

DEPARTMENT OF CERAMIC ENGINEERING

NATIONAL INSTITUTE OF TECHNOLOGY, ROURKELA

JULY 2015

Department of Ceramic Engineering
NATIONAL INSTITUTE OF TECHNOLOGY,
ROURKELA
Orissa-769008

CERTIFICATE

This is to certify that the thesis entitled ***"Processing of Mullite-based Ceramics using Bauxite-Fly ash Mixture"*** submitted by ***Ms. Devavarapu Soumya*** for the degree of **Master of Technology (Research)** in **Ceramic Engineering** to the National Institute of Technology, Rourkela, is a record of bonafide research work carried out by her under my supervision and guidance. Her thesis, in my opinion, is worthy of consideration for the award of the degree of Master of Technology (Research) in accordance with the regulations of the Institute.

The results embodied in this thesis have not been submitted to any other university or institute for the award of a Degree.

S. Bhattacharyya

Professor

Department of Ceramic Engineering

National Institute of Technology, Rourkela.

Declaration

I hereby declare that my M.Tech (Research) thesis is entitled as **"Processing of Mullite Based Ceramics Using Bauxite-Fly ash Mixture".** This thesis is my own work and has not been submitted in any form for another degree or diploma at any university or other institution of tertiary education. Information derived from the published and unpublished work of others has been acknowledged in the text and a list of references given in this thesis.

Devavarapu Soumya

_____ _____

Date Signature

Contents

Acknowledgement

It is with the most sincere thanks to who helped me to make this thesis possible.

I wish to express my deep, sincere gratitude to advisor ***Prof. S.Bhattacharyya*** for assigning me the project and for his inspiring guidance, constructive criticism and valuable suggestion throughout this research work.

I express my sincere thanks to Prof. Swadesh Pratihar, Head of the Department, Ceramic Engineering for providing me all the departmental facilities required for the completion of the project work. I am also thankful to all other faculty members of the Department of Ceramic Engineering, NIT Rourkela for their constructive suggestions and encouragement at various stages of the work.

My sincere thanks to all non-teaching staffs in Department of Ceramic Engineering for providing full of high- spirited delight in the lab and helping me throughout this project.

My sincere thanks to OCL and Tata Steel Refractories for helping me in carrying out the XRF.

My sincere indebted to all my senior research colleagues for their unconditional support and constant motivation whenever needed. I am very grateful my friends who have given me their friendship, put up with my odd hours, and provided me with lifts and practical help.

Last but not least, I would like thank to my ***dear parents & my loving brother*** who have patiently extended all kinds of help for accomplishing this work.

Devavarapu Soumya

Abstract

The present work discusses the preparation and characterization of mullite based ceramics from bauxite-fly ash mixture. Two different varieties of bauxites viz. Bauxite 1 (B1) and Bauxite 2 (B2) were used, and each bauxite variety was mixed with different weight percent (30, 40, 50 and 70) of same fly ash (FA). The B1-FA compositions were processed through two stage firing, and the B2-FA mixture was processed through single stage firing schedule. Both the B1- FA and B2 – FA compositions were sintered at 1400, 1450 and 1500^{o}C.

The mullitization reaction in the bauxite-fly ash commenced with the dissolution quartz and corundum followed by the appearance of mullite and corundum. The fraction of quartz and alumina decreased from 900^{o}C onwards while that of mullite and glass increased. The mullite percentage in the sintered bauxite-fly ash samples was dependent on the bauxite type and the higher percentage of mullite in B1 –FA compositions could be attributed to the finer crystallite size of B1. No difference in the mullite percentage was observed between single stage and two stage firing schedule. High bauxite compositions had corundum and mullite, whereas, high fly ash compositions had cristobalite and mullite. The microstructure of the sintered B1-FA samples showed dense crystalline microstructure for 30% FA samples and mullite grains and more glassy phase for 70% FA sample. The B2 microstructure showed the presence of glassy phase and porous microstructure both for 30% and 70% FA. Equiaxed primary mullite was present in 30% FA containing samples.

The bending strength and ISB fracture toughness was measured using Ring on Ring test method. A linear relationship was observed between the fracture strength and fracture toughness, particularly, for the compositions sintered at the highest temperature. In the B1-FA compositions, samples with predominantly mullite phase had low strength and toughness while the samples with a combination mullite and another phase had high strength, hardness, and toughness. In the B2-FA compositions, the strength and toughness were high in 40 and 50 % FA containing compositions. It was also observed that the samples that exhibited high strength and toughness had two different type of elongated mullite grains. Some of the selected samples were also subjected to thermal shock from 1250^{o}C for 5 cycles. The samples did not show any visible crack but showed a change in the mullite and glass content after cycling.

List of Figures

List of Tables

CHAPTER-1

INTRODUCTION

1. Introduction

Mullite ($3Al_2O_3.2SiO_2$) is a well-known alumino-silicate compound having wide applications in ceramic industries. The low thermal conductivity, high thermal shock resistance and high creep resistance makes mullite and mullite based ceramics an important candidate material for many applications. Some of these are the heat exchangers, metal filters, catalyst supports, radiant burners, sensors [1.1], lining for the upper parts of the melting furnaces, hot blast stoves, continuous casting furnaces, torpedo ladles [1.2], thermal and heat insulating materials for kiln furnaces, as heat resistant fillers, as substrates for catalysts, as heat resistant packaging for car engines [1.3]. Some of the important physical properties of mullite have been listed in Table 1.1 [1.4]

Table 1.1 Properties of Mullite

Melting point (^oC)	≈1830
Density (g cm^{-3})	≈3.2
Linear thermal expansion ($*10^{-6o}C^{-1}$) 20–1400°C	 ≈4.5
Thermal conductivity (kcal m^{-1} $h^{-1}{}^{\circ}C^{-1}$) 20°C 1400°C	 6 3
Strength (MPa)	≈200
Fracture toughness K_{IC} ($MPam^{0.5}$)	≈2.5
Flexural Strength (MPa)	150-360

1.1 Phase Diagrams of mullite

The main controversy regarding mullite is its ambiguous behaviour during melting i.e. whether mullite will exhibit congruently or incongruently behaviour. This particular aspect has been discussed in a later section. However, it can be said that the nature of precursor and the processing routes do control the melting behaviour [1.5]. Bowen and Grieg in 1924 [1.6] showed for the first time that mullite was a distinctly separate phase in Al_2O_3-SiO_2 system. The phase was different from sillimanite and exhibited incongruently melting behaviour. However, in 1949 Bauer, Gordon and Moore [1.7] reported the production of a single crystal of mullite by flame fusion method. The results of their experiments hinted that the mullite can also melt incongruently or else the growth of single crystal would not have been possible. Congruent melting of mullite was also reported by Toropov et.al [1.8] and Budnikov [1.9] but their results were refuted by Filonenko and Lavrov [1.10] who reported incongruent behaviour. Much later Aramaki and Roy [1.11] studied fusion of Al_2O_3-SiO_2 mixture on a

sealed Pt/Rh capsule and studied the phase diagram of a quenched sample. They observed congruently melting behaviour for mullite using three different Al/Si diffusion couples. In 1968, Aksay and Pask [1.12] reported incongruent melting of mullite. They further concluded that the mullite phase stability depended on the cooling rate from the processing temperature. It has also been reported that the presence of α-Al_2O_3 nuclei results in alumina rich mullite with incongruently melting behaviour. On the other hand, congruently melting mullite is produced from a homogeneous melt where the scale of mixing is in the molecular level. The diphasic mullite precursors require a higher densification temperature and produce elongated mullite crystal network.

1.2 Crystal Structure of mullite:

Mullite is derived from sillimanite group of minerals ($Al_2O_3.SiO_2$), the parent composition of the alumino-silicate family. The substitution of Si^{4+} by Al^{3+} at the tetrahedral sites results in mullite composition. The substitution of Si^{4+} by Al^{3+} removes oxygen ion in (Al, Si)O_4 tetrahedra and creates an oxygen vacancy. The removal of oxygen ion also leads to the repositioning of some of the cations [1.13]. The overall substitution in the tetrahedral unit can be written down as

$$2Si^{4+} + O^{2-} \longrightarrow 2Al^{3+} + \square \qquad (1.1)$$

Where $\square$ represents the oxygen vacancy. Since the octahedral [AlO_6] units remain unaltered, the generalized chemical formula for mullite can be written as [1.13]

$$Al_2^{VI}[Al_{2+2x}^{IV} Si_{2-2x}] O_{10-x}$$

The Roman numerals IV and VI denote the coordination states of Al and x represents the missing oxygen. Thus, in mullite Al is present both in 4 coordinated as well as 6 coordinated states. The value of x decides the mullite composition. Normally x varies between 0.17 to 0.6. At x= 0.25 the mullite composition is 3:2 and at x=0.57, the composition changes to 3:1. The oxygen vacancies can be arranged in an ordered or disordered array. In case of ordered oxygen vacancies, an additional or extra reflection is observed in both X-Ray and electron diffraction as satellite reflection [1.14]. Among the factors that affect the ordering-disordering phenomena in mullite, temperature, composition (hypo or hyper alumina) and reaction kinetics are important ones. Highly ordered mullite are observed which have been produced from a hyper alumina quench melt [1.15]. For such mullite, the solid solubility of alumina can be as high as 83.2% (76 mole %). The Al_2O_3/ SiO_2 ratio for these types of ordered mullite may vary from 1.5 to 3.17 [1.16].

On the other hand, mullite processed through diffusional couples of Al_2O_3 and SiO_2 are more stable, and the mullite lattice is highly disordered [1.17]. The composition of this stable mullite is 3:2. Because of the random distribution of vacant oxygen sites, 3:2 mullite do not produce additional scattering. However, in spite of the many studies carried out in the structural analysis of mullite, the issue of alumina solubility remains a matter of dispute [1.12]. It has also been observed that under a specific processing condition with a given set of precursors, several types of mullite may coexist in a single sample. These wide distributions of mullite structure have been correlated with the inhomogeneous distribution of oxygen ion, oxyge

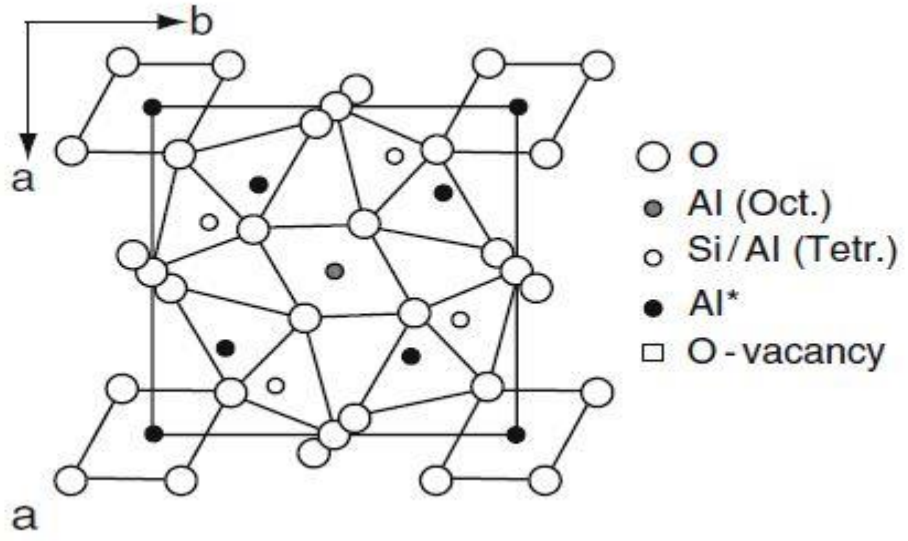

Figure 1.1.Structure of Mullite

1.3 Synthesis of Mullite:

Depending on the end applications, a wide variety of raw materials and precursors have been used to synthesize mullite. Solid state route involving two oxide powders for Al_2O_3 and SiO_2 source have conventionally been used for preparing mullite for refractories and whitewares. On the other hand, mullite intended to be used for structural or electronic applications mostly use a chemical route or a sol-gel route. On a general note, the processing routes can be classified into three categories. They are:

a) Solid state route involving mixing and reaction of two oxide powders. The oxide powders can be either pure Al_2O_3/ gibbsite /diaspore and SiO_2/α-quartz/Cristobalite/fused silica etc.
b) A combination of silica sol and colloidal alumina or vice versa like tetraethoxysilane (TEOS) and Aluminium hydroxide ($Al(OH)_3$). It can also be Al-sol (Aluminium isopropoxide) and silica sol (fume silica, colloidal silica).
c) A combination of Al-sol (Al-tri-sec-butoxide) and silica sol (silicon ethoxide).

Okada and Otsuka [1.19] have given the following schematic diagram on the various approaches that have been used for the processing of mullite ceramics.

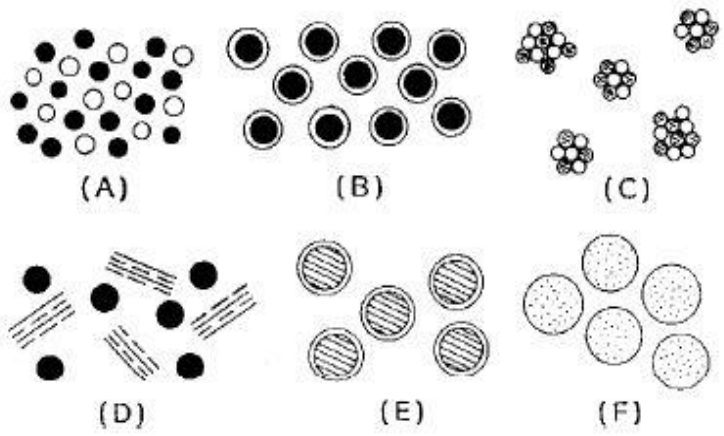

Figure 1.2. Schematic microstructural models of mullite starting materials prepared by the various approaches (A) sol mixing; (B) composite particles; (C) hydrolysis of alkoxides; (D) conventional mixing of clay minerals and alumina; (E) co-precipitation; (F) spray pyrolysis

Irrespective of the raw materials or the starting precursors used for mullitization, the synthesis process can be broadly classified as

a) Processing from monophasic precursors, and
b) Processing from diphasic (or biphasic) precursors.

The monophasic precursors exhibit atomic level mixing of Al and Si. Such a precursor directly transforms to mullite at 980^{o}C. Examples are the mullitization reaction in spray pyrolyzed amorphous precursors or the product from CVD process [1.20]. Inorganic salt solutions or mixed alkoxides also retain atomic level mixing and therefore also directly transforms to mullite below 1000^{o}C [1.21].

The scale of mixing in diphasic precursors is in the nanometer range (1-100nm). Examples of diphasic precursors are the gels or powders obtained through rapid hydrolysis of the inorganic salt solution or alkoxides sols, natural sources like kaolinite. The mullite formation with such type of precursors is preceded by the crystallization of cubic alumina (spinel or γ-alumina) at 980^{o}C. The mullite formation is shifted to 1200^{o}C. In most of such precursor, a segregation of alumina and silica is observed which may result in spinel (or γ-alumina) formation along with quartz or cristobalite. The mullite formation reaction will depend on the dissolution of alumina in silica-rich liquid and its precipitation as mullite. Thus, the kinetics of mullite formation depends on the nucleation rate of mullite in a siliceous matrix as the matrix reaches saturation concentration of alumina.

1.4 Densification and reaction sintering of mullite:

Although different research groups have established a number of improved processing routes for the synthesis of mullite, its densification issues have not been properly addressed. A reduction of initial particle size of Al_2O_3 and SiO_2 helps to achieve molecular level mixing constituents thereby reducing mullitization temperature, but densification issues remain unsolved. As already mentioned, low ion mobility of Si^{4+} prevents rapid inter-diffusion of Al^{3+} and Si^{4+}. It has been reported that the activation energy for the lattice diffusion of Si^{4+} is 700 KJ/mol, and that of Al^{3+} is 580 KJ/mol [1.22]. Thus, Si^{4+} diffusion is the rate controlling step for the mullite diffusion. Two other factors also affect the densification of mullite. One of them is the change in material density on mullitization. For 3:2 mullite, the density decreases by 4.53%. Secondly, the molar volume change on mullite formation is 9%. All these factors retard the densification. Therefore, the mechanism of reaction sintering appears to be most feasible for the reaction

$$3Al_2O_3+2SiO_2 = 3Al_2O_3.2SiO_2 \qquad (1.2)$$

Many authors [1.23-1.25] have also reported that pressureless sintering at (1650^{o}C) with a long holding time helps to achieve full densification. The use of hot pressing [1.26] and hot isostatic pressing [1.27] has also been employed successfully. Some of the recent literatures have mentioned the use of spark plasma sintering for achieving full densification of mullite. Another approach to solving the densification issue is to achieve low-temperature densification (<1350^{o}C). In this case, densification is achieved through transient viscous phase deformation of the amorphous matrix [1.26]

The key issue is to achieve densification before mullitization and to shift the mullite formation to higher temperatures. Some authors have also commented that most of the mullite forming systems retains SiO_2 as an amorphous phase. At the sintering temperature (1275-1350^{o}C) the crystallization of amorphous silica to cristobalite also retards the densification. Therefore, the densification of mullite from diphasic precursor systems experience two opposing effects. Firstly, the crystallization of mullite involves the presence of silica-rich liquid phase. However, if this liquid persists during densification, it retards densification due to the crystallization of the liquid phase

1.5 Effect of additives on mullitization:

In section 1.3, it has been mentioned that liquid precursors provide a low-temperature synthesis of mullite. Alkoxides [1.28], colloidal silica and boehmite [1.29], inorganic salts and alkoxides combination has been used [1.30]. These precursors provide advantages like molecular level mixing and are usually achieved in monophasic precursors. In case of

diphasic precursors, as the scale of mixing changes to the nanometer level, mullitization shifts to a higher temperature. Recently, it has been reported that certain additives like B_2O_3, Y_2O_3, La_2O_3, TiO_2 and V_2O_5 can promote low-temperature synthesis of mullite in a diphasic precursor system.

B_2O_3 lowers the viscosity of the SiO_2-rich liquid and also react with Al_2O_3 to form $9Al_2O_3.2B_2O_3$. It is reported that aluminum borate promotes nucleation of mullite crystal from the low viscosity of silica-rich liquid [1.31].

Y_2O_3 has been found to react with SiO_2 and form two types of yttrium silicate between 1300^{o}C and 1400^{o}C. The presence of these yttrium silicates increases mullitization as well as reaction bonding phenomenon of mullite ceramics [1.32].

Similar studies were also conducted with La_2O_3, TiO_2, and V_2O_5. All the above three oxide additives promoted lower temperature mullitization. But unlike the above additives, Nb_2O_5 and Ta_2O_5 retarded the mullitization reactions [1.33-1.34].

1.6 Mullite based ceramics using flyash:

Fly ash is generated in bulk quantities in thermal power plants. These waste products are not eco-friendly and, therefore, continuous efforts are being made for its useful industrial utilization.

Since the late 1990s, many researchers have tried to utilise fly ash for mullite ceramics preparation [1.35-1.38]. Usually, high Al_2O_3 fly ash (>40% Al_2O_3) have been used for this purpose. Owing to the lower Al/Si ratio as compared to clay and other alumino silicates, the mullitization process involving fly ash were directed in the following ways. Fly ash has been widely used as a raw material for high wear resistant ceramic tile, ash alloys, glazed floor and wall tiles, ceramic fibres. Some of the other applications are in oil well cement; continuous casting moulds powder, fire bricks, synthetic wood, an adsorbent for toxic organics, foam insulation products

a) The addition of Al_2O_3, $Al(OH)_3$ or bauxite to increase Al_2O_3 content.
b) Decreasing the silicon content of fly ash by a desilication process.

The coal fly ash- a by-product of the combustion of coal in electric generating plants is generally used for the fabrication of mullite ceramics because of its high alumina and silica content. The complete mullitization was achieved at higher sintering temperatures i.e. 1600^{o}C [1.39].

Thus, in this chapter a brief introduction on the properties and processing of Mullite has been provided. Among the different topics discussed in this chapter, the processing of mullite from

Industrial Waste is an eco-friendly system. This process and the available literature will be discussed in greater detail in the next chapter

CHAPTER-2

LITERATURE REVIEW

2.1 Phase Diagrams of Mullite:

In the Al_2O_3-SiO_2 system, single phase mullite could be obtained by different processes at atmospheric pressure. Some of these processes are melt quenching through an amorphous to crystalline transformation, solid state reaction, etc. Thus mullite is among one of the stable phases in Al_2O_3-SiO_2 systems [2.1]. However, since the time of first synthetic mullite, two subjects are still being revised by the researchers. The two questions are:

(a) How mullite will behave during melting?

(b) What is the composition range over which mullite will exist as a single phase material?

The answer to the first question will eventually decide if mullite exhibits "congruently melting behaviour" or "incongruently melting behaviour". The answer to the second question will finalize if mullite has a fixed composition or a range of compositions- i.e. the solubility range [2.2]. The melting behaviour of mullite has been a matter of controversy since the time of the publication of the first phase diagram of Al_2O_3-SiO_2 system by Bowen and Greig [1.6]. Since then, a large number of research papers [2.3-2.5] have been published to date on the phase stability issues in the Al_2O_3-SiO_2 system. Most of the phase diagrams of the Al_2O_3-SiO_2 system were determined at room temperature either on the sample that has been quenched from high temperature or through differential thermal analysis. Bowen and Grieg in 1924 were the first to report a systematic and reproducible Al_2O_3-SiO_2 phase diagram. In their study, mullite was prepared by quenching a mechanical mixture of Al_2O_3-SiO_2 from high temperature. The results showed that mullite melted incongruently at 1810^oC giving α-Al_2O_3 and liquid. The composition of the liquid was different from that of the mullite. The differential thermal analysis is the other method that has been used for phase diagram determination. Since the kinetics of mullite growth depends on the inter-diffusion of Al^{3+} and Si^{4+}, the exact nature of experiments required an isothermal study. However, both melt quenching and DTA methods were dynamic in nature. Thus, the mullite phase kinetic study was hampered by nucleation and growth issues. Therefore, these two methods gave non-reproducible and often misinterpreted results. In 1949, Bauer, Gordon and Moore [1.7] produced mullite single crystal of 3/1 composition ($3Al_2O_3.SiO_2$) by flame fusion method. The as grown mullite single crystal had 83 wt.% Al_2O_3. This work and the later work of Toropov et.al [1.8] raised questions on the existence of the incongruent nature of mullite. However, there were other reports like that of Shears and Archibald [2.6] and others, on the incongruently melting behaviour of mullite. The much referred work of Aramaki and Roy (1962) [1.11] on Al_2O_3-SiO_2 phase diagram confirmed that mullite is congruently melting. In

their study, Aramaki and Roy prepared the mullite samples from a mechanical mixture of α-alumina powder and silica glass which were held above the melting temperature for complete and homogeneous melting followed by quenching in mercury or water. The results indicated that mullite melted congruently with a solid solution ranging from 71.8 to 74.3 wt.% of Al_2O_3. In 1968, Aksay and Pask [1.12] worked with a diffusion couples made from sapphire and fused silica. The report of Aksay and Pask contradicted the result of Aramaki and Roy and concluded that mullite is an incongruently melting compound (melting point-1828^{o}C). In Askay's work, the solid solution range of mullite was observed to be between 70.5 to 74.0 wt. % of Al_2O_3 below 1753^{o}C and between 71.6 to 74.0 wt.% of Al_2O_3 at 1813^{o}C. David and Pask (1972) [2.7] used a semi-infinite diffusion couples of sapphire (α-alumina) and fused silica at temperatures up to 1750^{o}C. They determined the solid solution range of mullite between 71.0 to 74.0 wt.% of Al_2O_3. Guse and Mateika (1974) [2.8] grew single crystals of mullite via Czochralski technique. The obtained mullite single crystals were 2:1 composition instead of 3:1 observed with flame fusion process. In 1980, Shindo [2.9] grew single crystals of mullite by the "Slow Cooling Float Zone (SCFZ) method". The grown mullite crystals exhibited incongruent melting behavior. Prochazka and Klug (1983) [2.10] observed congruent melting behaviour of mullite. It was also observed that at 1600^{o}C, solid solution range shifted to higher Al_2O_3 content. Klug et.al [2.11] used the sol-gel method to prepare mullite and stated that 2:1 mullite was stable from 1600^{o}C up to melting temperature. The starting homogeneous powder was free of α-alumina particles. He observed that the liquidus position of Al_2O_3 needed modification to frame the proper phase diagram. Klug described and reported incongruent melting behaviour of mullite at 1,890^{o}C. In their study, the observed solid solution range was above the eutectic temperature of 1,587°C, and it tended towards higher alumina content (2:1) mullite. Recently, Mao et.al [2.12] have carried out the modeling of Al_2O_3-SiO_2 phase equilibrium. In their study, mullite was modeled with sillimanite as end member. They predicted a congruently melting behaviour. Thus, quoting Askay it can be concluded that "uncertainties about the phase equilibria of the silica-alumina system still continue. Conflicting views mainly arise when only *one* method of analysis is used to determine the phase diagram. More properly, in addition to the microstructural characterization, the overall composition must also be profiled to determine the stable and metastable equilibrium conditions" [2.13].

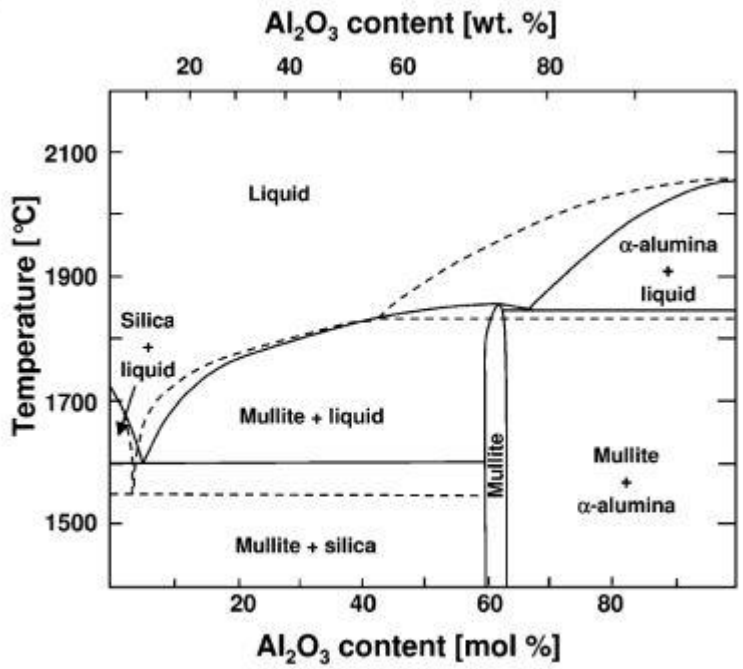

Figure 2.1 Phase Diagram by Bowen and Greig (dashed lines) [1.6] and of Aramaki and Roy (full lines) [1.11]

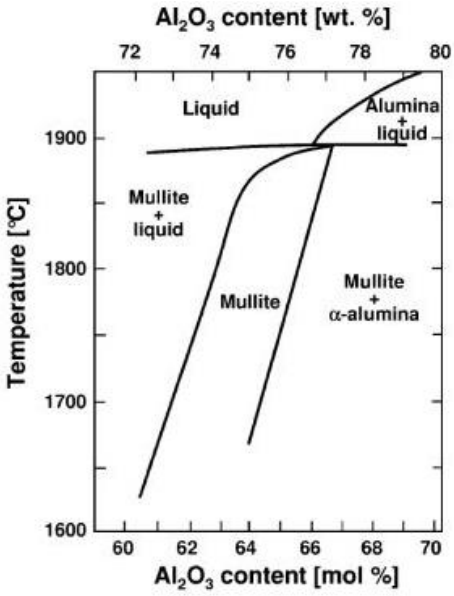

Figure 2.2 Phase Diagram by Klug [2.10]

2.2 Synthesis and properties of mullite- Effect of different raw material combination:

In the Introduction chapter, a large number of processes for mullite synthesis have been mentioned. The phase stability and phase boundaries of the synthesized mullite depended on the nature of precursors and the degree of mixing. Since mullite formation requires inter-diffusion of cations, the precursor combination resulting mixing on a finer scale is expected to yield a higher degree of stoichiometric mullite. In view of this, the list of precursors has been divided into six classes [2.14]:

(a) A mixture of oxides, hydroxides, salts and clays minerals [2.15-2.16]

(b) A mixture of sols [2.17]

(c) A mixture of sols and salts [2.18]

(d) A mixture of Si-alkoxide and Al-salt [2.19]

(e) A mixture of Al-alkoxide and Si-alkoxide, and [2.20]

(f) A mixture of other materials. [2.21-1.20]

A naturally occurring aluminosilicate (clay, sillimanite), as well as sol-gel method involving liquid precursors, provides more intimate and molecular level mixing. On the other hand, the solid oxide or colloidal particles provide nanometer or micrometer level. This difference in mixing will result in a difference in stoichiometry and properties of synthesized mullite.

Table 2.1 provides a summary of the more popularly used raw material combinations/precursors and the processing used for mullite preparation.

Table 2.1 Method of Processing Depending on Starting Raw Materials

Starting raw materials/Precursors	Method of processing	Mullitization Temperature
Clays minerals, oxides of Al_2O_3 and silica salt of Al and Si salts, Al-hydroxides and fume silica [2.15-2.16]	Conventional processing method	1600 -1700^oC
A mixture of sols [2.17]	Sol-gel method	1200 - 1300^oC
A mixture of sols and salts [2.18]	Sol-gel method	1200 - 1300^oC
A mixture of Si-alkoxide and Al-salt [2.19]	Precipitation method	1150^oC
A mixture of Al-alkoxide and Si-alkoxide [2.20]	Hydrolysis Method	1300^oC
A mixture of other materials [2.21-1.20]	Spray Pyrolysis, Chemical Vapor Deposition (CVD)	1500^oC

The mullite formation temperature is also affected by nature and the structure of the precursor phase. Depending on the precursor, there are two different variations of mullite precursors [2.22]:

(a) **Monophasic Mullite Precursor**: Direct mullitization from the amorphous precursors at a low temperature (~950^oC).

(b) **Diphasic Mullite precursor**: In this case, Mullitization takes place only above 1200^oC through the transient intermediate phases of spinel-type alumina with silica

While the first variety is called the low temperature synthesized mullite, the second one is called the high temperature synthesized of mullite. Single phase mullite is obtained using either of the two precursors.

Fig 2.3 shows the densification behavior of mullite samples prepared by different precursors viz. Colloidal mixing of α-alumina and kaolinite (conventional) [2.23], colloidal consolidation of composite powders, a diphasic sol-gel route and CVD-processed powders [1.20]. It is observed that the mullite processed from the conventional route has slow densification route. The mullite prepared through composite particles and the sol-gel route densifies faster. The densification rate of CVD mullite is slow. This is due to the different densification rate of films in contrast to the bulk powders. Viscous deformation of the

amorphous silica-rich matrix permits low-temperature sintering of sol-gel and composite-processed powder systems.

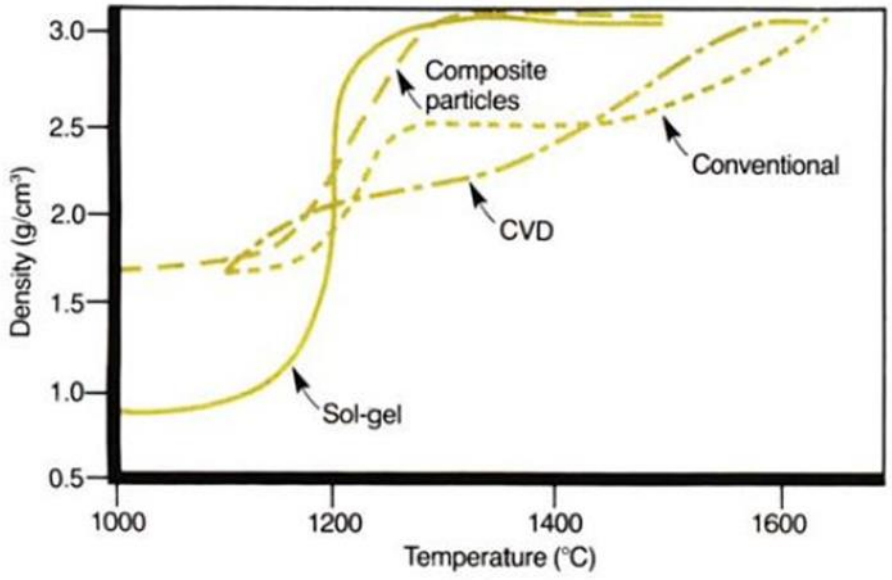

Figure 2.3 Densification Behavior of Mullite based on processing routes [2.24]

2.2.1Preparation of mullite-based ceramics using natural raw materials:

Traditionally, natural raw materials like alumino-silicate minerals were used for mullite preparation. These natural resources have molecular level mixing of Al_2O_3 and SiO_2. Hence, it was best suited for mullite preparation. Some of the commercially used natural alumino-silicate minerals are clay minerals (kaolinite, illite, halloysite), alumino hydro silicate and non-clay alumino silicate (sillimanite, andalusite and kyanite). Besides these, pure alumina and refractory grade Bauxite have also been used with different silica source (e.g. colloidal silica, fume silica) to synthesize mullite [2.25].

Gaida Sedmale et.al [2.15] prepared mullite ceramics from illite clay and aluminium hydroxide. Different weight fractions of illite clay and aluminium hydroxide were used. The mixture was sintered at different temperatures between 1200^{o}C to 1500^{o}C. The XRD analysis showed that mullite, quartz and corundum phases were present at 1100^{o}C. With the increase in the sintering temperature to 1500^{o}C, the fraction of mullite phase increased. The maximum compressive strength of 32MPa was observed for 50wt. % illite clay sintered at 1300^{o}C. With further increase in sintering temperature, the compressive strength decreased, probably, due to the liquid phase formation.

Abdulmula Ali Albhilil et.al [2.26] prepared cordierite-mullite ceramics through solid state route using natural kaolin, quartz and magnesite as the starting materials. The powder

mixture was sintered at different temperatures between 1250 to 1500^{o}C. The XRD analysis showed that with the increase in sintering temperature, cordierite fraction increased while the quartz was converted to cristobalite. The mullite peak was observed at 1250^{o}C.

V. Viswabaskaran et.al [2.27] prepared mullite using three different types of clay; Neyveli (36.11 % of Al_2O_3), Panruti (33.07% of Al_2O_3) and Udayarpalayam (52.09 % SiO_2). Three different alumina sources such as reactive alumina, gibbsite and boehmite were used. The as received clay was calcined at 1400^{o}C and mixed with different alumina sources. The mixture was sintered at 1600^{o}C. It was observed that the sample prepared from Panruti clay and boehmite exhibited the highest porosity (6.33 %) and that of Udayarpalayam clay and gibbsite showed the highest bulk density of 2.83g/cc. The samples prepared from Neyveli clay and Reactive alumina exhibited a maximum strength of 135 MPa. During heating, α-alumina reacted with the liquid silicate to form a large volume of liquid at 1500^{o}C. The liquid formation was very rapid at 1600^{o}C. Complete mullitization took place at 1600^{o}C. The vacancies were not completely removed in the mullite obtained from green clay–reactive alumina batch. The presence of residual vacancies reduced the density and flexural strength.

N.S.Raut et.al [2.28] prepared mullite ceramics from bauxite and clay mixture. They studied the effect of varying fraction of bauxite addition (wt.%) on the densification behavior and the mullitization reaction. It was observed that bauxite helped in the densification and the maximum densification was observed at 50wt% of bauxite addition when fired at 1500^{o}C. The higher densification at 50wt.% bauxite was due to the sintering aid effect of Fe_2O_3 present in bauxite. At low bauxite content, Fe_2O_3 was dissolving in mullite lattice, but at higher bauxite content, Fe_2O_3 was reacting with Al_2O_3 and improving densification. A glassy phase in bauxite helped alumina and cristobalite dissolution and re-precipitation as secondary mullite.

Ibram Ganesh et.al [2.29] prepared mullite aggregates from beach sand sillimanite and aluminum hydroxide. The mullite aggregates were prepared by both single and double stage firing process. It was observed that the mullite aggregates prepared by two-stage firing process had a high fraction of mullite, and high bulk density could be achieved at a lower temperature (1550^{o}C). In single firing stage, the process of mullitization (involving expansion) and densification (involving shrinkage) occur simultaneously. The two contrasting process retard the densification process, and higher temperature (1725^{o}C) was necessary to complete the densification.

2.2.2 Preparation of mullite-based ceramics using synthetic materials:

The processing of mullite from synthetic materials include different processing methods such as Sol-gel method, Precipitation method, Hydrolysis method, Spray Pyrolysis and Chemical Vapor Deposition (CVD) method [1.19]. In all these processing routes, either a chemically processed extra pure raw material or salt or alkoxides or sol is used. As all the precursors are pure, and the mixing is in the molecular level, these synthetic precursors are expected to yield single-phase mullite at a relatively lower processing temperature. The following paragraphs discuss the available literature for mullite processing through the above methods.

2.2.2.1 Sol-gel method

Yabin Zhang et.al [2.30] synthesized mullite fibers using the sol-gel method. The precursors were Aluminum Nitrate, TEOS. The samples were compacted and sintered at 1200^{o}C. The XRD analysis showed that Al-Si spinel formed before complete mullitization. The complete mullitization occurred at 1200^{o}C. The fibers showed a rough surface and lateral cracks when sintered at 800^{o}C.

Yabin Zhang et.al [2.17] synthesized mullite fibers via sol-gel method using aluminum chloride, aluminum isopropoxide and TEOS. The complete mullitization took place at 1200^{o}C. At a faster heating rate (10^{o}C/min), the fibers were cracked but had a uniform diameter and smooth surface without any defects when the samples were sintered at 5^{o}C/min.

S. Sundaresan et.al [2.18] studied the effect of sol-gel precursor homogeneity on the mullite formation. The mullite was prepared using TEOS and either aluminum isopropoxide or boehmite. The impact of homogeneity of sol-gel precursors on the mullite formation was studied. Some structural and thermodynamic characterizations were also carried out. It was observed that the homogeneous gels crystallize to mullite at 980^{o}C, but gels with segregated silica and alumina phases crystallize above 1250^{o}C. It was noted that better was the homogeneity of Al-Si mixing at 900^{o}C, the higher is the degree of crystallization and lower is the mullitization temperature. The crystallization and growth of mullite occurred on increasing the sintering temperature from 950^{o}C to 1400^{o}C.

2.2.2.2 Co-Precipitation method

J. S. Lee et.al [2.19] prepared mullite by co-precipitation method using an aqueous solution of $Al(NO_3)_3$, colloidal silica and NH_4OH. The precipitated powder was calcined at different temperatures (1200^{o}C, 1250^{o}C, 1400^{o}C , 1650^{o}C). The phase transition to mullite and the associated microstructural changes were studied in the calcined powder. It was observed that the fraction of mullite phase increased with the increase in calcination temperature. Mullite as high alumina mullite (73.9% Al_2O_3) took place but with the increase in calcination

temperature to 1650°C, the mullite composition shifted to stoichiometric mullite (71.8% Al_2O_3). When the Al_2O_3 content of the mullite was <74%, prismatic, elongated mullite grains were observed. However, mullite samples with Al_2O_3 content 75.5wt% were the granular type.

Minghua Zhou et.al [2.31] prepared mullite-alumina composite containing 10vol.% of excess alumina over and above the stoichiometric mullite composition. The composite was sintered at 1600°C by both pressureless and pressure-assisted sintering. The presence of excess alumina reduced the vitreous phase. In the low-temperature zone (1400°C), the densification was due to the combined effect of the plastic flow of the small mullite grains by dislocation movement and the viscous flow of a vitreous grain boundary phase. In the high-temperature regime (1600°C), the densification occurred due to the combined effect of lattice diffusion and grain boundary diffusion. In case of pressure assisted sintering, the densification happened due to particle rearrangement and viscous flow.

2.2.2.3 Spray Pyrolysis Method

Daniel M. Dabbs et.al [2.21] synthesized mullite from Aluminum Nitrate Nonahydrate and Tetraethoxysilane (TEOS) and sintered at 1400°C. 3/2 nano-mullite was found to precipitate in a 2/1 mullite matrix. The transformation of 2:1 mullite to 3:2 mullite occurred with the exolution of α-Al_2O_3. The presence of a highly coherent interface and ordered matrix indicate that the phase transformation could produce a matrix similar to dispersion strengthened the matrix. Such a matrix is expected to have high mechanical properties.

2.2.2.4 Hydrolysis Method

Katsumi Yoshida et.al [2.20] synthesized mullite through hydrolysis method. The precursors were Al-isopropoxide and TEOS. The as received mixture was amorphous containing Si-O-Al chain. Mullite formed between 1000-1300°C. Although this method could produce single phase mullite at a low temperature, the disadvantages of the process was the high cost of the precursor, low yield and tedious processing steps.

2.2.3 Processing of mullite from fly ash:

Flyash is an industrial waste containing SiO_2 and Al_2O_3. Typically most of the Indian flyash are high silica flyash with SiO_2 content varying from 30-63% [2.32]. Flyash have traditionally been used for common brick making, floor tiles, in cement and concrete. Flyash is also useful in castable manufacturing as well for the processing of some specialized structural ceramics (SiAlON).

In the use of flyash for mullite processing, different raw materials have been used with flyash for mullite formation. The choice of raw materials depended on the flyash composition i.e. whether it was high alumina flyash or high silica flyash. Accordingly, the flyash was used with Bauxite, $Al(OH)_3$, china clay, silica sol, Al_2O_3 powder etc. These different combinations of raw materials resulted in different mullite percentage with different morphology and density. The other factor that affected the mullite fraction considerably was the presence of impurities. The major impurities that have been observed in flyash are Fe_2O_3, TiO_2 and CaO, Na_2O/K_2O. The third factor that affected the mullitization reaction was the use of additives that acted as a sintering aid for higher densification and also helped in getting acicular mullite grains. Accordingly, the literature on mullite processing from flyash will be discussed in three subsections:

(i) Mullite processing using flyash as a raw material.

(ii) Effect of flyash impurities on mullite formation.

(iii) Effect of sintering aid on the densification of mullite using flyash.

2.2.3.1 Mullite Processing using Flyash as a raw material:

Three different kind of studies have been observed with flyash as a raw material for mullite processing. They are

(a) The study of mullite formation in coal ash only (without any other raw material) with or without an additive.

(b) Mullite formation in flyash and alumina, or alumino-silicate source (bauxite, $Al(OH)_3$, Al_2O_3, clay) and

(c) Mullite formation in flyash and a silica source (silica sol).

The available literature on the above three combinations (a, b, c) have been discussed in the following paragraphs.

2.2.3.1.1 Mullite formation in coal ash only

Guo et.al [2.33] prepared mullite ceramics from flyash and de-silicated flyash. The as received flyash had mullite and quartz (57%) as the crystalline phase and a glassy silicate phase. Sintering the flyash in the temperature range 1300^{o}C to 1600^{o}C resulted in the lowering of mullite content with corresponding increase in the glassy phase. The increase in the glassy phase was due to the amorphous silica present. It appears that the glassy phases have also partially dissolved the mullite phase. In contrast, the de-silicated flyash were found to strong mullite peaks in the sintered flyash samples. The authors concluded that the de-silicated flyash was a better candidate for mullite processing.

Parveen Sultana et.al [1.40] studied the flyash particle size effect on the mullite and glassy phase. The authors used different flyash particle size (50mesh to 250 mesh) and observed the mullite formation rate. It was observed that a finer flyash particle increased the mullite fraction to 15% at 1600^{o}C. It was concluded that the finer flyash was more conducive for mullite formation.

Guo [2.33] also observed that impurities present in flyash (Fe_2O_3) helped in the liquid phase formation and ultimately enhanced the mullite formation. The liquid phase also changed to mullite particle morphology to an acicular one.

Parveen Sultana et.al [2.34] observed the effect of MgO content on the mullite formation reaction rate. 1-5 wt% MgO was added to flyash. It was observed that the addition of MgO increased the extent of mullite formation and also increased the size of the mullite grains. It was concluded that MgO addition accelerated the reaction between Al_2O_3 and SiO_2 due to a possible decrease in the viscosity of the MgO added glassy phase.

2.2.3.1.2 Mullite ceramics using coal ash and another raw materials:

Researchers who have tried to maximize mullite phase content or to make a mullite based ceramics have used flyash in combination with another raw material. Depending on the chemical composition of bauxite, this other raw material was either an alumina source or a silica source. The following paragraphs briefly discuss the processing of mullite using flyash along with an Al_2O_3 or silica source.

Jung et al [1.39] prepared stoichiometric mullite ceramics using a silica rich coal flyash and Al_2O_3 powder. The investigators had also used 3Y-PSZ powder in some selected compositions. Reaction sintering was done till 1600^{o}C. The mullite phase started appearing at 1300^{o}C with an associated decrease in cristobalite and α- Al_2O_3 phases. It was observed that mullitization was complete at 1400^{o}C and sintering at higher temperature only increased the bulk density. Beyond 1500^{o}C, mostly elongated mullite grains were observed. The addition of 3Y-PSZ inhibited the grain growth rate of mullite and enhanced densification.

Kumar et.al [2.35] prepared mullite aggregates by reaction sintering of beneficiated flyash and calcined alumina at 1600^{o}C. The beneficiated flyash had lower Fe_2O_3 (1.9%) content in comparision to the as received flyash (4.7%). It was observed that the prepared aggregate consisted of a dense network of mullite and corundum crystals.

Park et al [2.36] prepared mullite whiskers by reacting coal flyash with Ammonium Aluminium Sulphates Hydrate ($NH_4Al(SO_4)_2.12H_2O$) and sodium dihydrogen phosphate ($NaH_2PO_4.2H_2O$). Al_2O_3/SiO_2 ratio of the mixed batch was 0.32. It was observed that with

the optimized amount of $(NH_4)Al(SO_4)_2.12H_2O$, mullite whiskers could be prepared at 1300°C. The presence of a liquid phase allowed Al_2O_3-deficient mullite grains to crystallize out. The presence of the liquid also permitted to shape change to an elongated one. The liquid content could be related to the presence of large percentage (5.96%) of Fe_2O_3 in the flyash precursor.

Dong et al [2.37] used $Al(OH)_3$ coated flyash for porous mullite ceramics preparation. Mullitization was carried out by reaction sintering at different temperatures between 1000 to 1500°C. It was observed that when flyash was coated with 33.3 wt% Al_2O_3, the mullitization reaction intiated at 1250°C and the reaction was completed at 1400°C. High Al_2O_3 containing flyash samples had more equiaxed mullite grains. The use of $Al(OH)_3$ also contributed to the porosity development by reducing the shrinkage during densification. The addition of $Al(OH)_3$ also widened the densification temperature range without excessive liquid formation.

Suriyanarayanan et al [1.37] used high temperature arc plasma to prepare mullite based glass ceramics using coal flyash and alumina. The results showed that single phase mullite formed when the flyash: alumina was 1:1. At high temperature, the mullite were needle shaped in the glass ceramics matrix. The high temperature plasma helped to obtain single phase mullite only in 5 minutes.

Li et al [2.38] studied the in-situ synthesis of mullite using flyash and two different sources of Al_2O_3 viz $Al(OH)_3$ and Al_2O_3. Additionally, AlF_3 was used as an additive. The use of AlF_3 helped mullite whisker preparation at a low temperature of 1400°C. It was also observed that among the two Al_2O_3 sources, $Al(OH)_3$ was more suitable for mullite whisker preparation. The presence of mullite crystals helped to increase the fracture strength to 100MPa.

Lee et al [2,39] prepared porous mullite using coal flyash and an appropriate amount of Al_2O_3. The Al_2O_3/SiO_2 ratio of the starting mixture was 1.8. However, inspite of a higher ratio α-Al_2O_3 was not detected. This indicated that the glassy silicate present in flyash reacted with Al_2O_3 to produce mullite.

Kim et al [2.40] fabricated porous mullite- alumina composites from a mixture of coal flyash and Al_2O_3. The presence of high silica and impurities resulted in a glassy phase at a low temperature. The liquid helped in the growth of rod-shaped mullite between 1300-1500°C. It was concluded that the alkalies present in the flyash had a role in low temperature glassy phase formation.

Sanjay Kumar et.al [2.41] developed mullite-corundum composites from fly ash and calcined alumina by reaction sintering at 1600°C. The major phases were corundum and mullite. The

inter-diffusion of Si^{4+} and Al^{3+} lead to the growth of mullite crystals. A glassy phase was also formed due to the reaction between Al_2O_3 and SiO_2. The primary mullite was produced from the fly ash whereas the reaction between SiO_2 of fly ash and Al_2O_3 in the bauxite resulted in secondary mullite. Randomly oriented and interlocked mullite grains resulted in a dense microstructure. It was concluded that mullite crystallizing out of an intergranular glassy phase exhibited acicular or elongated morphology. Although no improvement in strength was observed, the fracture toughness increased to 3.58MPa $m^{1/2}$.

2.2.3.1.3 Processing of mullite ceramics using flyash and bauxite:

Dong et al [1.36] prepared low cost mullite ceramics from flyash and bauxite. The batch of flyash and bauxite were mixed in the ratio 45.87:100 in order to produce 3:2 mullite. Primary mullite and cristobalite was formed at 1100^{o}C. At 1300^{o}C, cristobalite and alumina reacted to form secondary mullite. Above 1400^{o}C, mullite and corundum were the major phases and Al_2TiO_5 was the minor phase. The densification proceeded via liquid phase sintering.

Li et al [2.42] studied mullite formation using bauxite and flyash and also studied the effect of V_2O_5 addition on the mullitization reaction. The composition under had 30% bauxite and 70% flyash. Addition of V_2O_5 has accelerated liquid phase sintering. The multivalent V^{3+}/V^{5+} ion also causes an increase in the lattice parameter. At 1500^{o}C, V_2O_5 added mullite had cuboidal mullite.

Dong et al [2.43] prepared bulk porous mullite membrane by reaction sintering of flyash and bauxite. It was observed that during sintering, the samples initially shrunk followed by expansion between 1326 and 1477^{o}C. The expansion was related to the secondary mullitization. The shrinkage above 1477^{o}C was ascribed to the densification of secondary mullite. The increase in bending strength of the membrane with increase in sintering temperature was attribute to the growth of mullite grains.

Dong et al [2.44] prepared mullite ceramics from bauxite and flyash mixture. TiO_2 was added to alter the sintering behaviour. It was observed that TiO_2 inhibited the densification at lower temperatures due to the formation of Al_2TiO_5. However, the completion of final densification occurred at a lower temperature. This was caused by the presence of TiO_2 rich glassy phase in the SiO_2-Al_2O_3-TiO_2 system. Only mullite was present above 1450^{o}C. The flexural strength increased with TiO_2 content and reached the peak value of 35MPa at 6wt% TiO_2 addition.

Dong et al [2.45] studied the sintering of flyash-bauxite mullite ceramics with MgO addition. The mullite ceramics were densified between 1500-1550^{o}C. MgO addition was observed to

promote sintering markedly above 1450^{o}C. In the presence of MgO, the mullite had long elongated morphology with interlocking structure. This microstructure helped to increase the mechanical strength. Moreover, the addition of MgO slightly decreased the thermal expansion coefficient at 1300^{o}C due to cordierite formation. However, above 1400^{o}C, cordierite decomposed to corundum and spinel, thereby increasing the thermal expansion coefficient.

2.2.3.1.4 Effect of Additives on the sintering Behaviour of Bauxite and Mullite:

Xiang Chong et al [2.46] studied the sintering behaviour of Chinese bauxite. The Chinese bauxite was of diaspora-kaolinite type. It was observed that the sintering behaviour of bauxite was dependent on the Al_2O_3 content. The closer was the percentage of Al_2O_3 to the mullite, the more difficult was to sinter the bauxite. It was also observed when the Al_2O_3/SiO_2 ratio was less than 2.55, the glassy phase was 10-12%. The presence of 3-5% impurities resulted in 43-57% of secondary mullite at 1600-1700^{o}C.

Tripathi et al [2.47] studied the effect of TiO_2 on the synthesis and mechanical properties of mullite prepared from Beach Sand Sillimanite and Calcined Alumina mixture. TiO_2 (upto 6 wt%) was used as an additive. The densification of the mixture was controlled by Al_2O_3/SiO_2 ratio. Upto 4 wt.% TiO_2 promoted the densification behaviour of the composite and at 1550^{o}C, a near zero porosity compact was produced. The TiO_2 entered the mullite lattice and the produced mullite was 1:1 type.

Montanaro et al [2.48] studied the sintering of Industrial mullite with MgO addition. Upto 3 wt% MgO was added to act as a sintering aid. The authors observed that the MgO addition promoted liquid phase sintering of mullite. The sintered samples contained mullite, corundum and $MgAl_2O_4$ as the crystalline phases. The liquid phase promoted mullite dissolution and induced mullite grain growth.

Jayaseelam et al [2.49] studied the Pulsed Electric Current Sintering of industrial mullite at 1500^{o}C. The sintering study was carried out using two additives, viz. 0.5 wt.% SrO and 0.2 wt.% MgO. It was observed that while the MgO added mullite grains had equiaxed morphology, the SrO added mullite had a mixed (equiaxed and anisotropic) grain morphology. The different grain morphology affected the fracture behaviour of mullite differently.

Y.Dong et al [2.50] studied the sintering behaviour of coarse industrial grade mullite and mullite-corundum powder. A mixture of kaolin and basic carbonate magnesium was used as the sintering additive. The use of the additive, especially the MgO resulted α-cordierite at

1200-1400°C in the mullite-corundum matrix. Above 1400°C, α-cordierite decomposed into mullite and a glassy phase. The densification improved because of the liquid phase produced from kaolinite-MgO addition.

Tripathi et al [2.16] studied the microstructure and properties of sintered bauxite based mullite. The mullite was prepared from two different bauxite source using one silica sol. The authors observed that the mullite grain morphology was dependent on the impurity level. A lower impurity containing bauxite had more equiaxed mullite grains. On the other hand, mullite developed from higher impurity bauxite (particularly CaO impurity) were needle shaped. It was also observed that TiO_2 and Fe_2O_3 impurities enter the mullite lattice and produce less glassy phase. On the other hand, CaO produced large liquid phase and degraded mullite properties.

J. Roy et.al [2.51] prepared mullite from the Al_2O_3-SiO_2 diphasic gel using CoO as a sintering additive. The samples were sintered between 1400-1600°C. It was observed that the addition of CoO promoted the mullite formation by the interaction between Al_2O_3 and SiO_2 via the intermediate formation of cobalt silicate and cobalt aluminate. The crystallite size of mullite was also modified by the addition of CoO. It was also observed that the density and flexural strength were improved by 10%, and the fracture toughness was improved by 5%.

V. Viswabaskaran et.al [1.32] prepared mullite from clay and reactive alumina and used magnesia and yttria as a sintering additive. The samples were sintered between 1500, 1550 and 1600°C for 3h. The addition of Y_2O_3 helped in the liquid formation at low temperature and also favored the formation of equiaxed mullite and MgO improved the density and flexural strength. The addition of boehmite increased the size distribution of mullite grains.

Saikat Maitra et.al [1.33] prepared mullite from aluminosilicate diphasic gel and sintered the samples between 1400-1600°C. TiO_2 and V_2O_5 were used as the sintering additives. It was observed that the addition of these additives enhanced the mullitization and improved the mechanical properties.

L.B. Kong et.al [1.34] studied the effect of Nb_2O_5, Ta_2O_5 and V_2O_5 on the phase transformation and microstructural changes of mullite. It was found that V_2O_5 enhanced the liquid phase formation of SiO_2. As a result, the mullitization temperature lowered and helped in anisotropic grain growth, which resulted in low density. It was also observed that equiaxed grains were grown from samples doped with Nb_2O_5 and Ta_2O_5. Samples doped with Nb_2O_5 and Ta_2O_5 is having a higher density than the theoretical density that is due to high density of Nb_2O_5 and Ta_2O_5.

CHAPTER-3

OBJECTIVE OF THE WORK

3. Objective of the work:

The literature review on the processing of mullite ceramics from flyash revealed that some work has been carried out to prepare mullite from flyash. However, in order to overcome the inherent weakness of flyash (i.e. high impurity content), many studies have utilized a rather pure source of Al_2O_3 namely, $Al(OH)_3$, calcined alumina etc. Some researchers have also worked on beneficiated flyash. Very few studies have been made on the as received flyash and as received bauxite combination. Secondly, most of the studies on the bauxite-flyash combination have concentrated on the maximization of mullite phase. No study has been made with the different bauxite-flyash ratio. Thus, this study aims to study the mullite formation with different bauxite-flyash ratio. The composition range will be chosen between excess bauxite to excess flyash range. Such a wide composition range is expected to give a varying microstructure as well as varying mullite grain morphology. Therefore, the objective of the study can be summarized as follows:

a) Use of bauxite and flyash in different proportions to prepare mullite based ceramics through solid state route. The composition range chosen will be from alumina excess mullite composition to silica excess mullite composition.

   Since two different varieties of bauxite will be used having the different Al_2O_3/SiO_2 ratio, it will be worthwhile to study the effect of precursor type on the mullitization reactions.

b) Four different weight percentage of FA (30, 40, 50 and 70 %) will be used with bauxite.

   As mentioned earlier, the composition range was chosen so as to study the high alumina batch to high silica batch on the mullite phase formation. Accordingly, bauxite: Fly Ash ratio was varied.

c) The effect of two different bauxites (B1 and B2) on the mullite phase formation and densification will be studied.

   Besides having different silica amount, the minor amount impurities (CaO, MgO) are different in B1 and B2. It is reported in the literature that minor amount of CaO and MgO also affect the densification and phase. Thus, the effects of two bauxites on the densification will be studied

d) The effect of the single stage and two stage reaction process on the extent of mullitization and properties will be studied.

   The effect of two-stage sintering on the mullitization behavior has been reported by many authors. Therefore, in this study, one of the bauxite – Fly Ash mixture (B1- FA)

will be subjected to pre-calcination step while the other bauxite (B2-FA) will be directly heated to the different sintering temperature in order to study the mullite formation with and without pre-calcination step

e) The prepared mullite based ceramics will be characterized for density, porosity, phase, strength, hardness, toughness, microstructure and thermal shock behaviour.

The sintered samples are expected to have the different combination of the following phases- mullite, corundum, cristobalite and glass. Since the work is on mullite based composite, the effect of these different phase combinations on the physical properties, mechanical behavior and microstructure will also be studied.

CHAPTER-4

EXPERIMENTAL WORK

In this study, the processing of mullite based ceramics was through solid state route. The raw materials were bauxite and fly ash. Two types of bauxite were used. One variety was Bauxite-1, and the other variety was Bauxite-2. The fly ash was obtained as a waste product of thermal power plant of Rourkela Steel Plant. The following sections discuss the processing and analysis of raw materials and the subsequent processing of mullite through solid state mixing of bauxite and fly ash.

4.1 Raw material sources and their analysis:

The Bauxite-1 (B1) and Bauxite-2 (B2) were obtained from Tata Krosaki Refractories Limited (TKRL) and the fly ash (FA) was obtained from Rourkela Steel Plant (RSP). The as received granular B1 was subjected to wet planetary milling for 12 hours in a silicon nitride jar using silicon nitride as grinding media and water as a medium. The ground slurry was oven dried for 24 hours. The as received fly ash was fine with a mean particle size of 301.72nm. The chemical composition, particle size analysis, XRD, DSC/TG was done on the raw materials.

4.2 Preparation of B1 and fly ash precursor powder mix:

The precursor powder mix was prepared from milled B1 and FA. The different weight fractions of B1 and FA that were used are 70:30, 60:40, 50:50 and 30:70. The powder mix was first mixed in an agate mortar followed by milling in a pot mill for 1h. The milled slurries were oven dried and were ground to a fine powder. The powders were calcined at 1250^{o}C for 2hours at a heating rate of 3^{o}C per minute. The calcined powders were wet milled for 30 min in a planetary mill using silicon nitride jar and silicon nitride grinding media. The milled slurry was oven dried. The flow diagram for the preparation of B1-FA precursor was shown in Fig.4.1

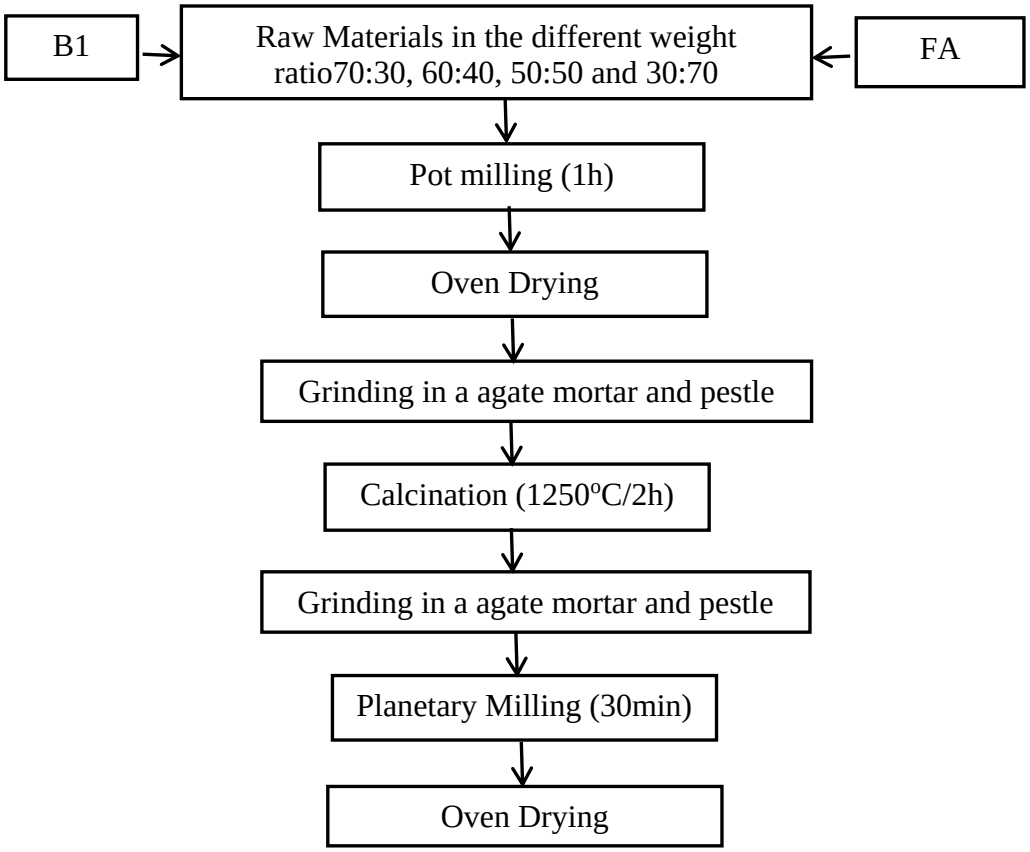

Figure 4.1 Flow chart for processing of Bauxite-1 and Fly Ash Precursor

4.3 Compaction of pellets and sintering:

As already mentioned before, two different batches of bauxite and fly ash mixture were prepared. One batch was with B1+FA, and the other batch was B2+FA. For both the batches, the identical weight ratio of bauxite and fly ash i.e. 70:30, 60:40, 50:50 and 30:70 were used. 5 weight% of PVA was added to the dried powder, and the powders were wet mixed thoroughly in an agate mortar pestle. Both the powders (i.e. the calcined B1+FA mixture and the uncalcined B2+FA mixture) were compacted to cylindrical pellets (25 mmϕ) in a hydraulic press (Model 3887, Carver Inc. USA) at a 165MPa. The green pellets were sintered at different temperatures i.e. 1400^{o}C, 1450^{o}C and 1500^{o}C for 2 hours at a heating rate of 2^{o}C per minute with a hold time of 1h at 650^{o}C. In the case of B2 + FA samples, an additional hold of 2h was provided at 1250^{o}C to compensate for the calcination process. The sintered pellets were subjected to different characterizations such as dilatometry, XRD, bulk density, apparent porosity, microstructure, strength, toughness and hardness. The following flow chart describes the compaction and sintering of bauxite + flyash powder mixture. The processing steps were identical for both the types of powder mixes i.e. B1+FA and B2+FA as shown in Fig.4.2

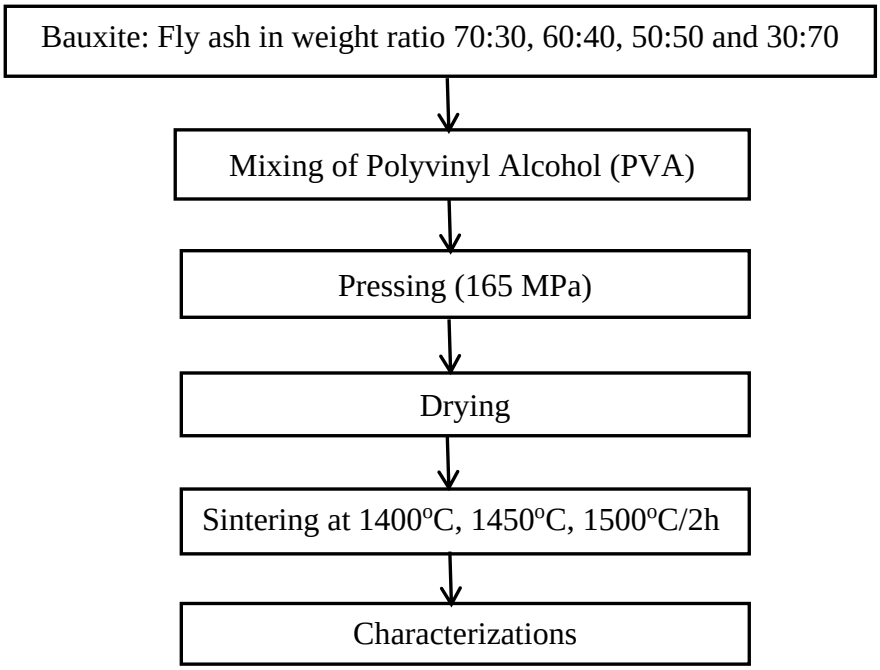

Figure 4.2 Flow chart for Compaction and Sintering of pellets

4.4 Characterizations:

The initial raw materials (B1, B2 and FA) were characterized for Particle Size, DSC/TG, Dilatometer and XRD whereas the sintered samples were characterized for Dilatometry, XRD, Bulk Density, Apparent Porosity, Microstructure, Strength, Toughness and Hardness.

4.4.1 Particle size analysis:

The particle size distribution was determined by Laser diffraction method. A He-Ne laser (633 nm) was used as the laser source. It was based on Mie-scattering theory. The powders were ultrasonically dispersed in water medium using an ultrasonic vibrator (Oscar, Sonopros PR-1000MP). The particle size analysis was carried out in computer controlled particle size analyzer [ZETA Sizers Nanoseries (Malvern Instruments Nano ZS)]. The medium particle size (D_{50}) of the samples were determined on the basis of the particle size - frequency curve

4.4.2 DSC/TG:

The decomposition and crystallization behaviour of FA was studied by simultaneous DSC/TG instrument [Netzsch STA (Model No 409C)] in an argon atmosphere at a heating rate of 5°C/ minute using α-Al_2O_3 as the reference material.

4.4.3 Densification Behaviour:

The densification behavior of bauxite-flyash mixtures were studied by the dilatometer (NETZSCH DL 402C) in a non-isothermal constant rate heating (CRH) mode. Rectangular

bar samples of length 15mm and width 5mm were used for the study. In the CRH mode, the green rectangular bars of the mixture samples were heated till 1400^{o}C at a heating rate of 10^{o}/min in an argon atmosphere. The study provided the information on the shrinkage due to densification and any expansion due to mullitization reaction.

4.4.4 Sintering of green compacts:

The sintering of the powder compacts was carried out in an electric furnace (Bysakh & Co) fitted with a heating element of $MoSi_2$ at a heating rate of 2^{o}/min. A holding time of 1 hour each was provided at 650^{o}C and 1000^{o}C for the decomposition and combustion of binder and other impurities. Beyond 1000^{o}C, the samples were also heated at the same heating rate to the final sintering temperature. A holding time of 2 hours was provided at the sintering temperature for completion of reaction sintering. The samples were furnace cooled to room temperature.

4.4.5 Phase Analysis:

The phases in the starting raw materials and the sintered samples were identified from XRD pattern. The study was performed in a Rigaku Japan/Ultima-IV Diffractometer using Cu Kα (λ= 1.5418 A^{o}) radiation. The samples were scanned in the 2θ range 15-80^{o} at a scan rate of 20^{o}/min. The generator voltage and current were set at 35KV and 25mA respectively. The peaks were identified using Philips X'pert High Score Plus Software.

The sample was placed on a sample holder and was kept for scanning. The diffracted X-rays were detected by an electronic detector placed on the other side of the sample. To get the diffracted beams, the sample was rotated through different Bragg's angles. The computer controlled goniometer tracked the angle (θ), and the detector recorded the detected X-rays in units of counts/sec and sent this information to the computer. After the scanning of the samples, the diffracted X-ray intensity (counts/sec) was plotted against 2θ. The angle (2θ) for each diffraction peak was converted to d-spacing, using the Bragg's law;

$$n\lambda = 2d \sin\theta \qquad (4.1)$$

where, λ = wave length of x-ray (1.5418 A^{o})

n = order of diffraction=1

The crystallite sizes of the raw materials (B1, B2 and FA) were determined from X-ray line broadening using the Scherrer's equation [4.1] as follows:

$$t = \frac{0.9\,\lambda}{\beta\,cos\theta} \qquad (4.2)$$

4.4.6 Bulk Density and Apparent Porosity:

The bulk density and apparent porosity of the samples were measured using Archimedes' principle. The dry weight (D) of the sample was taken, and the sample was submerged in a beaker filled with kerosene. The set up was placed in a vacuum desiccator and was evacuated for 30 min. The suspended weight (S) and soaked weight (W) of the samples was taken. The bulk density and apparent porosity of the samples were calculated using the following formulae [1.36]

$$\text{Bulk Density} = \frac{D}{S-W} * \rho \qquad (4.3)$$

$$\text{Apparent porosity} = \frac{\text{S}-\text{D}}{\text{S}-\text{W}} * 100 \qquad (4.4)$$

$$\text{Relative Density} = \frac{\text{Bulk Density}}{\text{Theoretical Density}} * 100 \qquad (4.5)$$

Where, D= Dry Weight of the sample

S= Suspended Weight of the sample

W= Soaked weight of the sample

ρ = Density of kerosene, 0.81g/cc

Theoretical Density was calculated from the rule of mixture based on the phase present and multiplying the X-ray density with the volume fraction of the phase

4.4.7 Hardness, Strength and toughness:

Hardness, flexural strength and fracture toughness of the sintered samples were measured on the disk samples of 25mm diameter and 1.6mm thickness. All the surfaces of the sintered samples were polished using 600 grit SiC powder. The polished samples were cleaned in an acetone medium in an ultrasonic vibrator.

4.4.7 (a) Vickers Hardness:

The Vickers Hardness of the samples was determined by a Vickers Semi-Macro Hardness Tester (LV-700 Leco, Japan). The indentations of the polished samples were carried out at different loads (1, 3, 5, 10 Kgf) with a dwell time of 10 sec. The hardness H_v was determined from the diagonal length using the formula [4.2].

$$H_v = 0.47 * \frac{P}{d^2} \qquad (4.6)$$

Where, H_v= Hardness (GPa)

P = Load (N)

d = half of the diagonal length (μm)

The hardness was calculated from the slope of the plot of applied load vs. the square of the half diagonal length (d^2) at no crack condition

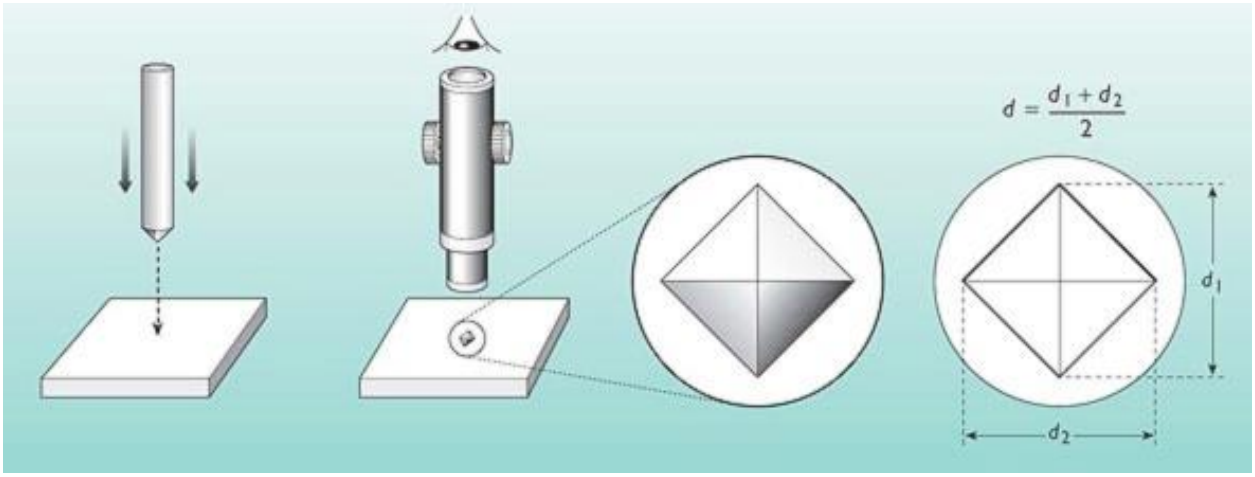

Figure 4.3 Schematic view of Vickers Hardness measurement

4.4.7 (b) Flexural Strength:

The biaxial flexural strength of the samples was determined by Ring- on- Ring bending test method (ASTM C1499) in a Materials Testing Machine (Tinius Olsen, UK) using a support ring of 16mm and loading ring of 6mm and cross head speed of 0.2mm/min. The flexural strength (σ_{fb}) of the samples was calculated from the formula [4.3].

$$\sigma_{fb} = \frac{3P_f}{2\pi t^2}\left[(1+\nu)\ln\left(\frac{D_s}{D_L}\right) + (1-\nu)\left(\frac{D_s^2 - D_L^2}{2D_v^2}\right)\right] \qquad (4.7)$$

Where, P_f= fracture load

t= disk thickness

ν= Poisson's ratio, 0.2

D_s= support ring diameter

D_L= loading ring diameter

D_v= test-specimen diameter

The equibiaxial bending method for strength measurement is an approved ASTM technique (ASTM C1499). This method is widely used for the strength measurement of dental ceramics, glass samples etc [4.4].

4.4.7 (c) Fracture Toughness:

Fracture toughness, K_{Ic} is defined as the critical stress intensity level at which a given flaw starts extending and provides insight into the potential resistance to crack growth of a material. The samples were indented using Vickers semi-macro hardness tester (LV-700 Leco, Japan) at the center of the tensile surface of the specimens at a load of 5 and 10kgf during 10s until a radial crack appeared on the sample which served as a pre-crack in this test.

The samples were then subjected to fracture toughness in Materials Testing Machine (Tinius Olsen, UK) using a support ring of 16mm and loading ring of 6mm and cross head speed of 0.2mm/min within 30min following the indentation. The fracture toughness K_{Ic} of the samples was calculated using the formula [4.5].

$$K_{Ic} = \eta(E|H)^{1/8}(\sigma_f P^{1/3})^{3/4} \quad (4.8)$$

Where η = geometrical constant (0.59)

E = Elastic modulus (GPa)

H= Vickers' hardness (GPa)

P = indentation load (N)

σ_f = Strength (MPa)

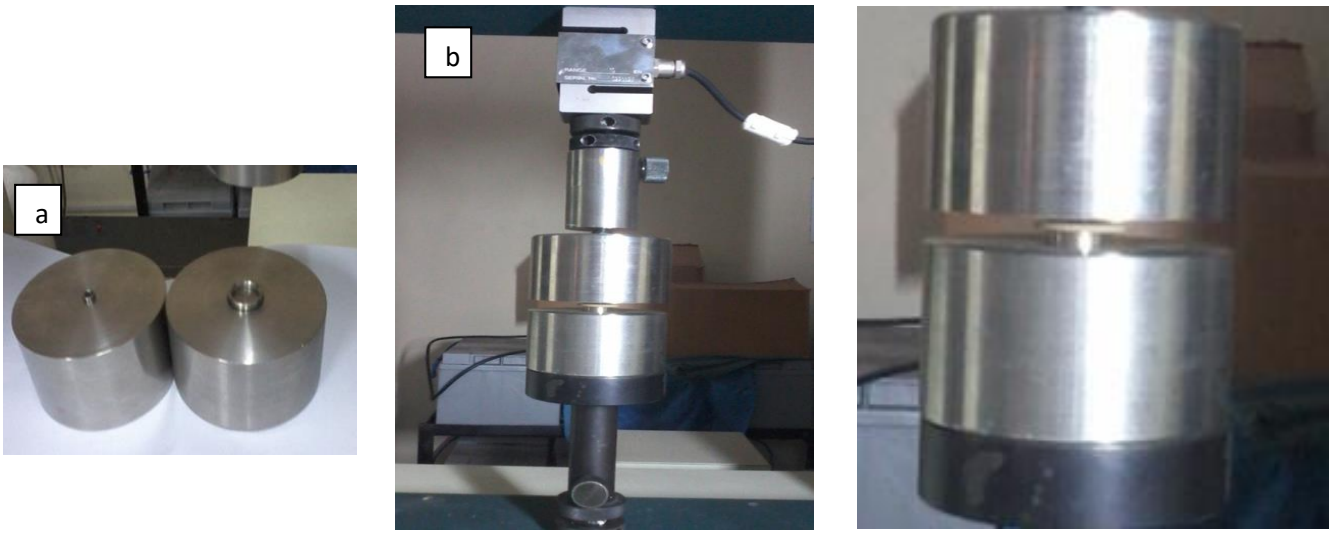

Figure 4.4 Test set up for Ring on Ring test method (a) Test Fixtures- Loading fixture on left and support fixture on right, (b) Test set up fixed with 10 KN load cell, (c) A closer view of test fixture with sample inside

4.4.8 Microstructural analysis:

For the microstructural observations, the sintered surface of the samples was polished on a glass plate using diamond paste on a glass plate. The polished samples were cleaned in acetone medium in an ultrasonic vibrator (Oscar, Sonopros PR-1000MP) and dried at 80^{o}C. The dried samples were thermally etched at 1250^{0}C for 5 minutes for microstructural study. The etched samples were gold coated in a Rotary-Pumped Sputter Coater (Quorum, Q150RES) for 4 minutes. The microstructural analysis of the gold-coated samples was carried out using a Field Emission Scanning Electron Microscope (Nova Nano SEM - 450).

4.4.9 Thermal Shock resistance:

The thermal shock resistance of the sintered samples evaluates the resistance to crack initiation or its propagation under thermal stress. To evaluate this parameter, the samples are

subjected to a thermal shock from high temperature (such as rapid cooling from high temperature to low temperature). The thermal shock resistance was studied by heating the samples up to a temperature of 1250°C with a soaking time of 1 hour and followed by rapid cooling in the air till the samples attained room temperature. The thermal shock resistance was determined by measuring Vickers Hardness. The microstructural study of the thermally shocked sample was also carried out to observe the change in the microstructure due to thermal shock.

CHAPTER-5

RESULTS & DISCUSSION

5.1 Chemical composition of the raw materials:

The chemical composition of the starting materials [Bauxite-1 (B1), Bauxite-2 (B2) and FA] was carried out by quantitative X-Ray Fluorescence (XRF) [ARL Thermofisher, Switzerland, Model:9900] spectrum analysis. The results are shown in Table 5.1. B1 has 86.6% alumina, 4.66% silica, 2.08 % ferric oxide and 3.97% titania. In B2, the content of alumina (84.62%) is less, and the content of silica is more (6.83%) compared to Bauxite-1. Some amount of ferric oxide (2.08%) and titania (3.97%) also exists in B2. FA consists of silica (62.37%) as a major phase and alumina (29.88%). In addition to ferric oxide (3.49%) and titania (1.96%), there are also small amounts of MgO, MnO, CaO, etc. Thus, it is seen from the analysis that B2 has lower alumina and higher silica content. The chemical analysis was also done by the wet chemical method that gave the similar results.

Table 5.1 Chemical Composition of Raw Materials

	Bauxite-1	**Bauxite-2**	**FA**
Al_2O_3	86.6	84.62	29.88
SiO_2	4.66	6.83	62.37
Fe_2O_3	2.08	2.46	3.49
TiO_2	3.97	3.67	1.96
MgO	0.141	0.222	0.537
MnO	0.01	0.01	0.01
CaO	0.52	0.25	0.7
Cr_2O_3	0.065	0.01	0.01
LOI	1.58	1.2	0.48

Based on the chemical composition of the raw materials, the actual Al_2O_3 and SiO_2 content present in the batch are calculated and are listed in Table 5.2 below. The excess Al_2O_3 and SiO_2 corresponds to the excess amount over and above the required for 3:2 mullite.

Table 5.2 The actual Al_2O_3 and SiO_2 content in the batch

Bauxite: Fly ash in the batch	B1-FA Batch		B2-FA Batch	
	Actual Al_2O_3 and SiO_2 in the batch		Actual Al_2O_3 and SiO_2 in the batch	
70:30	Al_2O_3 69.9 SiO_2 22	Al_2O_3 excess-13.1%	Al_2O_3 68.2 SiO_2 23.5	Al_2O_3 excess-7.8%
60:40	Al_2O_3 64 SiO_2 27.8	SiO_2 excess-2.8%	Al_2O_3 59.8 SiO_2 29.1	SiO_2 excess-5.8%
50:50	Al_2O_3 58.3 SiO_2 33.5	SiO_2 excess- 10.8%	Al_2O_3 57.3 SiO_2 34.6	SiO_2 excess-12.3%
30:70	Al_2O_3 47 SiO_2 45.1	SiO_2 excess-26.8	Al_2O_3 46.3 SiO_2 45.7	SiO_2 excess-27.7%

5.2 Phases in the as received raw materials:

The phases in the as received raw materials (B1, B2, and FA) were determined through XRD. Fig 5.1 (a, b, c) shows the XRD patterns of B1, B2 and FA respectively. The XRD pattern of

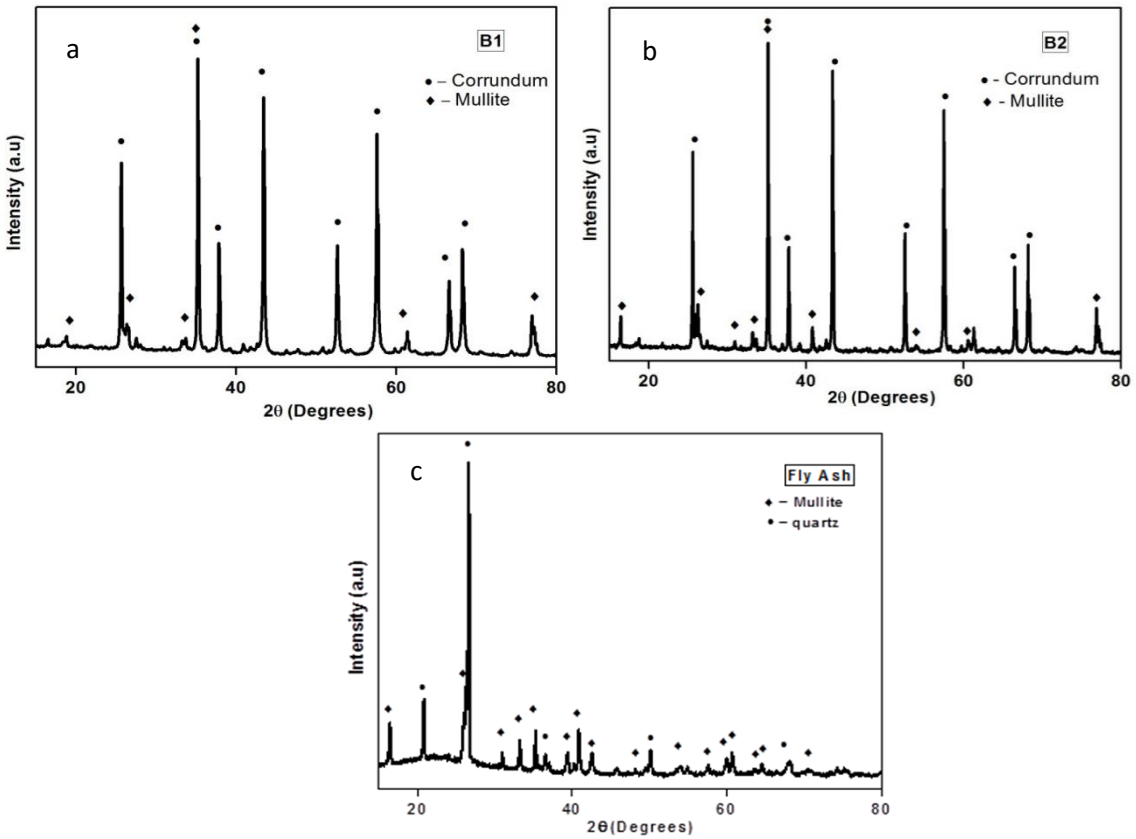

Figure 5. 1 XRD pattern of a) Bauxite -1 b) Bauxite - 2 c) Flyash

B1 and B2 contain corundum as a major phase, and some mullite peaks are also observed. The mullite phase appears on the calcination of the clay based impurity. The FA pattern shows that silica is the major phase, and some mullite is also observed in the sample. The appearance of mullite is due to the high-temperature reaction of silica and alumina during the burning of coal. A broad hump in the XRD pattern between $2\theta = 20^{o}$-30^{o} indicate that the FA also contains residual glassy phases. The glassy phase appears due to the melting of silica based impurity and the subsequent quenching of coal ash.

5.3 Thermal Decomposition behaviour of raw materials:

Fig 5.2 shows DSC/TG pattern of FA. The pattern shows a weight loss till about 1200^{o}C (occurring in 2 stages) and a broad exothermic peak between 600^{o}C and 1200^{o}C. The weight loss and exothermic peak in the DSC/TG curve are due to the combustion of volatile matters, carbon residues, impurities present in FA

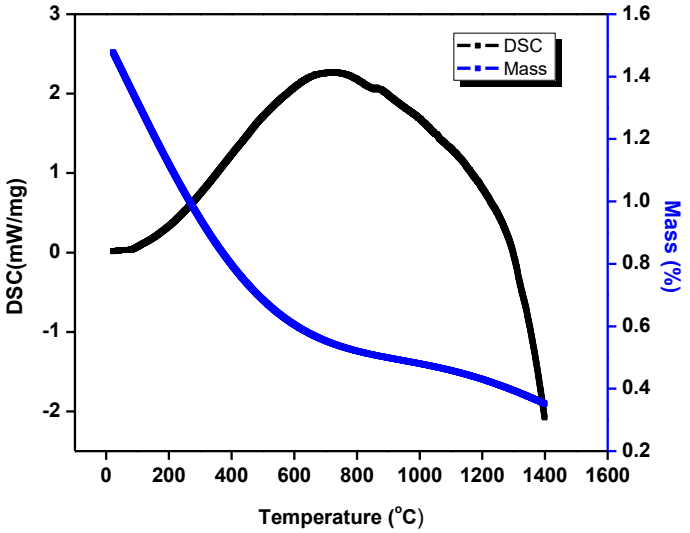

Figure 5. 2 DSC/TG of Fly ash

5.4 Particle Size of the raw materials:

Fig 5.3 a, b, c shows the particle size distribution of the starting materials i.e. B1, B2 and FA. The particle size of B1 and FA shows a monomodal type of distribution. B2 shows a bimodal type of distribution. FA shows a narrow particle size distribution with 96 vol.% of the particles lying in the range 255-342nm. The mean particle size calculated to be 301.72nm. B1 and B2 shows a broad particle size of distribution with 93 vol.% of the particles in the range 295-615nm and 92.8 vol.% of the particles in the range 396-955 nm respectively. The mean particle size of B1 and B2 calculated are to be 461.5 and 506.28 nm respectively. However, it is to be noted that the particle size calculated here essentially represents the agglomerate size

of the powder in the suspension. The actual particle size is expected to be smaller. A better idea on the reactivity of the powders can be obtained from the crystallite size.

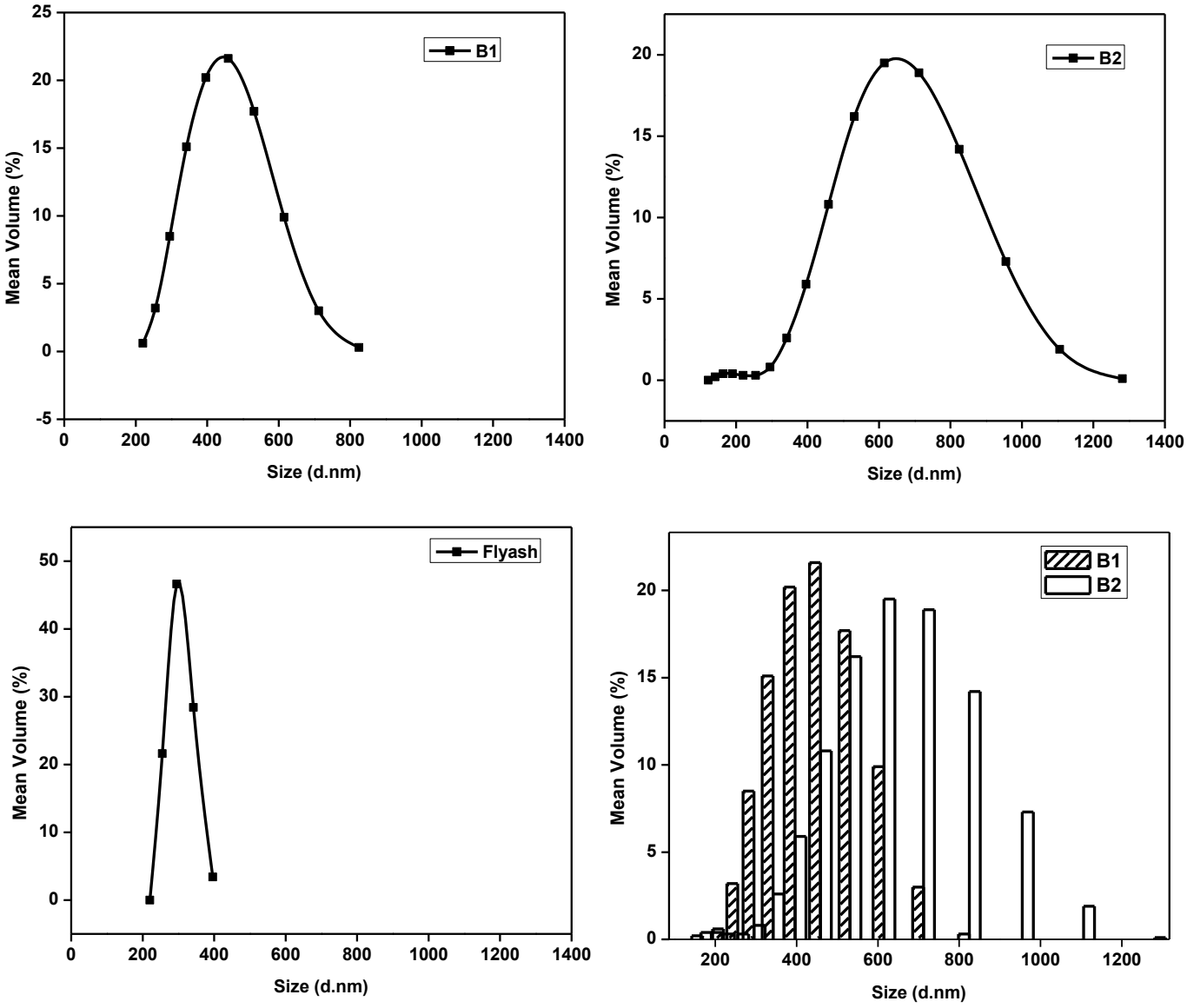

Figure 5. 3 a, b, c, d Particle Size Distribution of B1, B2 and FA and histogram of B1 and B2

The particle size results of B1 and B2 have been separately plotted (Fig5.3a and 5.3b). It is seen that B2 is having a bimodal particle size distribution. The fractional size analysis (Fig 5.3d) also reveal that the two bauxites have a distinctly different particle size. While the B1 variety has 60% particles less than 0.450 µm and only 27% between 0.50 and 0.80 µm, the corresponding figures for B2 are 19% and 74% respectively. Thus, the median particle size of B1 is almost half that of B2.

It is also possible that inspite of having a comparable agglomerate size, the primary particle size are different. In order to establish this fact, the FESEM image of the two bauxite powders were carried out (Fig 5.3 e,f). The Figure 5.3 e shows that the average primary

particle size of B1 is much smaller in comparison to B2. This implies that the number fraction of finer particles are more in B1 than in B2.

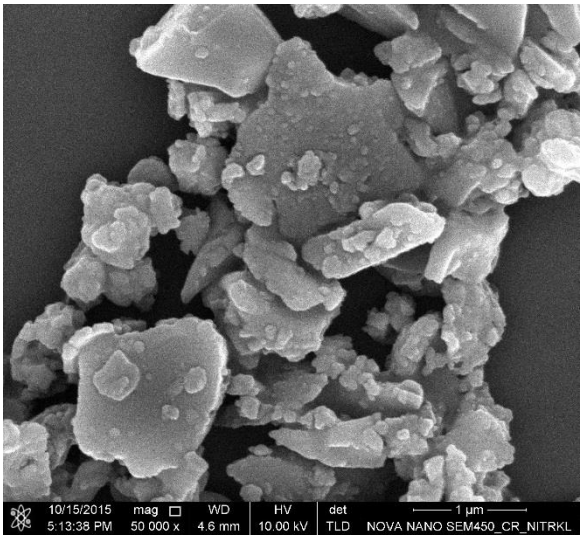

Figure 5.3 e FESEM of B1

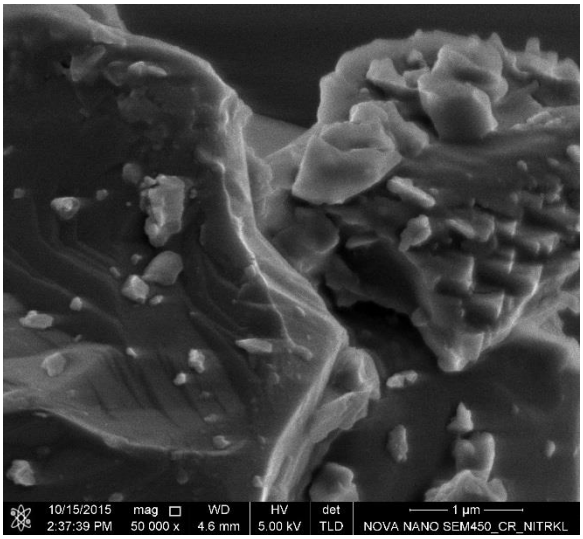

Figure 5.3 f FESEM of B2

5.5 Phase Analysis in the calcined powders:

All the compositions of B1-FA mixture were calcined as a powder at 1250^{o}C/2h. As already mentioned in the particle size distribution, FA had the finest particle size compared to B1 and B2. The particle size of B1 was less compared to B2. The crystallite size of B1 and B2 were calculated and were found to be 320 A^{o} and 1180 A^{o} respectively. So, to make the crystallite size of B1 comparable to that of B2, a calcination step was carried out for the B1-FA powder mixtures. The crystallite size of the calcined powder was also calculated which showed an increase in the crystallite size.

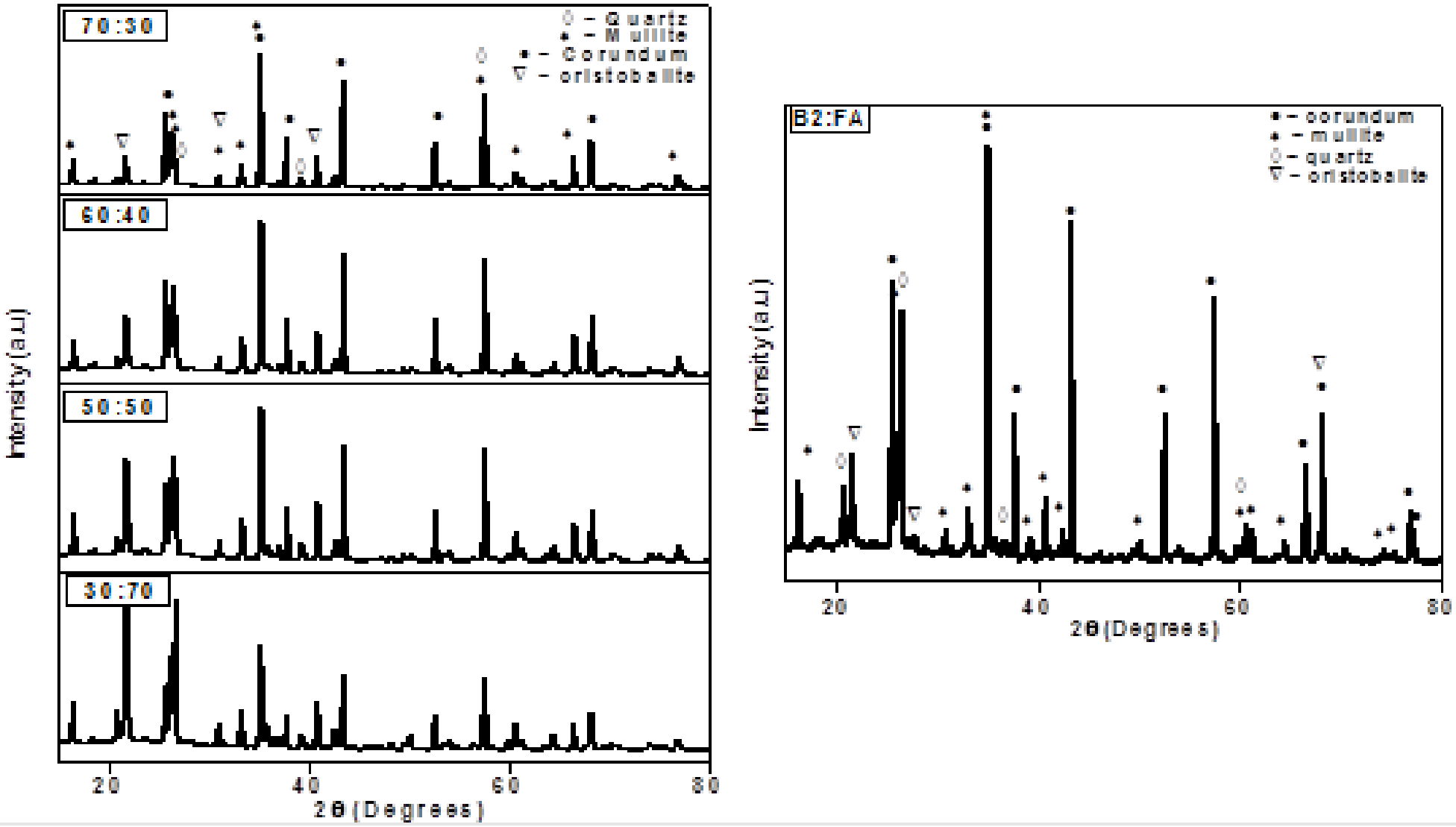

Figure 5.4 a, b XRD Pattern of B1-FA and B2-FA compositions calcined at 1250ºC

5.6 Comparison of Single-stage and two-stage firing for B1-FA and B2-FA composition:

Fig 5.5 a, b shows respectively the XRD analysis for Single-stage and two-stage firing of a specific composition (60:40) of B1-FA. Similarly, Fig 5.5 (c, d) show the XRD pattern of single – stage and two – stage fired B2-FA batches sintered at 1500^{o}C. In case of single stage firing, the raw mixture of bauxite-flyash was compacted and directly sintered at the desired temperature. In the double stage firing, the raw powder mixture was first calcined at 1250^{o}C, and the calcined powder was ground and compacted. The compacted sample was then fired to the desired temperature. The XRD analysis of the single stage and double stage firing (for both B1- FA and B2- FA compositions) show no significant difference in the percentage of mullite formed due to single or two- stage firing.

The XRD analysis was also done at 1250^{o}C to find out the increase in the intensity of the mullite peak. The result showed that when the powder was calcined at 1250^{o}C, there was an increase in the content of mullite in case of B1-FA. The increase in the mullite content in B1-FA was due to the reaction between corundum and quartz. In B2-FA, no significant increase in the mullite percentage was noted.

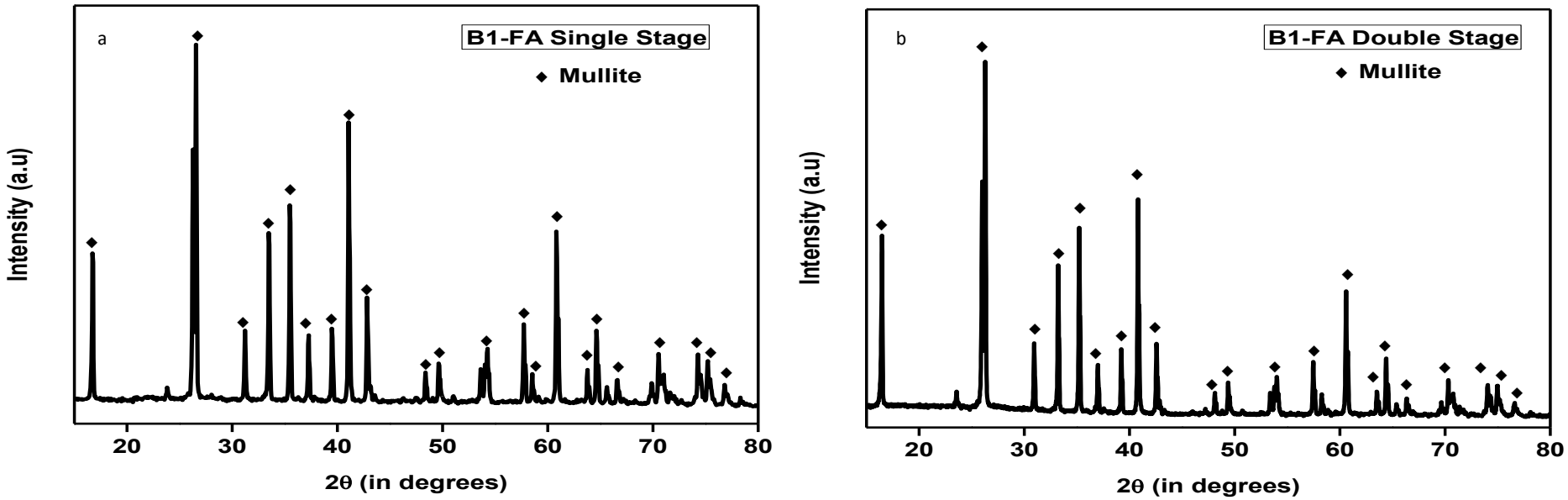

Figure 5. 5 a, b XRD Pattern of single stage and two stage firing of 60:40 B1-FA composition

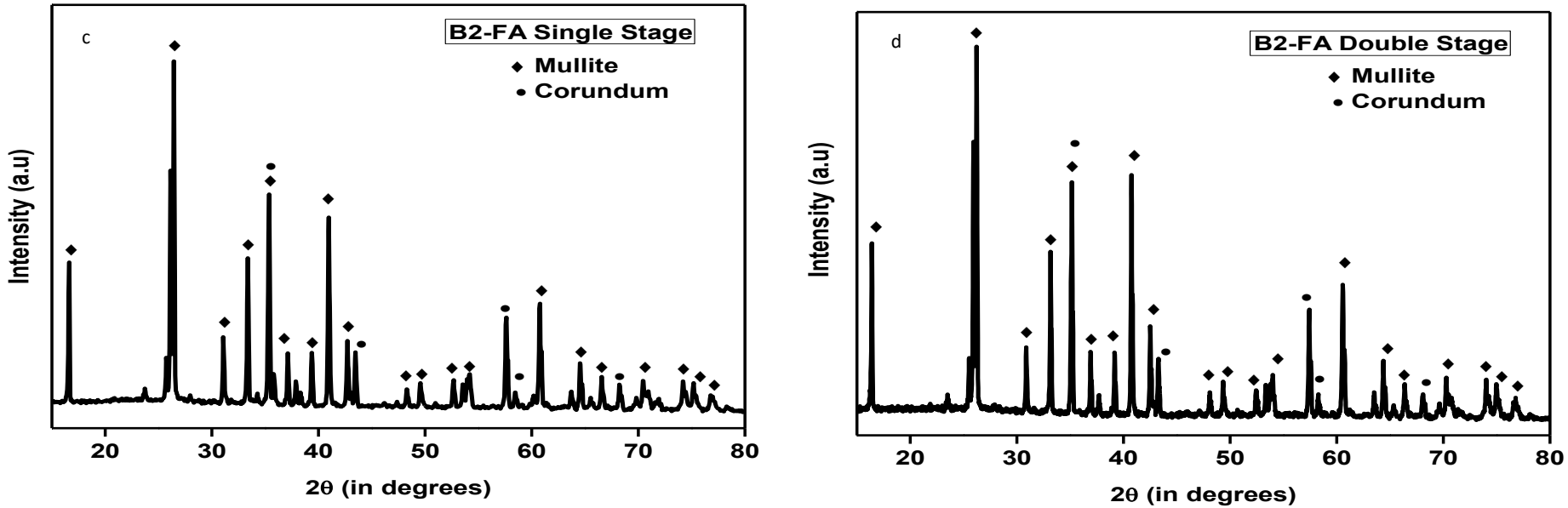

Figure 5. 5 c, d XRD Pattern of single stage and two stage firing of 60:40 B2-FA composition

5.7 Dilatometry study of bauxite and fly ash composition:

Fig 5.6 shows the dilatometric study for a specific composition (70:30) of B1-FA and B2-FA batches. Without considering the absolute value of shrinkage, it can be said that the densification of the mixtures start at around 900^{o}C, and it shows a shrinkage occurs till about 1250^{o}C. Beyond 1250^{o}C, the curve shows an expansion that is due to two opposing phenomena occurring from this temperature onwards. The first of this is the shrinkage due to densification and the second one is the expansion due to mullitization reaction. It may be noted that the volume expansion of 9% takes place during the conversion of Al_2O_3-SiO_2 mixture to mullite. Thus, mullitization adversely affects densification [1.22]. From the dilatometer plot, it can be noted that percentage expansion is higher (4%) for B1-FA relative to the B2-FA composition (1.5 %). Thus, B1 is expected to react faster with FA to produce higher mullite fraction. Secondly, the expansion for B1 -FA starts around 1250^{o}C and the expansion is completed around 1425^{o}C. On the other hand, the expansion of B2-FA is incomplete till 1475^{o}C and is expected to continue till at higher temperature. Thus B2 –FA batch will require a higher temperature for complete mullitization. The expansion of the samples due to the mullitization reaction adversely affects the sintered density.

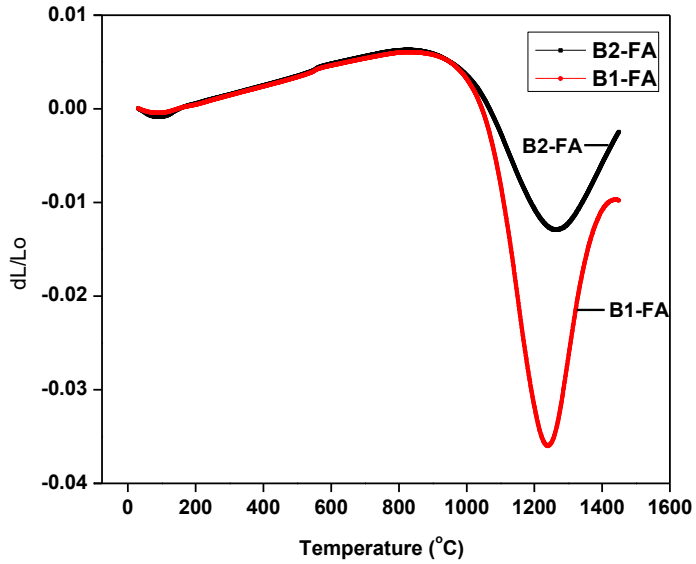

Figure 5. 6 Dilatometry Study of B1-FA and B2-FA

5.8 Phase Analysis of B1-FA powder mixture calcined at different temperatures:

Fig. 5.7 a shows the XRD pattern of a selected composition of B1+FA (70:30) powder mixture calcined at different temperatures i.e. 500, 900, 1050, 1250 and 1400^{o}C. Fig 5.7 b shows the zoomed in pattern of the same in the 2θ range 20-30^{o}, where all the 100%peaks of mullite, cristobalite and corundum are present. Fig 5.7 c shows the graphical representation of

the percentage of the phases present in a specific composition i.e. 70:30 B1+FA powder mixture calcined at different temperatures. The graphical representation shows that the intensity of mullite phase increased whereas the intensity of the corundum and quartz peaks decreased. The results indicate that with the increase in the calcination temperature, corundum reacted with quartz to form mullite. The glassy phase increased with increase in calcination temperature. The gradual decrease in the intensity of quartz peak along with an increase in cristobalite peak also indicated the transformation of quartz to cristobalite at 1250^{o}C. At the higher temperature, i.e., 1400^{o}C, the intensity of mullite increased sharply, and that of corundum decreased whereas the cristobalite and quartz peaks disappeared. The increase in the mullite content at this temperature indicates the formation of secondary mullite by dissolution of alumina to silica-rich glass and precipitation of secondary mullite [2.23]

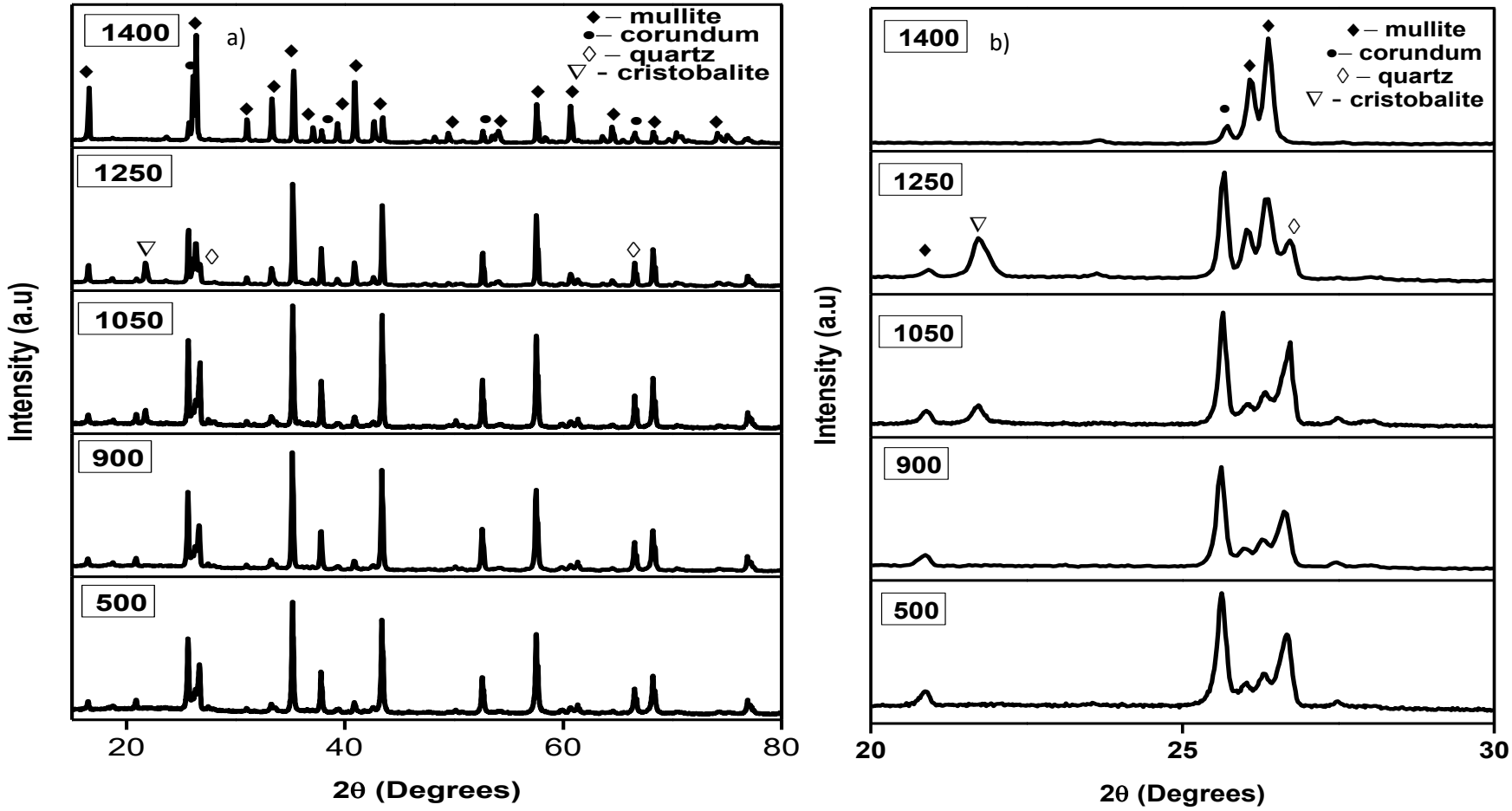

Figure 5. 7 a) XRD Spectra of 70:30 B1-FA calcined at different temperatures b) Zoomed in Pattern of 70:30 B1-FA at different temperatures

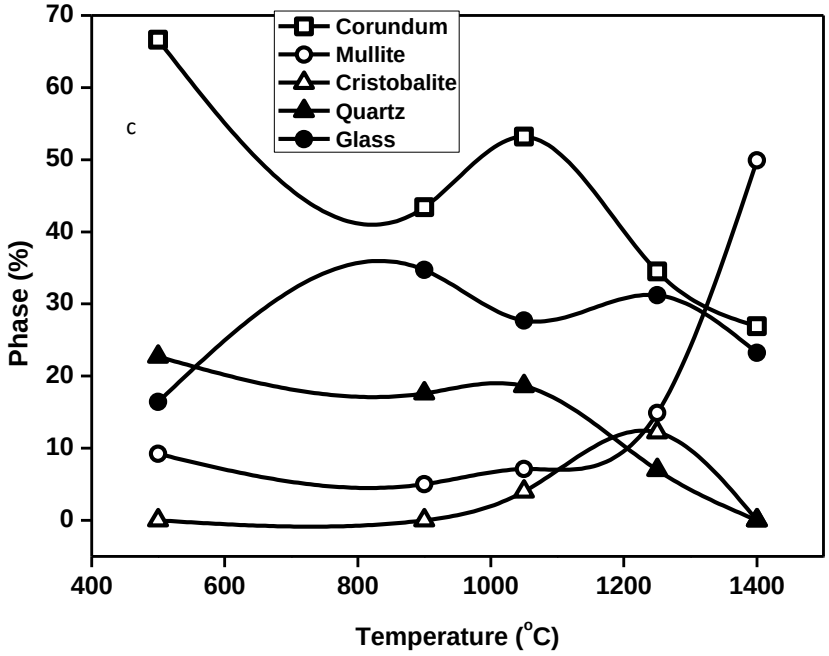

Figure 5. 7 c) Graphical Representation of phases in 70:30 B1-FA at different temperatures

5.9 Phase Analysis of B1-FA at high temperatures:

Fig 5.8, 5.9, 5.10 a shows the XRD patterns of different compositions of B1-FA samples sintered at high temperatures i.e. 1400, 1450 and 1500^{o}C respectively. Fig 5.8, 5.9, 5.10 b shows the zoomed in pattern of the same in the 2θ range 20-30^{o}. Fig 5.11 a, b, c shows the graphical representation of the percentage of the phases present in the different compositions sintered at different temperatures. . All the compositions contained glassy phases. The glassy phase variation was just the reverse of mullite phase variation. The result can be explained in line with the published results on the crystallization of mullite [2.30]. According to the reports at first an aluminosilicate glassy phase forms from which mullite crystallizes out. Thus mullite and glassy phase show the inverse relation. Corundum dissolves in the glassy phase and disappears at 1450^{o}C. Cristobalite appears at high FA containing batch. The appearance of cristobalite is due to crystallization from the glassy melt. It is further seen that mullite content is highest (90%) at 1400^{o}C in 60:40 B1: FA composition. At higher FA, mullite decreases due to the progressive dissolution of primary mullite and crystallization of secondary mullite. The drop in mullite content at higher temperature is due to the dissolution of mullite in the glassy phase which has started at a lower temperature. At 1450^{o}C, the glassy phase is more than mullite. At 1500^{o}C, the mullite content increases due to the crystallization of mullite and accordingly glassy phase are reduced.

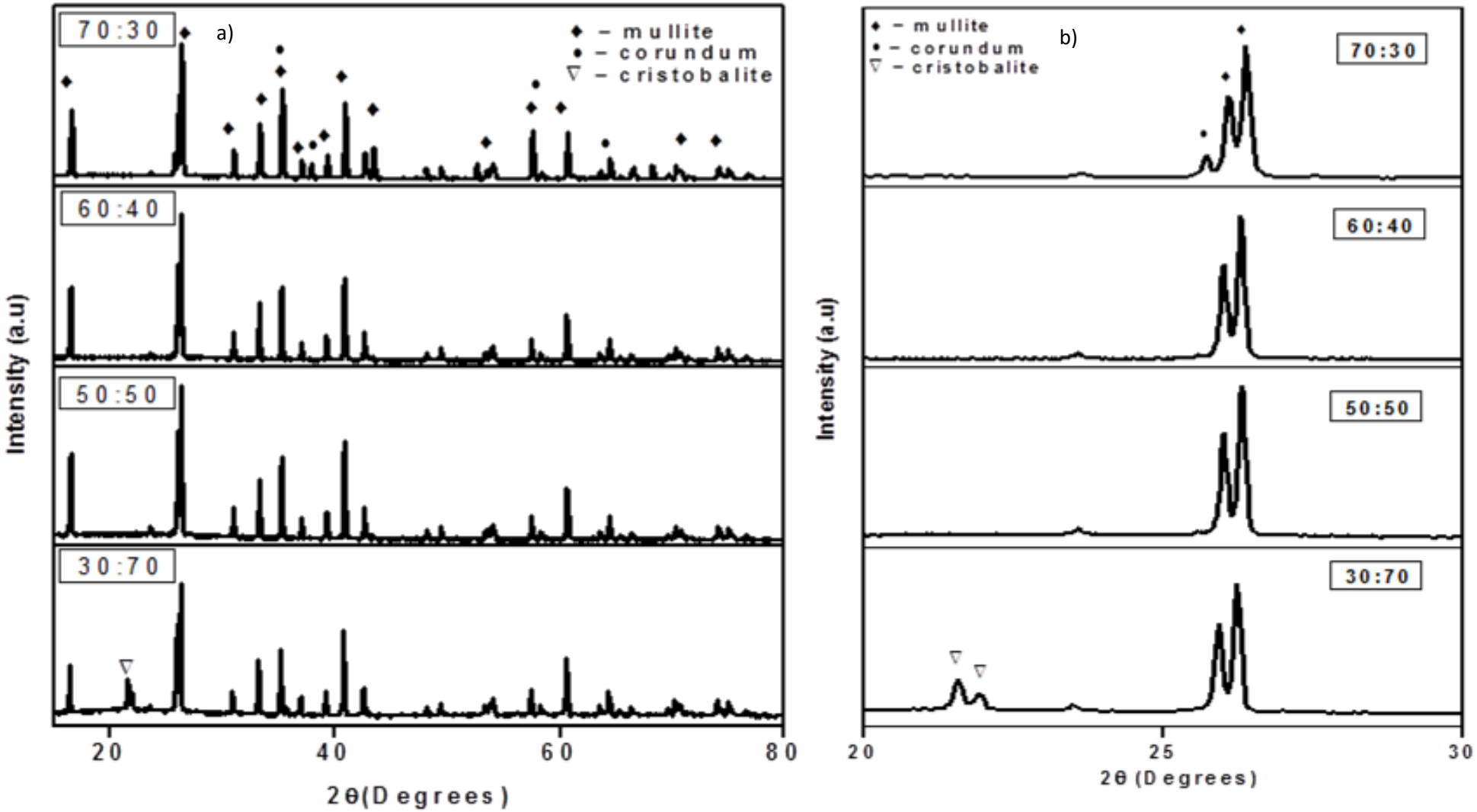

Figure 5.8 a) XRD Pattern of B1-FA sintered at 1400ºC b) Zoomed in pattern of B1-FA sintered at 1400ºC

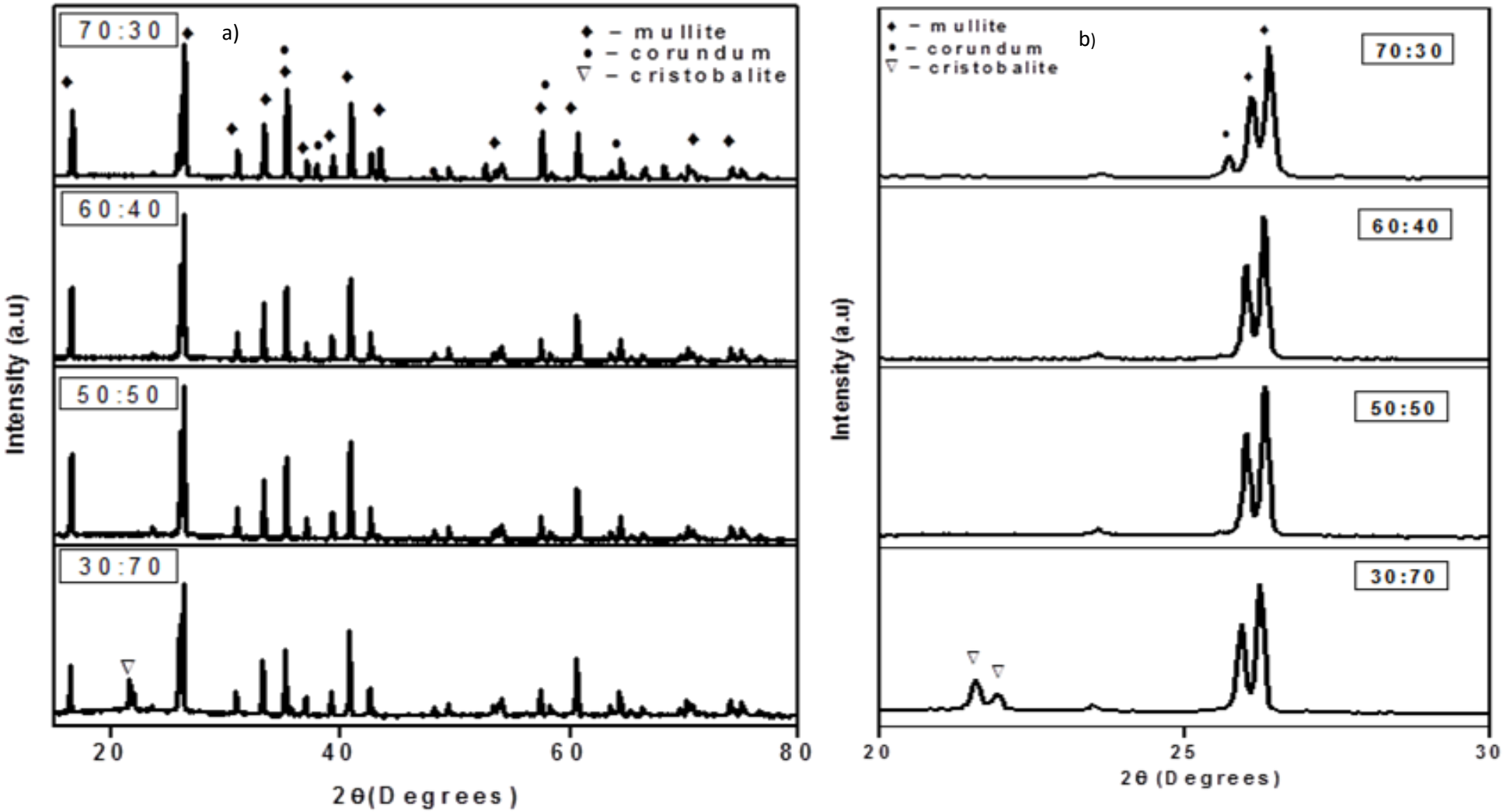

Figure 5.9 a) XRD Pattern of B1-FA sintered at 1450ºC b) Zoomed in Pattern of B1-FA sintered at 1450ºC

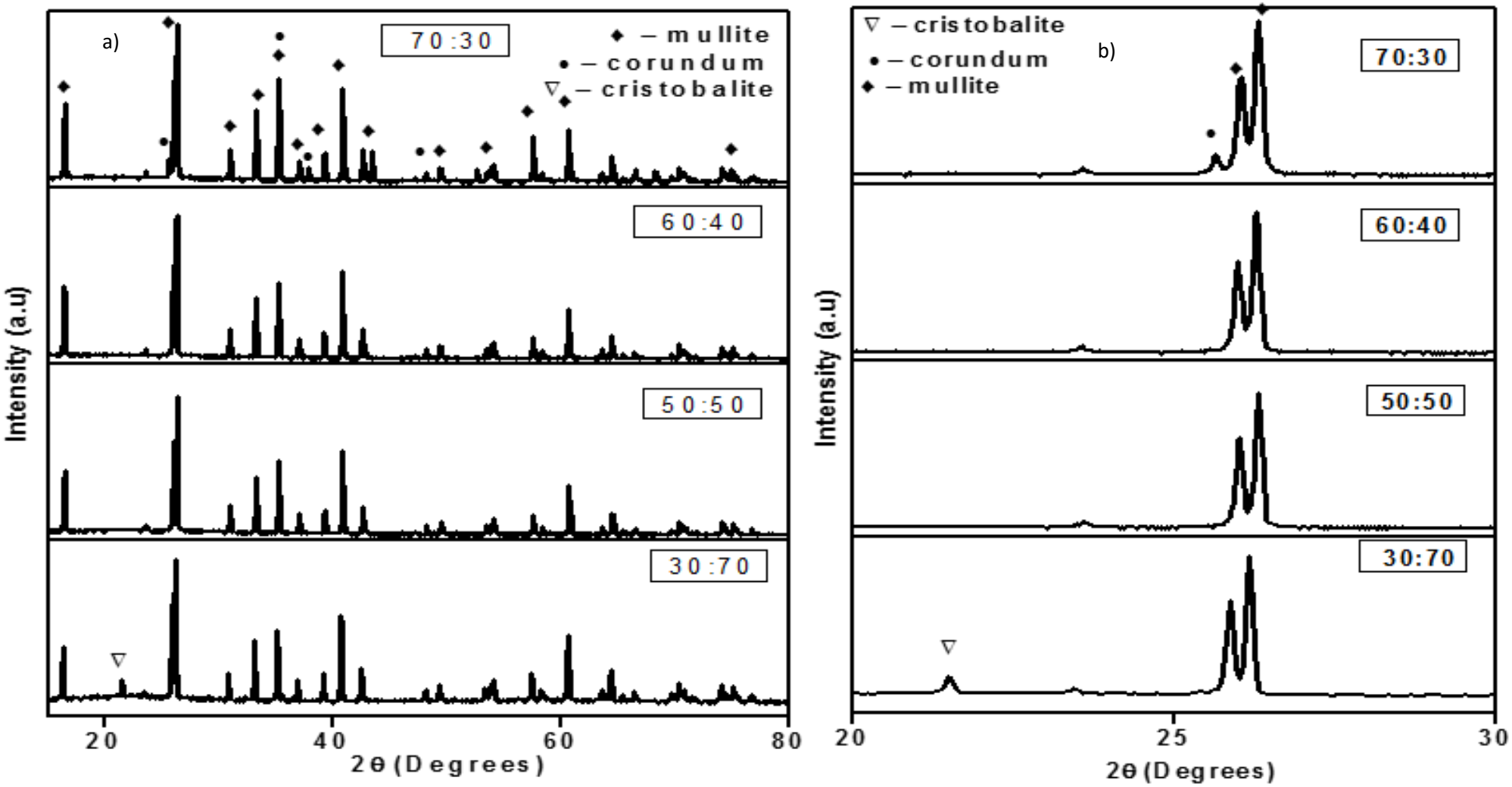

Figure 5.10 a) XRD Pattern of B1-FA sintered at 1500ºC; b) Zoomed in Pattern of B1-FA sintered at 1500ºC

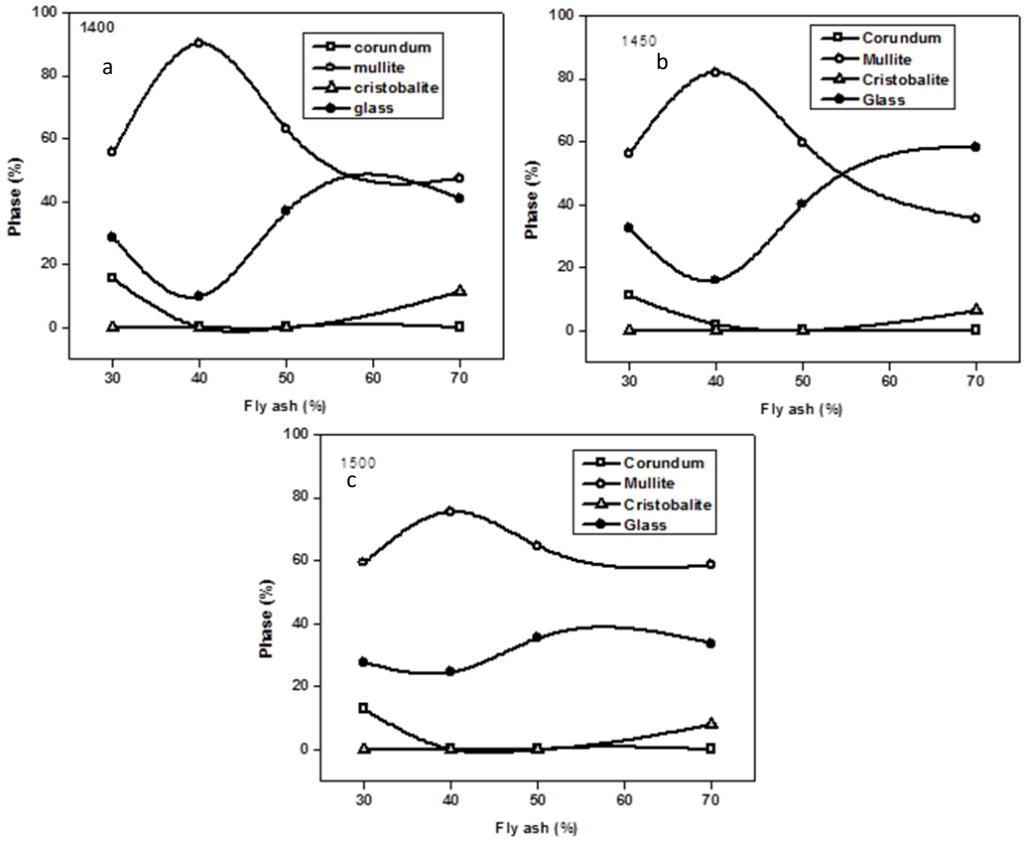

Figure 5.11 a, b, c Graphical Representation of percentage of phase of B1-FA composition sintered at 1400, 1450 and 1500ºC

5.10 Phase Analysis of B2-FA at high temperatures:

Fig 5.12, 5.13, 5.14 a, Fig 5.12, 5.13, 5.14 b respectively show the XRD patterns of different compositions of B2-FA samples, the zoomed in pattern of the same in the 2θ range 20-30º. Fig 5.15 a, b, c show the graphical representation of the percentage of the phases present in the different compositions sintered at high temperatures i.e. 1400, 1450 and 1500ºC respectively. It was observed that with the increasing in sintering temperature, the intensity of corundum decreased and the intensity of mullite increased for all the compositions. There was no cristobalite found in 70:30 and 60:40 B2-FA whereas in case of 50:50 B2-FA, a small amount of cristobalite was observed at 1400ºC which decreased as the sintering temperature increased. In 30:70 B2-FA, the content of cristobalite was higher, and the amount of mullite formed was lower compared to other compositions. At 1400ºC, both mullite and corundum decrease with increase in FA content. Thus, the glassy phase continues to dissolve corundum and mullite and secondary mullite starts forming at high temperature. At 1450ºC, mullite and alumina show a similar trend, and glassy phase shows the opposite trend. At 1450ºC, 70% FA compositions have lower glassy phase than mullite. This is in contrast to the pattern observed at 1400ºC. The mullite content increases at 1500ºC, most likely due to crystallization of secondary mullite from the melt.

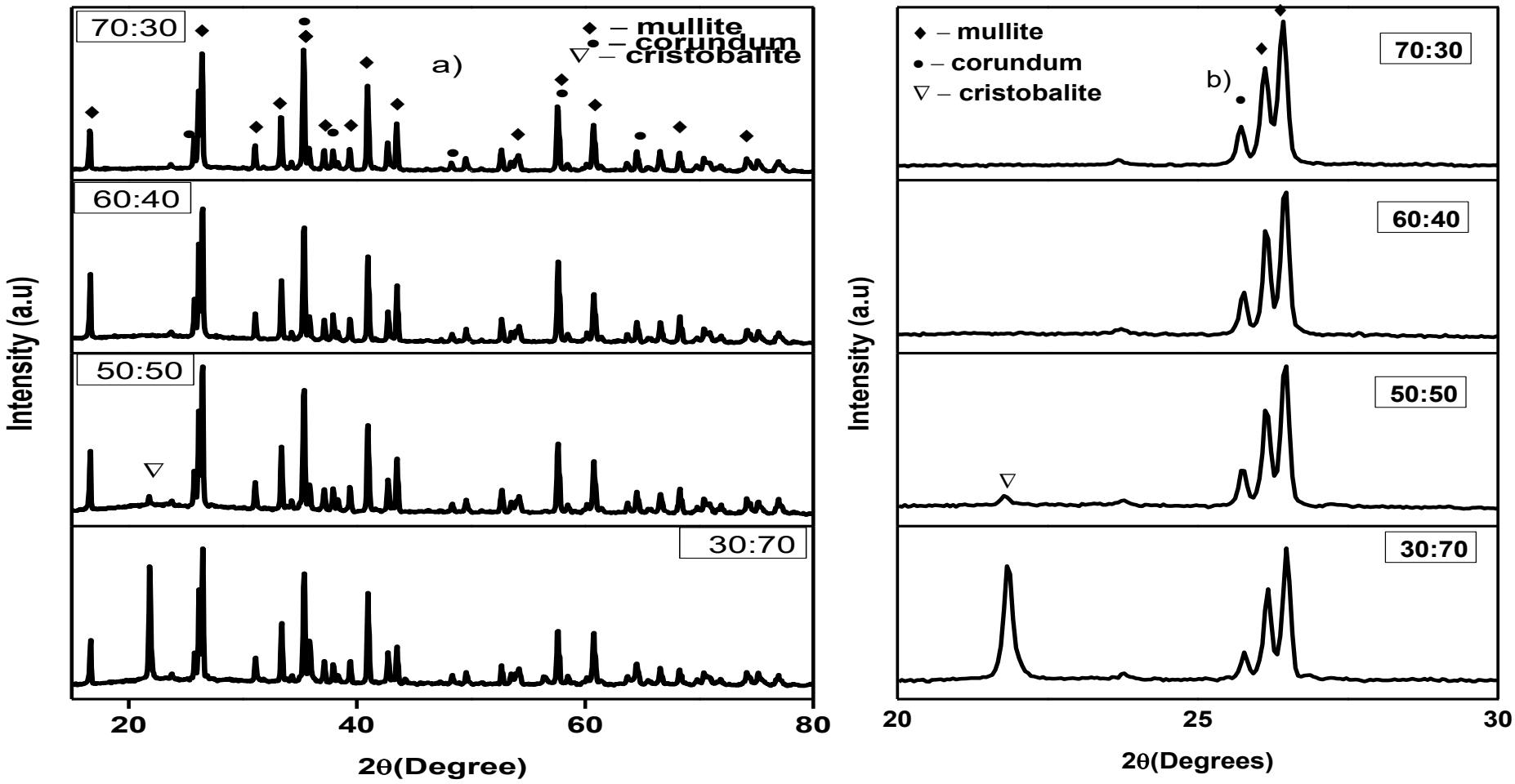

Figure 5.12 a) XRD Pattern of B2-FA sintered at 1400°C b) Zoomed in Pattern of B2-FA sintered at 1400°C

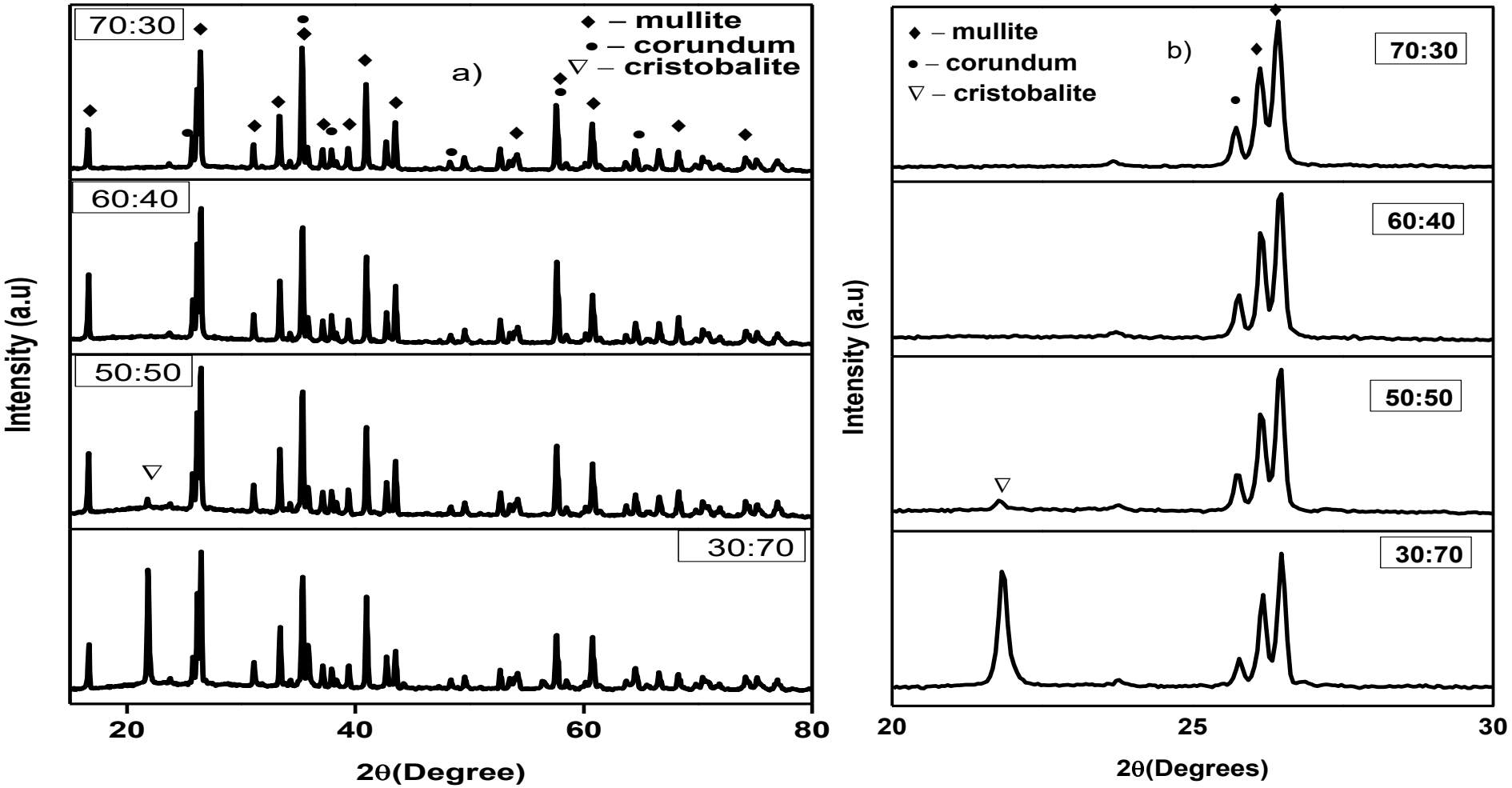

Figure 5.13 a) XRD Pattern of B2-FA sintered at 1450°C b) Zoomed in Pattern of B2-FA sintered at 1450°C

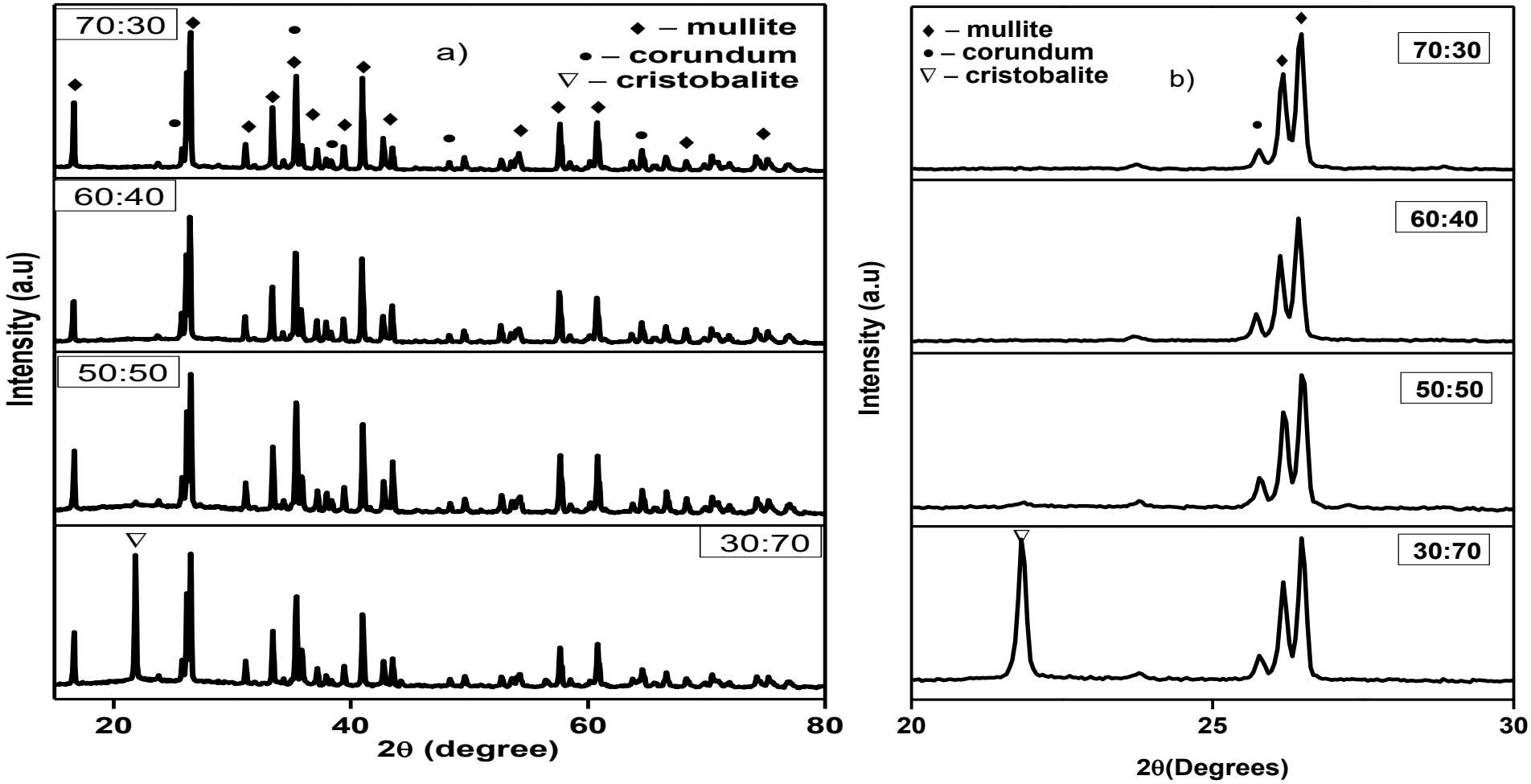

Figure 5.14 a) XRD Pattern of B2-FA sintered at 1500ºC b) Zoomed in Pattern of B2-FA sintered at 1500ºC

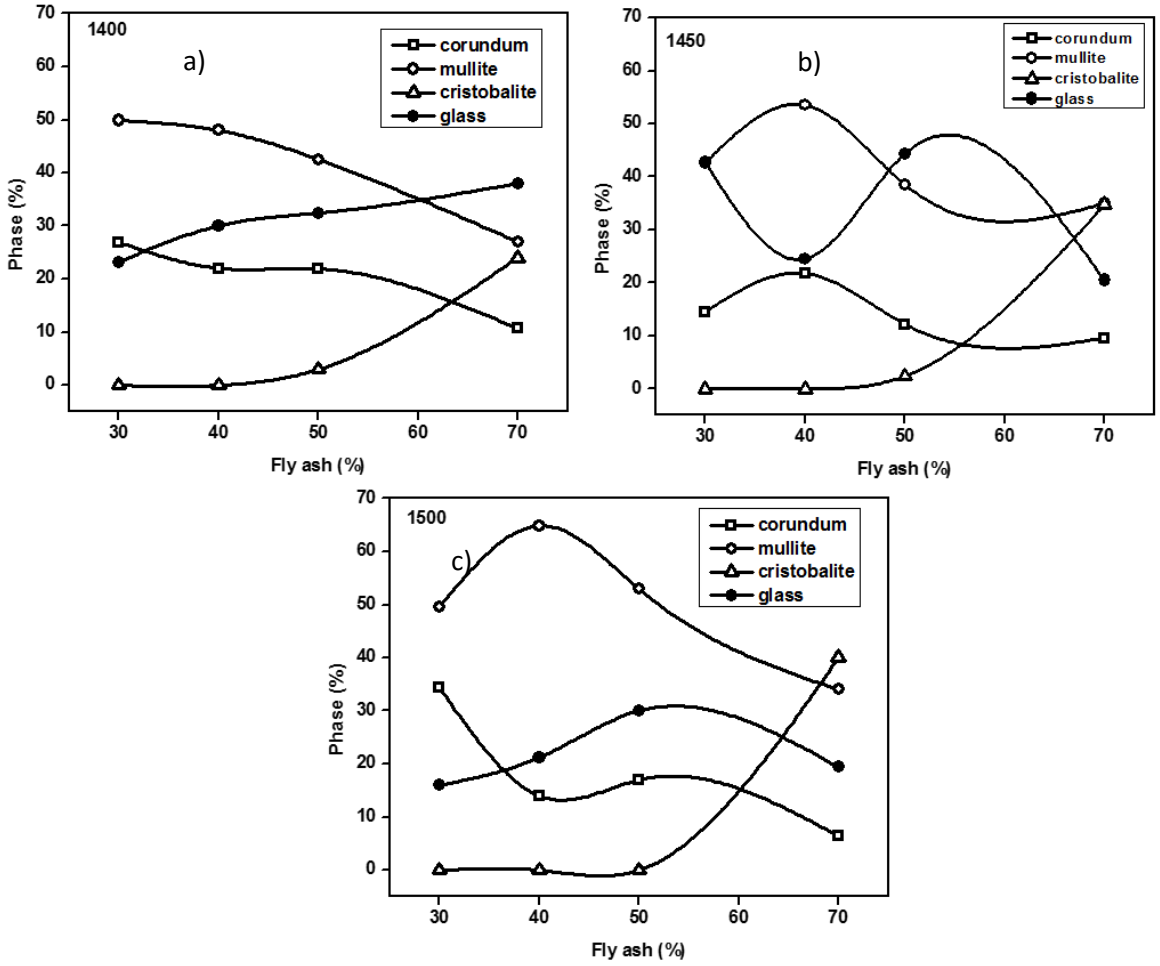

Figure 5.15 a, b, c Graphical Representation of percentage of phase of B2-FA composition sintered at 1400, 1450 and 1500°C

5.11 Relative density of the sintered samples:

Fig 5.16 a, b shows the relative density of different compositions of B1-FA and B2-FA samples as a function of FA addition. The relative densities were calculated considering the theoretical densities of corundum, mullite, cristobalite and glass to be 3.98, 3.2, 2.26 and 2.23g/cc respectively. In B1-FA compositions, the relative density of the samples increased with increasing sintering temperature except for one B1-FA composition (40% FA). The 40% FA containing B1-FA samples show a dip in the density at all the sintering temperatures. However, in all the B1-FA compositions, the density difference among the different compositions decreased as the sintering temperature was raised to 1500°C. The maximum density of 81% was achieved for 30:70 B1-FA compositions sintered at 1500°C. In B2-FA compositions, the relative density increased with increase in FA content. The data could be very well fitted by the linear fitting method, implying a direct correlation between FA and relative density in B2-FA compositions. The maximum relative density of 87.5% was obtained in the case of 30:70 B2-FA composition. The high density in the B2-FA samples

resulted due to the combination of the optimum fraction of crystalline and glassy phase. The presence of two crystalline phases, i.e. mullite and corundum resulted in high density for 70:30 B1-FA samples as compared to 60:40 and 50:50 B1-FA samples which contain predominantly mullite phase. In case of B2-FA compositions, it can be further noted that all the compositions contain corundum but in B1 only one composition (70:30) contain corundum. Other compositions have either single phase mullite or mullite + cristobalite

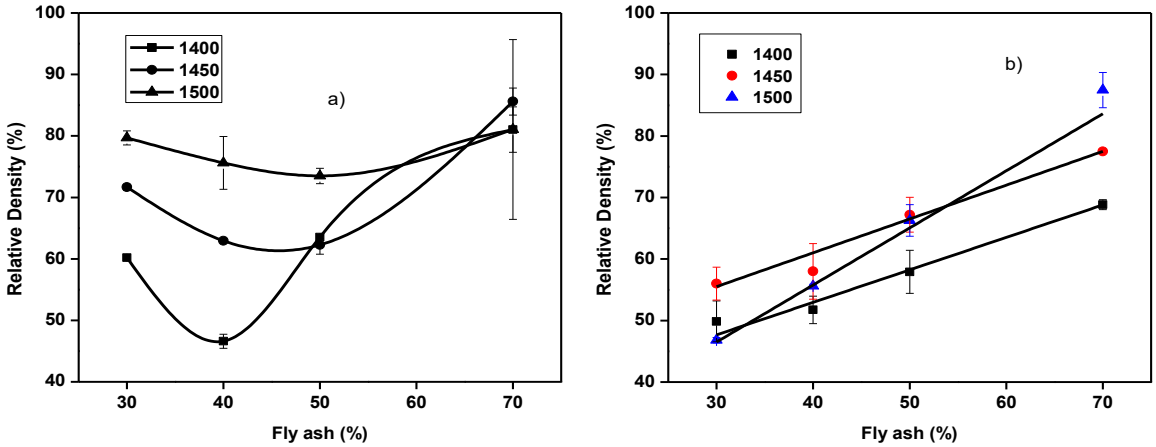

Figure 5.16 a, b Relative Density vs Fly ash of B1-FA and B2-FA compositions

5.12 Apparent porosity of the sintered samples:

Fig 5.17 a, b shows the variation of apparent porosity as a function of FA addition. It is seen that for both B1-FA and B2-FA compositions, the apparent porosity decreased with increase in FA except for 60:40 B1: FA composition. In 60:40 B1:FA composition, the porosity increases and at higher FA , the porosity decreases giving a peak at 60:40 composition Other than this sample, the porosity decreases with FA addition both for B1 + FA as well as for B2 + FA compositions. This implies that FA addition helps in densification of samples through the liquid phase formation. In both the composition, 30:70 batch had a maximum decrease in apparent porosity. In B2-FA samples, the drop in apparent porosity is most for 30:70 samples, indicating the large volume of liquid being formed at this composition.

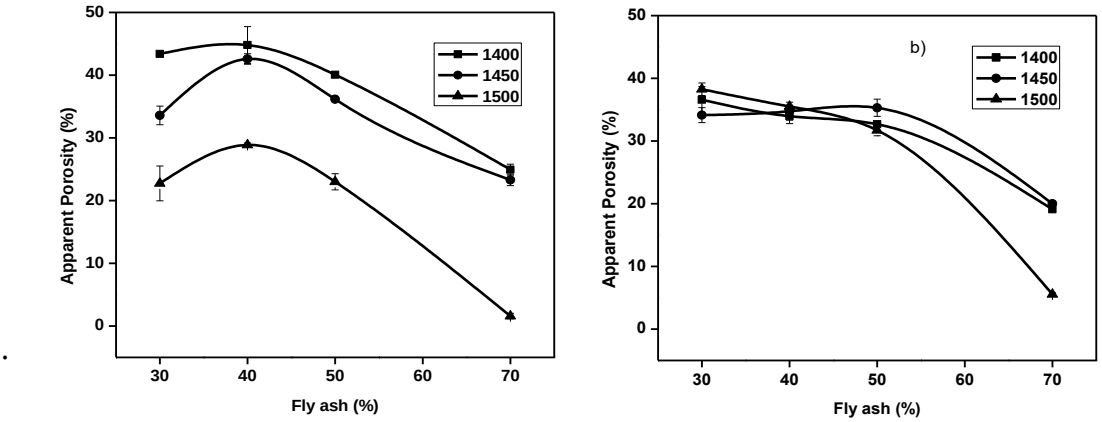

Figure 5.17 a, b Apparent Porosity vs Fly ash of B1-FA and B2-FA compositions

The above porosity result is also supported by the microstructure of the samples. Fig 5.18 a, b shows the microstructure of 60:40 B1-FA sintered at 1400ºC. It can be seen that both equiaxed (single arrow) and elongated mullite grains (double arrow) are present, and the structure is porous. Fig 5.19 a shows the microstructure of 50:50 B1- FA composition. This microstructure also shows mullite grains dispersed in the matrix. The presence of glassy phase is also clear from the microstructure. Fig 5.19 b shows the higher magnification microstructure of 50:50 B1-FA samples. At the center, we can see a large lump which shows two things: the dissolution of the crystalline phase in a glass (marked by an arrow) and the crystallization of mullite phase. Similarly fig 5.20 a, b shows the microstructure of 60:40 B2-FA composition. The structure is porous and elongated mullite grains are very few. The microstructure also shows sharp angular grains. According to XRD pattern, this sample has lower mullite content compared to B1-FA. Thus, the microstructure supports the XRD and porosity results

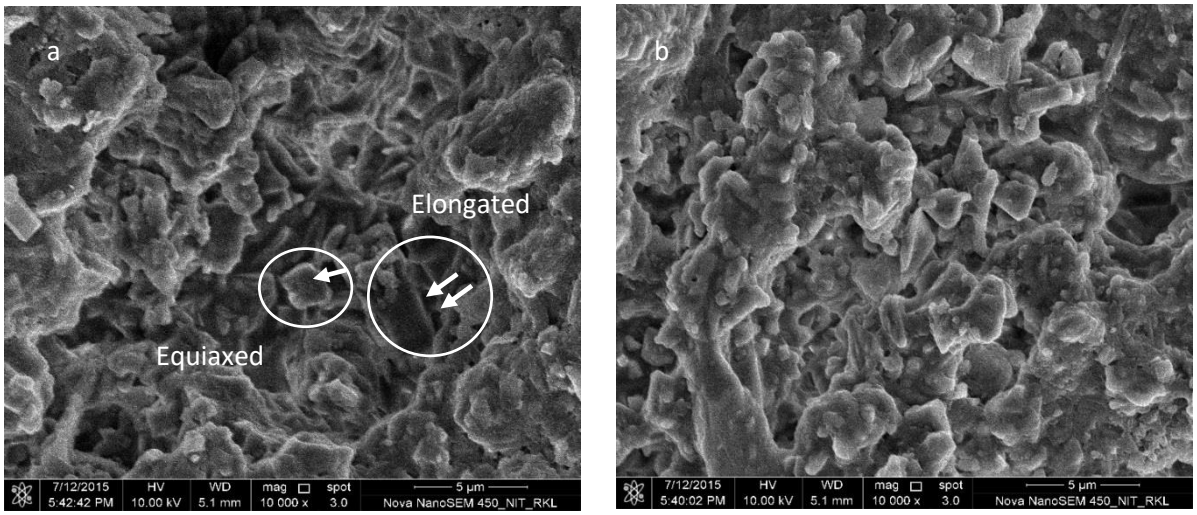

Fig 5.18 a, b FESEM images of 60-40 B1-FA composition sintered at 1400ºC

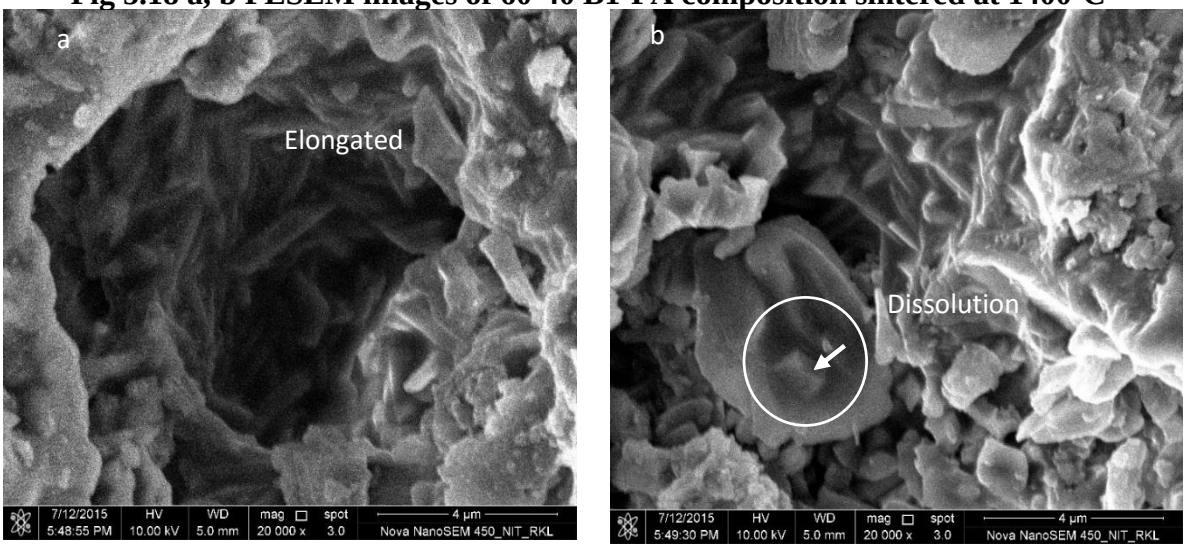

Fig 5.19 a, b FESEM images of 50-50 B1-FA composition sintered at 1400ºC

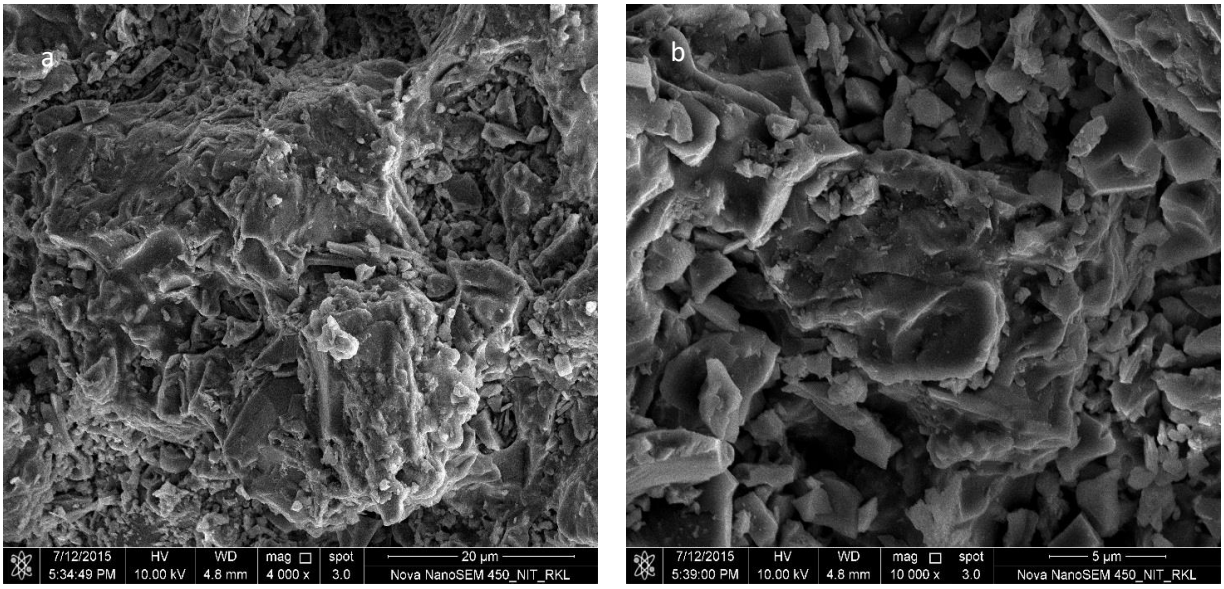

Fig 5.20 a, b FESEM images of 60-40 B2-FA composition sintered at 1400ºC

5.13 Microstructure:

Fig 5.21 (a, b, c, d) and 5.22 (a, b, c, d) shows the microstructure of 70, 60, 50 and 30% B1-FA and B2-FA compositions respectively sintered at 1500ºC. The microstructure of B1-FA compositions shows that at 30%FA, two types of mullite grains are present. The equiaxed grains are the primary mullite, and the elongated grains are the secondary mullite. The encircled area in Fig *5.21d* shows that elongated mullite grains have started developing from the surface of primary mullite through a dissolution precipitation reaction. In 50% FA samples, the primary mullite grains have started developing elongated mullite grains, and it can also be seen that some very long mullite grains are also developing at some places. In the literature [5.1], these fine mullite crystals have been termed as tertiary mullite. In 70% FA samples, besides the equiaxed mullite grains, two distinct type of mullite grains could be observed. One of them is wider elongated grains, and the other is finer and elongated mullite grain. Moreover, some spherical particles could also be seen (encircled area). These spherical particles are likely to be cristoballite which have precipitated out from the glass along with the precipitation of tertiary mullite. In the B2-FA compositions, the microstructure of 30%FA containing samples shows a different feature. Both primary mullite and corundum are observed. The equiaxed mullite grains are embedded in the glassy matrix. In the 50 %FA and 70 %FA samples, very fine elongated needle-like mullite grains could be observed. Thus, in these samples both secondary and tertiary mullite grains [5.2] are present.

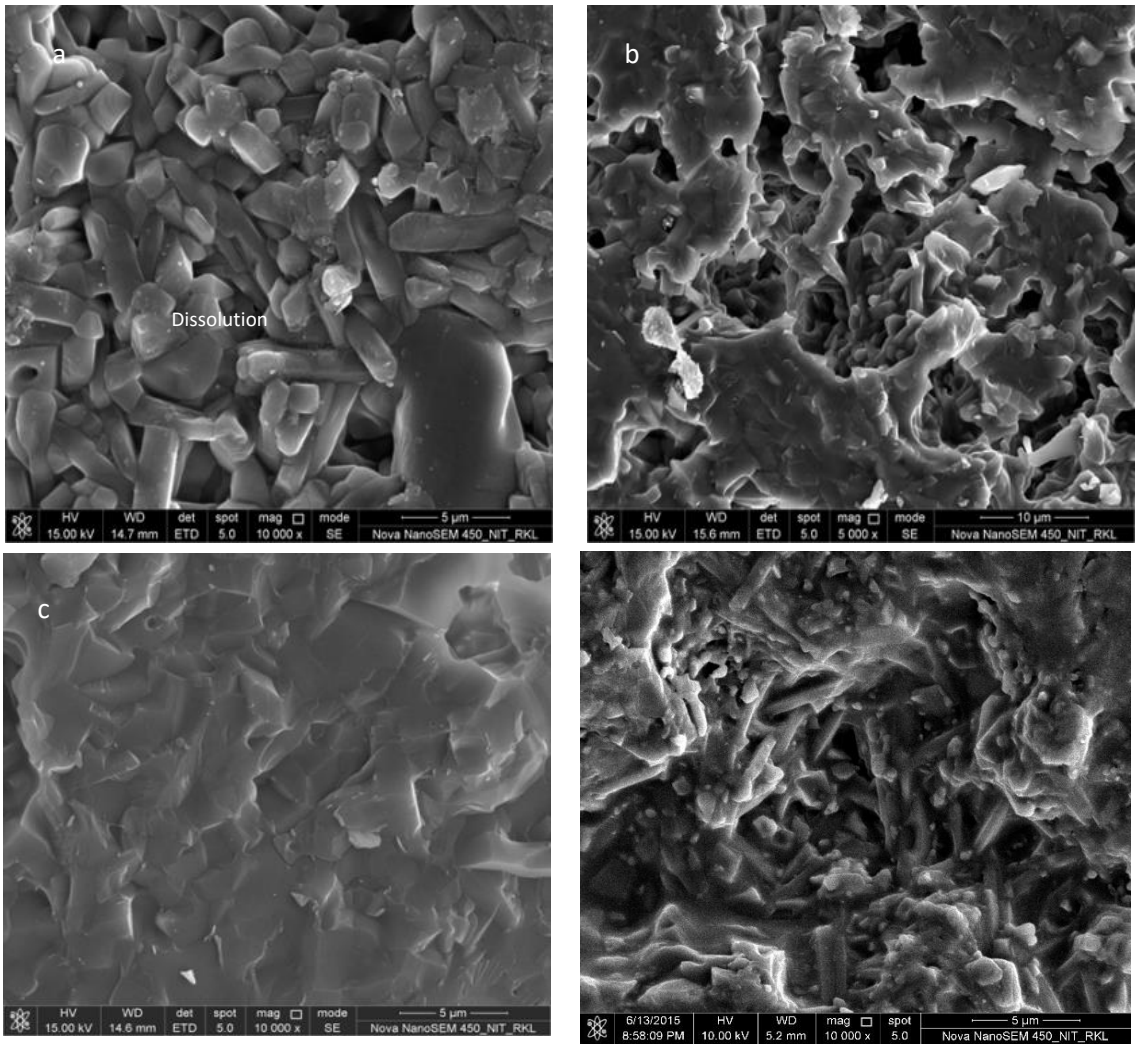

Fig 5.21 a, b, c, d FESEM images of B1-FA compositions sintered at 1500^{o}C

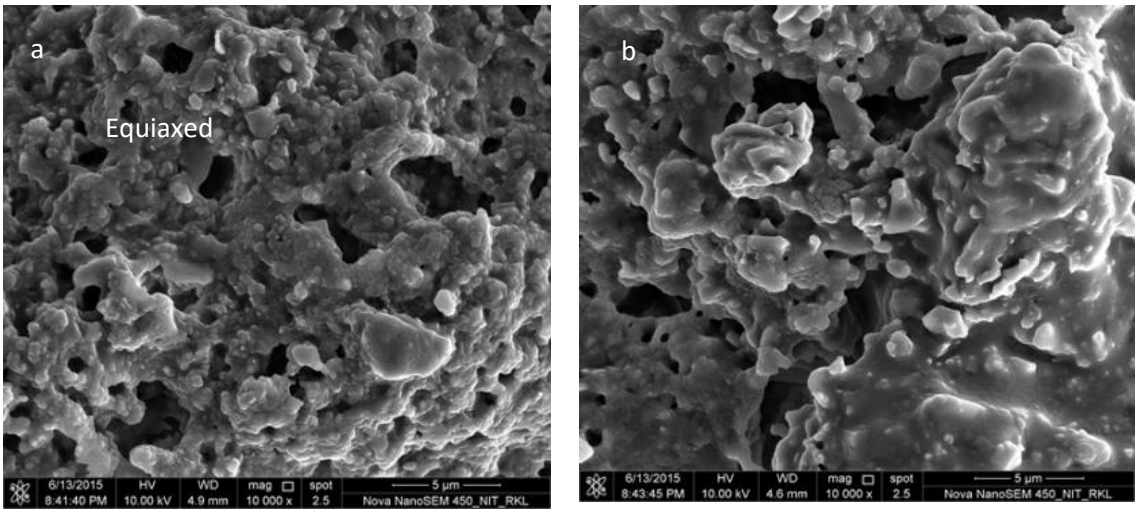

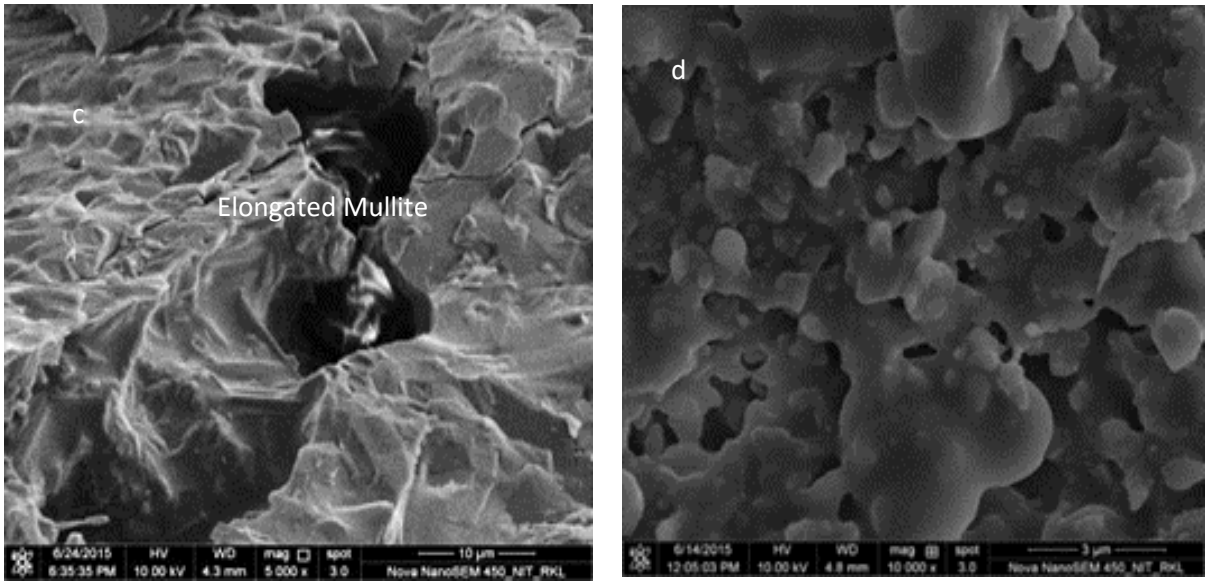

Fig 5.22 a, b, c, d FESEM images of B2-FA composition sintered at 1500ºC

5.14 Bending Strength of the sintered samples:

Fig 5.23 a, b shows the bending strength of different compositions of B1-FA and B2-FA samples as a function of fly ash content. The bending strength of B1-FA samples increased with the increase in sintering temperature from 1400-1500ºC. The increase in bending strength in 70:30 B1-FA samples at 1450ºC is because of the combination of two phases (mullite and corundum) and the very dense structure of the matrix.The matrix is hard which can be seen from the indentation impression of the sample in Fig 5.24 a. The indentation shows a very sharp image of the diamond pyramid. There was no deformation at the edges of the indent. No crack can be seen originating from the corners at 5kgf (Fig 5.24b). At 1500ºC, the indent has become smaller (Fig 5.24 c) which means that the sample has densified as compared to the sample sintered at 1450ºC. A closer look of the indent (1500ºC sintered) area at higher magnification show that within the indent and very close to the diagonal lines, multiple cracks have started appearing. Thus, the microstructure indicates that some crack – particle interaction taking place as shown in Fig 5.24 d. Thus, this composition of sample is probably resistant to crack propagation. In the 60:40 B1-FA composition, the outline of the indent is not sharp as the sample is porous as shown in Fig 5.24 e. The indent appears to have deformed the samples that are representative porous microstructure (Fig 5.21b). This type of microstructure is probably responsible for the decrease in the sample strength. In the sintered 30:70 B1-FA composition, irrespective of the sintering temperature, no alumina could be detected. All the samples contained mullite and cristobalite. The samples sintered at 1400-1450ºC also contain some free silica that was identified as quartz by XRD. It is to be also mentioned that the samples sintered at 1500ºC have extensive black coring. The

microstructure shows that at all the three sintering temperatures, liquid phase has formed, and the extent of liquid phase increases as the sintering temperature increases from 1400-1500^{o}C. The presence of glassy phase binds the mullite crystals and, as a result, the strength is high. The mismatch in density and porosity data for 1500^{o}C samples is because of black coring in the samples.

For B2-FA compositions, fired at 1400^{o}C the bending strength increases with FA content and it slightly decreases at 30:70. For samples fired at 1450^{o}C, the strength increases with FA addition and in 30:70 composition, the highest strength of 32.38 MPa was recorded. The hardness also increases. This is evident from the indentation image, which shows the typical indent with glassy fracture (Fig 5.24 f) However, at 1500^{o}C, the peak strength is observed around 50% FA composition and then it drops drastically for 70% FA composition. The increase in strength with FA at 1400 and 1450^{o}C can be attributed to increased densification. At 1500^{o}C, the mullite and cristobalite phase are in comparable fraction, and glassy phase is around 20%. Such a microstructure offers a crack resistant structure. It is to be noted that at 70% FA, high FA content resulted in a high glassy phase and black coring of the sintered sample. The microstructure shows that both secondary and tertiary mullite crystals are dispersed in a continuous glassy matrix.

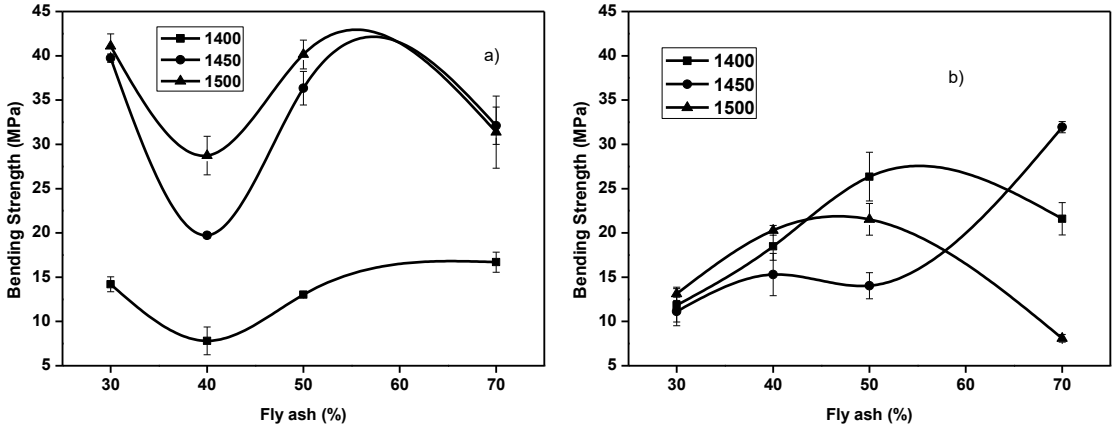

Figure 5.23 a, b Bending Strength VS Fly ash of B1-FA and B2-FA compositions

The results of equi-biaxial bending strength obtained by the ring on ring test method were low compared to the three-point bending method. The lower strength value in equi-biaxial bending test method was due to the larger effective volume under load for the ring on ring test in comparison to that of a three-point bend test.. The effective volume for equi-biaxial bending and three-point bending strength were calculated from the following formula:

Effective volume calculation for ring on ring test method [5.3]

$$V_{eff}=\frac{\pi}{2}D_L^{\,2}\left[1+\left[\frac{44(1+\mu)}{3(1+m)}\right]\right]\left[\frac{5+m}{2+m}\right]\left[\frac{D_S-D_L}{D_S}\right]^{2}*\left[\frac{2D^{2}(1+\mu)+(D_S-D_L)^{2}(1-\mu)}{(3+\mu)(1+3\mu)}\right]\frac{h}{2(m+1)} \qquad (5.1)$$

Effective volume calculation for three point bending test method [5.6]

$$V_{eff} = [\frac{1}{2(m+1)2}] * b * d * L_o \quad (5.2)$$

Where, m=Weibull modulus. The Weibull modulus for these samples was assumed to be 5.

D_s= support ring diameter, mm

D_L= loading ring diameter, mm

D_v= test-specimen diameter, mm

b=breadth, mm

d=depth, mm

L_O=Length, mm

The calculated effective volume under load for equi-biaxial bending was 1.8 times more than the effective volume under three-point bending. Due the higher effective volume the samples failed at lower load and exhibited lower strength than the normally reported strength of 100-150 MPa [1.33]

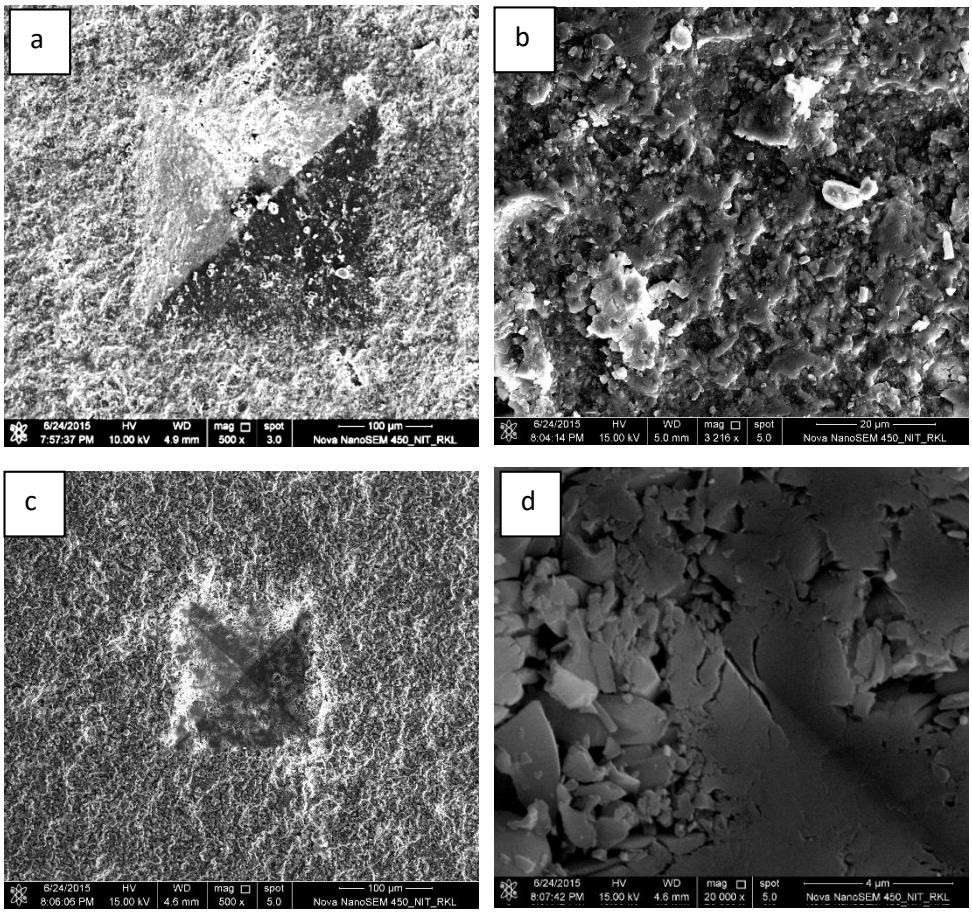

Figure 5.24 a, b) FESEM images of indented 70:30 B1-FA composition sintered at 1450ºC c,d) FESEM images of indented 70:30 B1-FA composition sintered at 1500ºC

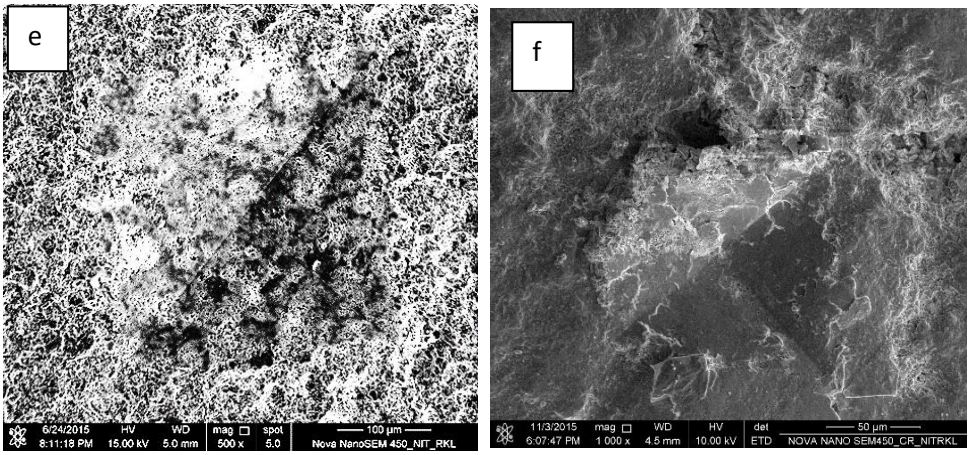

Figure 5.24 e) FESEM image of indented 60:40 B1-FA composition sintered at 1450ºC f) FESEM image of indented 30:70 B2-FA composition sintered at 1500ºC

5.15 Hardness of the sintered samples:

Fig 5.25 (a, b) show the hardness of B1-FA and B2-FA compositions respectively as a function of fly ash content. The hardness of B1-FA compositions shows that at 1400 and 1450ºC, the hardness is reduced. This is due to the lower relative density of the samples, higher mullite content and lower glassy phase for these compositions. All the other compositions of B1-FA batch show higher density and hence the hardness is high. In B2-FA compositions, at all temperatures the hardness followed the same trend. The hardness is increased with increasing fly ash content. The increase in hardness at 1500ºC is due to the formation of more amount of glassy phase compared to other temperatures which make the sample dense and resistant to indentation.

.

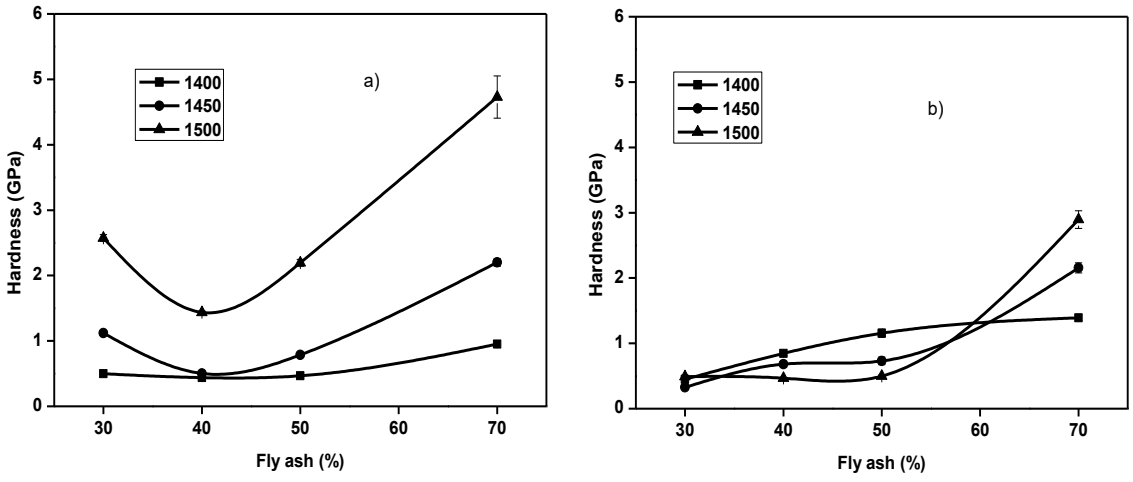

Figure 5.25 a, b Hardness vs Fly ash of B1-FA and B2-FA compositions

5.16 Fracture Toughness

The fracture toughness of B1-FA and B2-FA compositions as a function of FA percentage is shown in Fig 5.26 (a, b). It is seen that the trend of fracture toughness for 1450^0C and 1500^0C are similar but for 1400^0C, the trend is different. Samples sintered at 1400^0C exhibit low

toughness value, presumably because of poor densification. At 1450^0C and 1500^0C, the toughness increases but the minimum toughness is observed for 40% FA compositions. The minimum toughness also correlates well with strength and hardness values where the minimum of the respective properties were also observed. In the B2-FA compositions, the toughness trend is entirely different from B1-FA compositions. In these compositions, high toughness is obtained for 40% and 50% FA addition. The trend in the toughness also follows the strength value trend for B2-FA compositions. On the basis of above observations, it was thought that for these ceramics there may be a correlation between strength and toughness. It is well known that the fracture strength (σ_f) and fracture toughness (K_{IC}) are related by the following equation [2.17].

$$\sigma_f = \frac{YK_{IC}}{\sqrt{C}} \qquad (5.3)$$

Therefore, a plot of σ_f and K_{IC} should show a linear fitting curve. Fig 5.27 a, b shows the plot of σ_f vs K_{IC} for B1-FA composition and Fig 5.28 a, b for B2-FA composition. It is seen that good fitting curve is obtained for higher temperature sintered sample. This result indicates that the mullite based ceramics prepared in this work exhibit a direct correlation between strength and toughness.

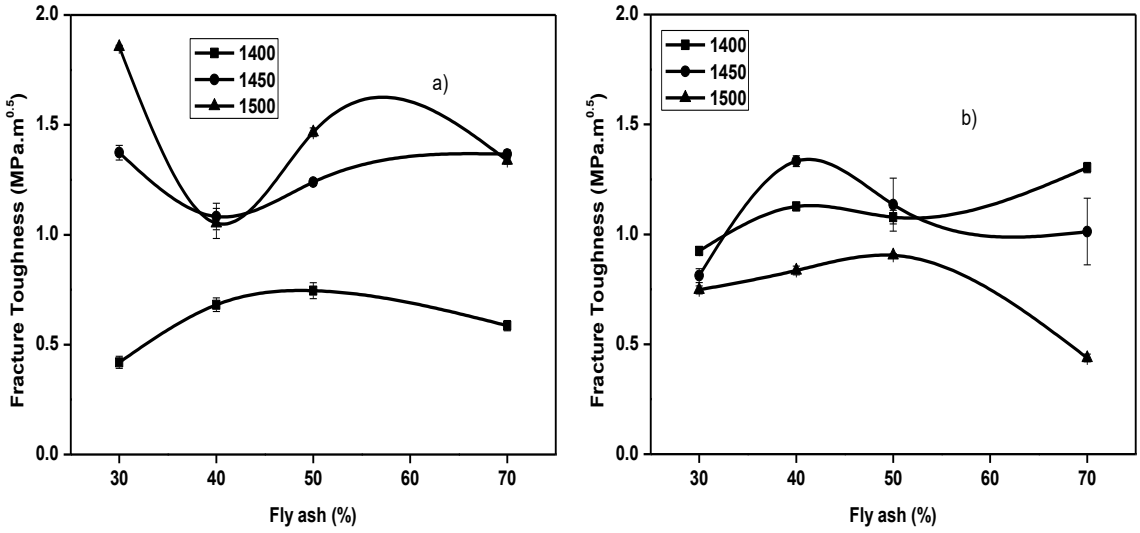

Figure 5.26 a, b Fracture Toughness vs Fly ash of B1-FA and B2-FA compositions

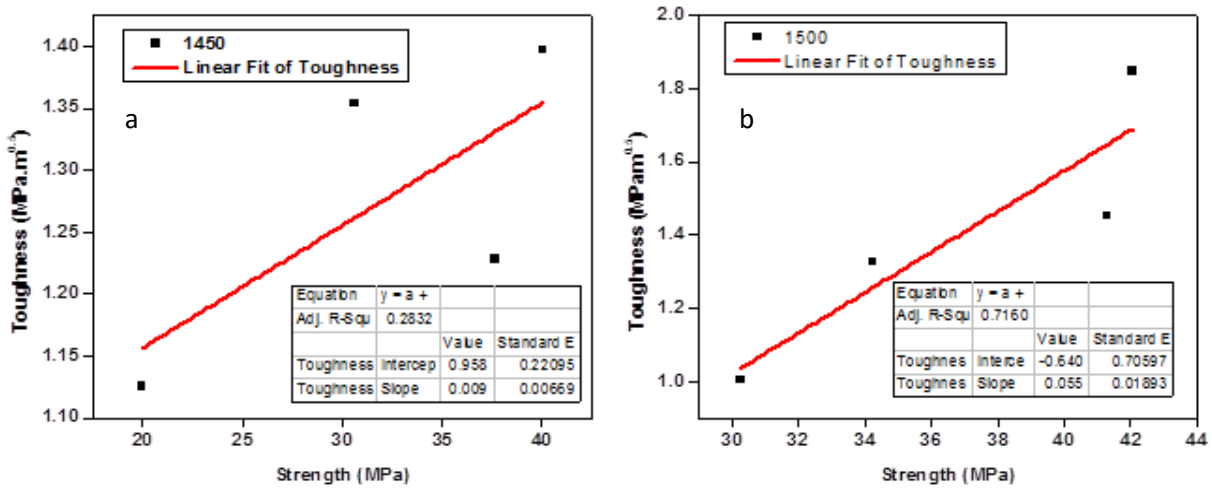

Figure 5.27 a, b σ_f vs K_{IC} of B1-FA at 1450°C and 1500°C

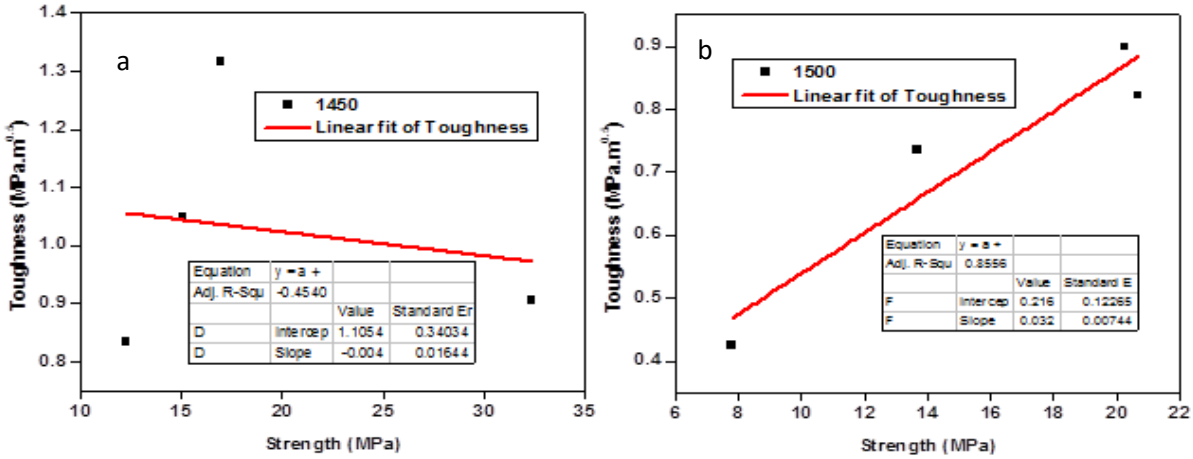

Figure 5.28 a, b σ_f vs K_{IC} of B2-FA at 1450°C and 1500°C

5.17 Thermal Shock Resistance:

Table 5.3 shows the Vickers hardness of both B1-FA and B2-FA compositions after the samples have been subjected to thermal shock cycles. For thermal shock 1500°C sintered samples were considered. It can be seen from the table that only in B1-FA, 70% FA samples the hardness decreased. For all the other compositions, the hardness increased after 5 cycles. The decrease in hardness can be correlated with the change in microstructure. This particular sample was having "black coring". However, after thermal cycling the sample turned white due to oxidation of carbon residue. This probably resulted in a porous sample that reduced the hardness. Similarly for 70:30 B2-FA composition porous structure is formed. Hence, thermal shock gives easy crack propagation. Fig 5.29 (a, b) and 5.30 (a, b) shows the microstructure of 30:70 B1-FA and 70:30 B2-FA sample before and after thermal cycling. Two points can be noted from the microstructures. Firstly, the structure becomes porous after thermal cycling. Secondly, the elongated mullite grains and the dense microstructure has changed after thermal cycling, and a large number of small bright grains have appeared in the microstructure. A detailed study of this aspect is required. But at this stage, it can be

concluded that the decrease in hardness can be related to the change in the microstructure of the thermally cycled sample. Similarly, for B2-FA compositions, only 70:30 B2-FA composition exhibited a decrease in hardness. However, microstructure comparison between the sintered and thermally cycled samples shows that elongated mullite grains have appeared, and glassy phase is also observed. Thus here also, a microstructural change has taken place.

Table 5.3 Hardness of B1-FA and B2-FA compositions after thermal shock

Composition (Bauxite: Fly ash)	Hardness of B1-FA (GPa)		Hardness of B2-FA (GPa)	
	As Sintered	After 5 cycles	As Sintered	After 5 cycles
70:30	2.6	3.1	0.50	0.30
60:40	1.45	1.8	0.47	1.1
50:50	2.15	2.2	0.49	0.93
30:70	4.95	3.4	2.8	3.3

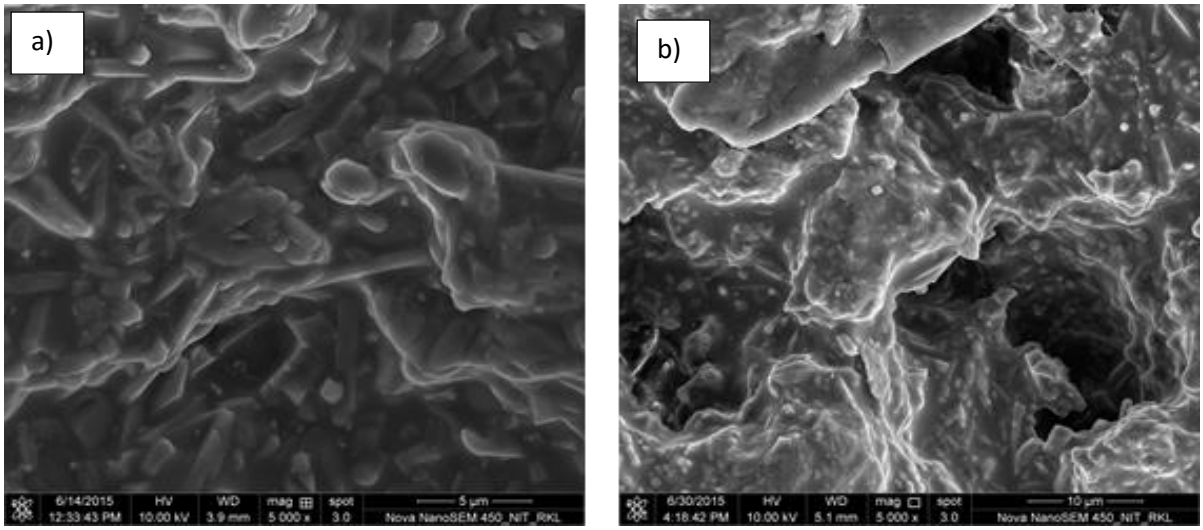

Figure 5. 29 a, b FESEM images of 30:70 B1-FA composition before and after thermal cycling

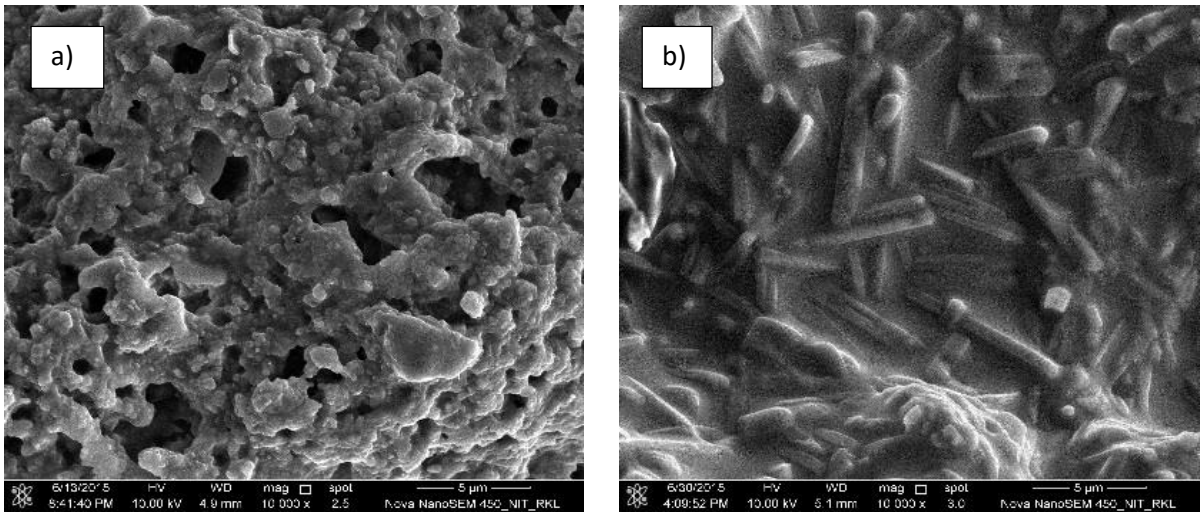

Figure 5.30 a, b FESEM images of 70:30 B2-FA composition before and after thermal cycling

Table 5.4 a Summary of the results obtained for B1-FA compositions:

Bauxite: Fly ash	Temperature (ºC)	Phase composition (%)				Relative Density (%)	Apparent Porosity (%)	Bending Strength (MPa)	Hardness (GPa)	Fracture toughness (MPa.m$^{0.5}$)
		Corundum	Mullite	Glass	Cristobalite					
70:30	**1400**	15.7	55.6	28.8	0	60.1	43.39	14.2	0.5	0.41
	1450	11.2	56.4	32.4	0	71.6	33.5	39.7	1.1	1.37
	1500	12.9	59.4	27.7	0	79.6	22.7	41	2.6	1.85
60:40	**1400**	0	90.1	9.9	0	46.6	44.8	7.8	0.4	0.68
	1450	2	82	16	0	62.9	42.5	19.7	0.5	1.08
	1500	0	75.5	24.5	0	75.6	28.8	28.7	1.4	1.05
50:50	**1400**	0	63	37	0	63.5	40	13	0.45	0.74
	1450	0	59.8	40.2	0	62.2	36.1	36.3	0.8	1.23
	1500	0	64.6	35.4	0	73.5	23	40.1	2.19	1.46
30:70	**1400**	0	47.5	41	11.5	81	24.9	16.6	0.95	0.58
	1450	0	35.5	58.2	6.3	85.6	23.3	32.1	2.2	1.36
	1500	0	58.5	33.7	7.9	81	1.6	31.3	4.7	1.33

Table 5.4b Summary of the results obtained for B2-FA compositions:

Bauxite: Fly ash	Temperature (°C)	Phase composition (%)				Relative Density (%)	Apparent Porosity (%)	Bending Strength (MPa)	Hardness (GPa)	Fracture toughness (MPa.m$^{0.5}$)
		Corundum	Mullite	Glass	Cristobalite					
70:30	1400	26.9	49.9	23.2	0	49.85	36.57	11.83	0.44	0.92
	1450	14.6	42.8	42.7	0	56	34.12	11.14	0.32	0.81
	1500	34.4	49.6	16	0	46.81	38.24	13.13	0.49	0.74
60:40	1400	22	48	30	0	51.73	33.96	18.49	0.84	1.12
	1450	21.8	53.6	24.5	0	58	34.74	15.29	0.68	1.33
	1500	14	64.9	21.2	0	55.6	35.51	20.29	0.46	0.83
50:50	1400	21.92	42.5	32.4	3	57.91	32.66	26.35	1.15	1.07
	1450	12.2	38.5	44.4	2.4	67.2	35.3	14.04	0.73	1.13
	1500	17	53	30	0	66.28	31.69	21.53	0.49	0.90
30:70	1400	10.7	27	38	24	68.84	19.11	21.59	1.39	1.30
	1450	9.6	35	20.5	34.75	77.5	19.98	31.94	2.15	1.01
	1500	6.4	34	19.4	40	87.47	5.53	8.095	2.89	0.43

CHAPTER-6

CONCLUSIONS

6. Conclusions:

The present study focused on the processing of mullite based ceramics using Bauxite (B)-Flyash (FA) mixtures. Different B-FA compositions were chosen (30% FA, 40% FA, 50% FA and 70% FA) which varied the overall compositions from alumina (excess) - mullite compositions to silica (excess) - mullite compositions. The compositions were studied for phase analysis, fracture strength and toughness, hardness and microstructure. On the basis of the results obtained in this study, the following conclusions can be drawn:

1) The mullite percentage in the sintered bauxite-fly ash samples was dependent on the bauxite type. 60:40 B1-FA had a higher percentage of mullite (90.1%) as compared to B2-FA (64.9%). The higher percentage of mullite in B1 –FA compositions could be attributed to the finer crystallite size of B1 and smaller particle size distribution of B1.
2) Dilatometric study revealed that initiation of the mullitization reaction (the onset of expansion in the dilatometric curve) for B1-FA mixture is 1250^{o}C and 1300^{o}C for B2-FA composition. Since, same FA powder was used with both the bauxite, a shift of the mullitization reaction to a higher temperature indicated a coarser particle size of B2. The dilatometric curve also indicate that in the B1-FA composition, the mullitization reaction completed by 1475^{o}C (exhibiting flattening of the curve) but in the B2-FA composition, the mullitization reaction is incomplete.
3) It is also noted from the dilatometric study that the percentage linear shrinkage due to densification is less for B2-FA (1.5%) and more for B1-FA (4%) composition. This fact also indicates a coarser particle size distribution for B2.
4) The mullitization reaction in the bauxite-fly ash commenced with the dissolution of quartz and corundum followed by the appearance of mullite and cristobalite.
5) In either of the B1-FA or B2-FA compositions, no difference in the mullite percentage was observed between single stage and two stage firing schedule.
6) Three types of mullite grains were observed. They were equiaxed primary mullite, elongated secondary mullite and very fine and elongated tertiary mullite. The equiaxed grains were observed in compositions with a lower glassy phase. In the higher glassy phase compositions, elongated mullite grains were observed. These grains resulted from the dissolution – precipitation reactions involving primary mullite.
7) The relative density of the sintered B1-FA samples showed a dip at 40% FA addition following which the relative density increased. The dip in the relative density corresponded to the maximum mullite formation (due to the associated expansion

retarding the densification). The maximum relative density of 85.6% was obtained for 30:70 B1-FA samples. This composition had higher glassy phase which accounted for high density of this composition.

8) In B2-FA sintered samples, the relative density increased with FA content, and no minima were noticed. A maximum relative density of 87.5% was obtained for 30:70 B2-FA samples.
9) In the B1-FA compositions, the highest apparent porosity was 28.8% for in the 1500^{o}C sintered samples of 60% B1-40% FA compositions. In the B2-FA compositions, the highest porosity was 38.24% for 1500^{o}C sintered 70% B2- 30% FA samples. The high apparent porosity samples also had relatively higher mullite fraction. The apparent porosity dropped rapidly in the 70% FA compositions – it was 1.6% for B1-FA compositions and 5.53% for B2-FA composition. High Fly ash content resulted in dense samples due to high glassy phase. The large volume of glassy phase also caused premature sealing of open pores thereby causing black coring.
10) The microstructures of the sintered 70% B1-30% FA samples showed dense crystalline microstructure and mullite grains. The glassy phase was more in the 30% B1- 70% FA sample. The B2 microstructure showed the presence of glassy phase and porous microstructure both for 30% and 70% FA. Equiaxed primary mullite was present in 70% B2 - 30% FA containing samples.
11) The highest bending strength of 41 MPa was observed for B1-FA samples and the highest strength was 32 MPa for B2-FA samples. The bending strength results exhibited almost the same trend as the Relative Density with the exception that the strength dropped for 70% FA composition. The drop in strength could be related to high cristobalite and glassy phase present in these samples. The black coring might also have contributed to the strength decrease. The results are comparable to the literature value.
12) The Vickers Hardness increased at 70% FA addition. The maximum hardness of 4.7 GPa was observed for B1- FA samples while the hardness was 2.9 GPa for B2-FA samples. The increase in hardness with the increase in FA content could be related to the increased amount of glassy phase that helped the samples to densify.
13) The maximum fracture toughness was 1.85 MPa.m$^{0.5}$ for 70% B1-30% FA composition. For B2-FA compositions, the highest toughness was 1.33 MPa.m$^{0.5}$ for 60% B2-40% FA samples. The fracture toughness variation of B1-FA and B2-FA

with FA addition showed the opposite trend. The toughness variation correlated well with the strength of the samples. For 1500^{o}C sintered samples, the toughness and strength were directly proportional.

14) After thermal cycling, the structure becomes porous. Secondly, the elongated mullite grains and the dense microstructure of 30:70 B1-FA has changed after thermal cycling, and a large number of small bright grains have appeared in the microstructure. Similarly, for B2-FA compositions, only 70:30 B2-FA composition exhibited a decrease in hardness. However, microstructure comparison between the sintered and thermally cycled samples shows that elongated mullite grains have appeared, and glassy phase was also observed. The reason for such a microstructural change has not been fully understood at this moment and require further detailed investigation.

REFERENCES

1.1. H. Horitsu, "Ceramics Bioreactor," Kinozairyou, **11** 14-28, 1991.

1.2. B. Hildmann and H. Schneider, "Thermal Conductivity of 2:1-Mullite Single Crystals," J. Am. Ceram. Soc., **88** [10] 2879-82, 2005.

1.3. M. Iwata, K. Oshima, T. Isoda, M. Arai, K. Nakano and A. Kamiya, "Mechanical Properties and Micro-structures of Fiber Reinforced Silicon Nitride and Mullite Composites. In: Abstracts of the Annual Meeting of the Ceramic Society of Japan," Ceram. Soc. Jpn. Paper No. 2E36, 1989.

1.4. H. Schneider, J. Schreuer, B. Hildmann," Structure and properties of mullite—A review", J. Eur. Ceram Soc **28**, 329–344, 2008.

1.5. T. Kumazawa, S. Kanzaki, J. Asaumi, O. Abe,and H Tabata, "Sinterability of SiO_2-Al_2O_3 Prepared by Spray Pyrolysis Effect of Chemical Composition," Yogyo Kyokaishi, **94** [5] 485-90, 1986.

1.6. N L. Bowen and J W Greig, "The System: Al_2O_3-SiO_2," J. Am. Ceram. Soc, **7** [4] 238-54, 1924.

1.7. W.H Bauer, I Gordon, and C H. Moore, "Flame Fusion Synthesis of Mullite Single Crystals," J. Am.Ceram Soc., **33** [4] 140-43, 1950.

1.8. N.A. Toropov and F. Ya. Galakhov, "Solid solutions in the system Al_2O_3–SiO_2", Izv. Aka. Nauk SSSR Otd. Khim. Nauk, 8 (1958).

1.9. P. P. Budnikov, S. G. Tresvyatskii. and V. I. Kushakovskil, "Making the Phase Diagram of the System Al_20_3-SiO_2. More Precise." Doklady Akad. Nauk *S.S.S.R.*, **93** [2] 281-83, 1953.

1.10. N. E. Filonenko and I. V. Lavrov. "Fusion of Mullite," Doklady Akad. Nauk S.S.S.R., 89 [1] as indexed in the Ceram. Abstr., 1955 , April, p. 61f 141-42 (1953)

1.11. S. Aramaki and R. Roy, "Revised Equilibrium Diagram for the system Al_2O_3-SiO_2", J. Am. Ceram. Soc. **45** [5], 229–222, 1962.

1.12. I.A. Aksay and J. A. Pask, "Stable and metastable phase equilibria in the system Al_2O_3–SiO_2", J. Am. Ceram. Soc. **58** [11–12] 507–512, 1975.

1.13. David J. Duval, Subhash H. Risbud, and James F. Shackelford, Chapter 2, in Ceramic and Glass Materials: Structure, Properties, and Processing, Eds. J Shackelford, R. H Doremus, Springer 2008.

1.14. S.O. Agrell and J V Smith, "Cell Dimensions, Solid Solution. Polymorphism, and Identification of Mullite and Sillimanite," J. Am Ceram Soc., **43** [7] 69-76, 1960.

1.15. W.M Kriven and J A Pask, "Solid-Solution Range and Microstructure of Melt-Grown Mullite," J Am. Ceram Soc., **66** [9] 649-54, 1983.

1.16. Y Nakajima and P H Ribbe, "Twinning and Superstructure of Al-Rich Mullite," Am Mineral. **66**, 142-47, 1981.

1.17. W, E. Cameron, "Mullite A Substituted Alumina," Am. Mineral, **62** [7-81] 747-55, 1977.

1.18. S. Freimann and S. Rahman, "Refinement of the real structures of 2:1 and 3:2 mullite", J. Eur. Ceram. Soc. **21**, 2453–61, 2001.

1.19. K. Okada and N. Otsuka, "Formation Process of Mullite in Ceramic Transactions 'Mullite and Mullite Matrix Composites", Vol. 6, pp. 375-387, Eds. S. Somiya, R. F. Davis and J. A. Pask, The American Ceramic Society, Westerville, (1990).

1.20. Y. Hirata and I A Aksay, "Colloidal Consolidation and Sintering Behavior of CVD-Processed Mullite Powders", pp 611-21 in Ceramic *Mi*crostructures *86.* Role of Interfaces, Materials Science Research, Vol. 21 Edited by J A Pask and A G Evans Plenum Press, New York, (1987).

1.21. A. Yasumori, M. Anma and M. Yamane, "Chemical Effects of Formamide and N, N Dimethylformamide on the Formation of Alkoxy-Derived Silica Gel", Phys. Chem. Glasses, **30** [5] 193-201, 1989.

1.22. P. D. D. Rodrigo and P. Boch, "High Purity Mullite Ceramics by Reaction Sintering", Int. J. High Technology Ceramics **1** 3-30, 1985.

1.23. K.S. Mazdiyasni and L M. Brown, "Synthesis and Mechanical Properties of Stoichiometric Aluminum Silicate (Mullite)", J. Am. Ceram. Soc., **55** [11] 548-52, 1972.

1.24. R.R.Tummala, "Ceramic and Glass-Ceramic Packaging in the 1990s", J Am. Ceram. Soc, **74** [5] 895-908, 1991.

1.25. E.A.Richards, C.J.Goodbrake, and H.G.Sowman, "Reactions and Microstructure Development in Mullite Fibers", J Am. Ceram. Soc, **74** [10] 2404-409, 1991.

1.26. M D Sacks, N Bozkurt, and G W Scheiffele, "Fabrication of Mullite and Mullite-Matrix Composites by Transient Viscous Sintering of Composite Powders", J Am Ceram Soc, **74** [l0] 2428-37, 1991.

1.27. **N** Shinohara, D. M. Dabbs, and I. A Aksay, "Infrared Transparent Mullite through Densification of Monolithic Gels at 1250"C",Infrared Opt. Transm Water, Proc SPIE, **683**, 19-24, 1986.

1.28. J A Pask, X W Zhang, A P Tomsia, and B.E Yoldas, "Effect of Sol-Gel Mixing on Mullite Microstructure and Phase Equilibria in the α-$A1_2O_3$-SiO_2 System", J Am. Ceram. Soc, **70** [10] 704-07, 1987.

1.29. S. Komarneni, Y Suwa. and R. Roy, "'Application of Compositionally Diphasic Xerogels for Enhanced Densification: The System Al_2O_3-SiO_2", J Am Ceram. Soc. **69** [7] C155-56, 1986.

1.30. H.Suzuki and H Saito. "Processing of the Fine Mullite Powder from Metal Alkoxides and Its Sintering", Yogyo Kyokaishi, **95** [7] 697-702, 1987.

1.31. C.L. Yehn, W.C. Kao," Effects of TiO_2, B_2O_3, and SiO_2 on the formation of TiB_2/mullite composites by thermite-based combustion synthesis", Ceram Int **41** 4558–63, 2015.

1.32. V. Viswabaskaran, F.D. Gnanam, M. Balasubramanian," Effect of MgO, Y_2O_3 and boehmite additives on the sintering behavior of mullite formed from kaolinite-reactive alumina", J Mat Proc Technol **142** 275–81, 2003.

1.33. Saikat Maitra and Jagannath Roy," Effect of TiO_2 and V_2O_5 Additives on Chemical Mullite", Adv Ceram Sci Engg (ACSE) **2** [3], August (2013).

1.34. L.B. Kong , Y.B. Gan , J. Ma , T.S. Zhang , F. Boey , R.F. Zhang," Mullite phase formation and reaction sequences with the presence of pentoxides", J Alloys Compd **351** 264–72, 2003.

1.35. Yingchao Dong, Xuyong Feng, Xuefei Feng, Yanwei Ding, Xingqin Liu and Guangyao Meng "Preparation of low-cost mullite ceramics from natural bauxite and industrial waste fly ash", J Alloys Compd **460**, 599–606, 2008.

1.36. Shaopeng Li, Jianbo Zhang, Zhanbing Li, Bin Lin, Yonghui Li and Huiquan Li",Preparation of Mullite Ceramics from Coal Fly Ash by Deep-desilication Technology",2015 World of Coal Ash Conference,May5-7, (2015).

1.37. N. Suriyanarayanan, K.V. Kannan Nithin, Enrico Bernardo," Mullite Glass Ceramics Production From Coal Ash and Alumina by High Temperature Plasma", J Non-Oxide Glasses, **1** [4], 247- 60, 2009.

1.38. J. S. Jung, H. C. Park and R. Stevens "Mullite ceramics derived from coal fly ash", J Mater Sci **20** 1089 – 91, 2001.

1.39. Parveen Sultana, Sukhen Das, Biswajoy Bagchi, Alakananda Bhattacharya, Ruma Basu and Papiya Nandy," Effect of size of fly ash particle on the enhancement of mullite content and glass formation", Bull. Mater. Sci., **34** [7] 1663–70, 2011**.**

2.1.F J Klug, S. Prochazka, and R.H. Doremus, 'Alumina-Silica Phase Diagram in the Mullite Region", **6** 15-43 in Ceramic Transactions, Mullite *and* Mullite *Matrix* Composites. Edited by S Somiya, R F Davis, and J.A Pask, American Ceramic Society, Westerville, OH, (1990).

2.2. IIhan A. Aksay, Daniel.M.Dabbs and Mehmet Sarikaya “Mullite for Structural, Electronic, and Optical Applications”, J.Am Ceram, Soc., **74** [l0] 2343-58, 1991.

2.3. W.H.Bauer, I.Gordon and C.H.Moore, “Flame Fusion Synthesis of Mullite Single Crystals” J.Am Ceram, Soc., **33** [4] 140-43, 1950.

2.4. S.Somiya, R.F.Davis and J.A.Pask, “Mullite and Mullite Matrix Composites”, American Ceramic Society, Westerville,OH Ceramic Transactions, **6** (1990).

2.5. Symposium F “Mullite Processing, Sructure, and Properties” (American Ceramic Society Pacific Coast Regional Meeting), Am.Ceram.Soc.Bull..,**69** [9] 1526-27, 1990.

2.6. E.C. Shears and W.A. Archibald, “Alumino-silicate refractories”, Iron Steel 27, 26–30 and 61–65 (1954).

2.7. R.F. Davis and J.A. Pask, Diffusion and reaction studies in the system Al_2O_3−SiO_2, J. Am. Ceram. Soc. **55** [10], 525–31, 1972.

2.8. Guse W and Mateika D,” Growth of mullite single-crystals ($2Al_2O_3.SiO_2$) by Czochralski method”, J. Cryst. Growth, **22,** 237-40, 1974.

2.9. Shindo Isam, “The melting nature and growth of mullite single crystals by the modified floating zone method”, Cer American Trans.**6**, 103-13, 1990.

2.10. S. Prochazka and F.J. Klug, Infrared-transparent mullite ceramics, J. Am. Ceram. Soc., 66, 874–880 (1983).

2.11. F.J. Klug, S. Prochazka, and R.H. Doremus, “Alumina–silica phase diagram in the mullite region”, J. Am. Ceram. Soc. **70**, 750–59, 1987.

2.12. H. Mao, M Selleby and B Sundman, “Phase Equilibria and Thermodynamics in the Al_2O_3- SiO_2 System- Modeling of Mullite and Liquid”, J Am Ceram Soc **88** [9] 2544-51, 2005.

2.13. A. Aksay and J. A. Pask, "The Silica-Alumina System. Stable and Metastable Equilibria at 1.0 Atmosphere”, 'Science (Washington, *D C.),* 183, 69-71, 1974

2.14. Juliana Anggono “Mullite Ceramics: Its Properties, Structure, and Synthesis”, Jurnal Teknik Mesin **7**, [1] 1 – 10, 2005.

2.15. Gaida Sedmale, Ingunda Sperberga and Uldis Sedmalis, “Phase composition and properties of mullite ceramic in high temperature testing”,Conference proceedings, Riga Technical University, Institute of Silicate Materials, Azenes str. 14/24, LV-1048, Latvia.

2.16. H S Tripathi, A Ghosh, M K Halder, B Mukherjee and H S Maiti," Microstructure and properties of sintered mullite developed from Indian bauxite", Bull. Mater. Sci.,**35** [4], 639–43, 2012.

2.17. Yabin Zhang, Yaping Ding, Yong Li, Jiqiang Gao, Jianfeng Yang, and Litong Guo," Mullite Fibers Prepared by Sol-Gel Method Using Aluminum Chloride Aluminum Isopropoxide and Tetraethylorthosilicate", Mater.Manuf Processes, **26**: 649–53, 2011.

2.18. S. Sundaresan and J. Benziger,"Structural Investigations and Energetics of Mullite Formation from Sol-Gel Precursors", Chem. Mater.,**6**, 160-70, 1994.

2.19. J.S.Lee and S.C.Yu,"Characterization and sintered bodies of mullite derived via coprecipitated alumina silica powders", Mat.Res.Bull.,**27** 811-821,1992.

2.20. Katsumi Yoshida, Hideki Hyuga, Naoki Kondo, Hideki Kita," Synthesis of precursor for fibrous mullite powder by alkoxide hydrolysis method", Mat. Sci.Engg B **173** 66–71, 2010.

2.21. Daniel M. Dabbs, Nan Yao, Ilhan A. Aksay", Nanocomposite Mullite/Mullite Powders by Spray Pyrolysis" J. Nanopart. Res, **1** [1] 127-30, 1999.

2.22. W.E. Lee and Mark Rainforth," Ceramic Microstructures: Property Control by Processing",p.p 23. Chapman & Hall, U.K (1994).

2.23. N Shinohara, D. M. Dabbs, and I. A Aksay, "Infrared Transparent Mullite through Densification of Monolithic Gels at 1250^{o}C", Infrared Opt. Transm Water, Proc SPIE, **683** 19-24, 1986.

2.24. B E. Yoldas, "Microstructure of Monolithic Materials Formed by Heat Treatment of Chemically Polymerized Precursors in the SiO_2-Al_2O_3 Binary," Am. Ceram. Soc. *Bull.*, **59** [4] 479-83, 1980.

2.25. H. Schneider, U. Seifert-Kraus and A. Majdic, "Microchemistry of Refractory-Grade Bauxites", Am. Ceram. Soc. Bull., **61**, 741-45, 1982.

2.26. Abdulmula Ali Albhilil, Martin Palou and Jana Kozankova," Characterization of cordierite-mullite ceramics prepared from natural raw materials", Acta Chimica Slovaca, **6** [1] 1-7, 2013.

2.27. V. Viswabaskaran, F.D. Gnanam and M. Balasubramanian," Mullitisation behaviour of calcined clay–alumina mixtures", Ceram Int **29**, 561–71, 2003.

2.28. N S Raut, P Biswas, T K Bhattacharya and K Das," Effect of bauxite addition on densification and mullitization behavior of West Bengal clay", Bull. Mater. Sci., **31** [7] 995–999, 2008.

2.29. Ibram Ganesh, Govindam Sundararajan and Jose M.F. Ferreira,"Formation and Densification Behavior of Mullite Aggregates from Beach Sand Sillimanite", J.Am.Ceram.Soc.,**91** [8] 2464-68, 2008.

2.30. Yabin Zhang, Yaping Ding, Jiqiang Gao, Jianfeng Yang," Mullite fibres prepared by sol–gel method using polyvinyl butyral", J Eur Ceram Soc **29** 1101–07, 2009.

2.31. Minghua Zhou, J.M.F. Ferreira, A.T. Fonseca, J.L. Baptista,"Sintering of mullite-alumina composites from diphasic precursors", Ceram Int **25**, 325-30, 1999.

2.32. Anjan K. Chatterjee," Indian Fly Ashes, Their Characteristics, and Potential for Mechano-Chemical Activation for Enhanced Usability", Second International Conference on Sustainable Construction Materials and Technologies, June 28-30, 2008.

2.33. Anran Guo, Jiachen Liu, Rui Xu, Hai Xu, Caifen Wang," Preparation of mullite from desilication-flyash", Fuel **89**, 3630–36, 2010.

2.34. Parveen Sultana, Sukhen Das, Alakananda Bhattacharya, Ruma Basu and Papiya Nandy, "Mullite formation in coal fly ash is facilitated by the incorporation of magnesium oxide", Rev.Adv.Mater.Sci.**27**,69-74, 2011.

2.35. S.Kumar, S.K.Das and P.K.Daspoddar,"Synthesis of mullite aggregates from flyash: effect on thermomechanical behaviour of low cement castables", Brit Ceram Trans. **103** [4] 176-80, 2004.

2.36. Y.M. Park, T.Y. Yang, S.Y. Yoon, R. Stevens, H.C. Park," Mullite whiskers derived from coal fly ash", Mat. Sci. Engg A 454–455, 518–522 (2007).

2.37. Yingchao Dong, Juan Diwu, Xuefei Feng, Xuyong Feng, Xingqin Liu, Guangyao Meng," Phase evolution and sintering characteristics of porous mullite ceramics produced from the flyash-$Al(OH)_3$ coating powders", J Alloys Compd **460**, 651–57, 2008.

2.38. Shihui Li, Haiyan Du, Anran Guo, Hai Xu, Duo Yang," Preparation of self-reinforcement of porous mullite ceramics through in situ synthesis of mullite whisker in flyash body", Ceram Int **38** ,1027–32, 2012.

2.39. J. H. Lee, H. J. Choi, S. Y. Yoon, B. K. Kim, H. C. Park," Porous mullite ceramics derived from coal fly ash using a freeze-gel casting/polymer sponge technique", J Porous Mater **20** 219–26, 2013.

2.40. Kyu H. Kim, Seog Y. Yoon and Hong C. Park," Recycling of Coal Fly Ash for the Fabrication of Porous Mullite/Alumina Composites," Materials, **7**[8] 5982-91**,** 2014.

2.41. Sanjay Kumar & K.K.Singh," Development of corundum/mullite composites from fly ash and alumina mix by reaction sintering", Conference paper National Metallurgical Laboratory, 198-205, 1998.

2.42. Jin-Hong Li , Hong-Wen Ma, Wen-Hui Huang," Effect of V_2O_5 on the properties of mullite ceramics synthesized from high-aluminum fly ash and bauxite", J Hazard Mater **166** 1535–39, 2009.

2.43. Yingchao Dong, Jian-er Zhou, Bin Lin, Yongqing Wang, SonglinWang, Lifeng Miao, Ying Lang, Xingqin Liu, Guangyao Meng," Reaction-sintered porous mineral-based mullite ceramic membrane supports made from recycled materials", J Hazard Mater **172**, 180–86, 2009.

2.44. Yingchao Dong, Stuart Hampshire, Jian-er Zhou, Bin Lin, Zhanlin Ji, Xiaozhen Zhang, Guangyao Meng," Recycling of fly ash for preparing porous mullite membrane supports with titania addition", J Hazard Mater **180**, 173–80, 2010).

2.45. Yingchao Dong, Stuart Hampshire, Jian-er Zhou, Zhanlin Ji, Jiandong Wang, Guangyao Meng," Sintering and characterization of flyash-based mullite with MgO addition", J Eur. Ceram Soc **31** 687–95, 2011.

2.46. Zhong Xiang Chong and Li Guangping (H.S. Chung and K.P. Li)," Sintering Characteristics of Chinese Bauxites", Ceram Int, **7** [2] 65-68, 1981.

2.47. H. S. Tripathi and G. Banerjee," Synthesis and Mechanical Properties of Mullite from Beach Sand Sillimanite: Effect of TiO_2", J Eur. Ceram Soc.**18** [14] 2081-87, 1998.

2.48. Laura Montanaro, Christophe Perrot, Claude Esnouf, Gilbert Thollet, Gilbert Fantozzi, and Alfredo Negro," Sintering of Industrial Mullites in the Presence of Magnesia as a Sintering Aid", J. Am. Ceram. Soc., **83** [1] 189–96, 2000.

2.49. D. Doni Jayaseelan, D. Amutha Rani, D. Benny Anburaj, T. Ohji," Pulse electric current sintering and microstructure of industrial mullite in the presence of sintering aids", Ceram Int **30** 539–43, 2004.

2.50. Yingchao Dong, Bin Lin, Kui Xie, SonglinWang, Hanping Ding, Daru Fang, Xingqin Liu, Guangyao Meng," Cost-effective macro-porous mullite-corundum ceramic membrane supports derived from the industrial grade powder", J Alloys Compd **477**,350–56, 2009.

2.51. J. Roy, N. Bandyopadhyay, S. Das and S. Maitra," Effect of CoO on the Formation of Mullite Ceramics from Diphasic Al_2O_3-SiO_2 Gel", J Eng Sci Tech Rev **3** [1] 136-41, 2010.

4.1. B.D.Cullity, “Elements of X-Ray Diffraction”, 2nd Ed, Addision-Wesley. INC (1978).

4.2. ASTM: C1327-99, Standard test method for Vickers indentation hardness of advanced ceramics, 1-8, 1999.

4.3. Xu Nie and Weinong W. Chen, “Dynamic Ring-on-Ring Equibiaxial Flexural Strength of Borosilicate Glass”, Int. J. Appl. Ceram. Technol., **7** [5] 616–24, 2010.

4.4. Jeffrey J. Swab, Parimal J. Patel, Xuan Tran, Luke Gilde, Ernest Luoto, Mariel H. Gaviola, Ashley Gott, Blake Paulson, and Steven Kilczewski,” Equibiaxial Flexure Strength of Glass: Influence of Glass Plate Size and Equibiaxial Ring Ratio”, International Journal of Applied Glass Science, **5** [4] 384–92, 2014.

4.5. P. Chantikul, G.R. Anstis, B.R. Lawn and D.B. Marshall, A critical evaluation of indentation techniques for measuring toughness: II, strength method, J Am Ceram Soc **64**, 539–43, 981.

5.1. Yaseen Iqbal and William Edward Lee, “Fired Porcelain Microstructural Revisited”, J.Am.Ceram.Soc., **82** [12] 3584-90, 1999.

5.2. W.E.Lee and Y.Iqbal,”Influence of mixing on mullite formation”, J Eur. Ceram Soc **21**, 2583-86, 2001.

5.3. Rahul Jain, “Effective area and volume calculations for ceramic test specimens”, Ph D Thesis submitted to the Dept. of Civil Engineering, The Cleveland State University, (2008).